AD-A193 774

AFWAL-TR-87-3101

DTIC FILE COPY

INVESTIGATIONS OF ROUGH SURFACE EFFECTS ON
FRICTION FACTORS IN TURBULENT PIPE FLOW

Robert P. Taylor
Hugh W. Coleman
W. F. Scaggs
Thermal & Fluid Dynamics Laboratory
Mechanical and Nuclear Engineering Department
Mississippi State University
Mississippi State, MS   39762

February 1988

Final Report for Period May 1984-August 1987

FLIGHT DYNAMICS LABORATORY
AIR FORCE WRIGHT AERONAUTICAL LABORATORIES
AIR FORCE SYSTEMS COMMAND
WRIGHT-PATTERSON AIR FORCE BASE, OHIO   45433-6533
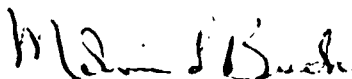
DTIC
ELECTE
APR 2 5 1988
S
D
H

88 4 25 010

NOTICE

When Government drawings, specifications, or other data are used for any purpose other than in connection with a definitely Government-related procurement, the United States Government incurs no responsibility or any obligation whatsoever. The fact that the government may have formulated or in any way supplied the said drawings, specifications, or other data, is not to be regarded by implication, or otherwise in any manner construed, as licensing the holder, or any other person or corporation; or as conveying any rights or permission to manufacture, use, or sell any patented invention that may in any way be related thereto.

This report is releasable to the National Technical Information Service (NTIS). At NTIS, it will be available to the general public, including foreign nations.
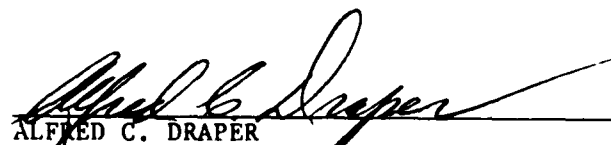
This technical report has been reviewed and is approved for publication.

MELVIN L. BUCK
Asst for Experimental Simulation
Aeromechanics Division

FOR THE COMMANDER

ALFRED C. DRAPER
Acting Chief, Aeromechanics Division
Flight Dynamics Laboratory

If your address has changed, if you wish to be removed from our mailing list, or if the addressee is no longer employed by your organization please notify AFWAL/FIMG, WPAFB, OH 45433-6553 to help us maintain a current mailing list.

Copies of this report should not be returned unless return is required by security considerations, contractual obligations, or notice on a specific document.

AD-A193 774

REPORT DOCUMENTATION PAGE

1a. REPORT SECURITY CLASSIFICATION	1b. RESTRICTIVE MARKINGS
2a. SECURITY CLASSIFICATION AUTHORITY	**3. DISTRIBUTION/AVAILABILITY OF REPORT**
2b. DECLASSIFICATION/DOWNGRADING SCHEDULE	Approved for public release; distribution unlimited.

4. PERFORMING ORGANIZATION REPORT NUMBER(S)	5. MONITORING ORGANIZATION REPORT NUMBER(S)
	AFWAL-TR-87-3101

6a. NAME OF PERFORMING ORGANIZATION Mississippi State University Engr. & Indus. Research Sta. Mech. & Nuclear Engr. Dept.	6b. OFFICE SYMBOL (If applicable)	7a. NAME OF MONITORING ORGANIZATION Flight Dynamics Laboratory (AFWAL/FIMG) Air Force Wright Aeronautical Laboratories
6c. ADDRESS (City, State, and ZIP Code) P. O. Drawer ME Mississippi State, MS 39762		7b. ADDRESS (City, State, and ZIP Code) Wright-Patterson Air Force Base, OH 45433-6553

8a. NAME OF FUNDING/SPONSORING ORGANIZATION	8b. OFFICE SYMBOL (If applicable) FIMG	9. PROCUREMENT INSTRUMENT IDENTIFICATION NUMBER F33615-84-K-3014

8c. ADDRESS (City, State, and ZIP Code)	10. SOURCE OF FUNDING NUMBERS			
AFWAL/FIMG Wright-Patterson Air Force Base, OH 45433	PROGRAM ELEMENT NO. 61102F	PROJECT NO. 2307	TASK NO. N4	WORK UNIT ACCESSION NO. 58

11. TITLE (Include Security Classification)
Investigations of Rough Surface Effects on Friction Factors in Turbulent Pipe Flow

12. PERSONAL AUTHOR(S)
Robert P. Taylor; Hugh W. Coleman, W. F. Scaggs

13a. TYPE OF REPORT Final	13b. TIME COVERED FROM May 84 TO Aug 87	14. DATE OF REPORT (Year, Month, Day) 1988, February	15. PAGE COUNT 100

16. SUPPLEMENTARY NOTATION

17. COSATI CODES			18. SUBJECT TERMS (Continue on reverse if necessary and identify by block number)
FIELD	GROUP	SUB-GROUP	Surface Roughness, Friction Factor
01	01		Discrete Element,
20	04		Turbulent Flow ;

19 ABSTRACT (Continue on reverse if necessary and identify by block number)

The results of an experimental investigation of the effects of surface roughness on turbulent pipe flow friction factors are presented and compared with predictions from a discrete element roughness model which had been developed previously. Friction factor data were acquired over a pipe Reynolds number range from 10,000 to 600,000 for eleven different rough surfaces, nine of which had uniform roughness elements and two of which were roughened nonuniformly. These surfaces covered a range of roughness element sizes, spacings and shapes. Predictions from the discrete element roughness model were in very good agreement with the data for both the uniform and nonuniform roughness cases. Keywords:

20. DISTRIBUTION/AVAILABILITY OF ABSTRACT ☒ UNCLASSIFIED/UNLIMITED ☐ SAME AS RPT. ☐ DTIC USERS	21. ABSTRACT SECURITY CLASSIFICATION Unclassified
22a. NAME OF RESPONSIBLE INDIVIDUAL Mel Buck	22b. TELEPHONE (Include Area Code) (513) 255-6156 22c. OFFICE SYMBOL AFWAL/FIMG

DD FORM 1473, 84 MAR   83 APR edition may be used until exhausted.
All other editions are obsolete.

PREFACE

This program was conducted by the Mississippi State University
Engineering and Industrial Research Station, P. O. Drawer ME,
Mississippi State, Mississippi 39762 under Contract F33615-84-K-3014
and Modifications P00003 and P00004 with the Air Force Wright Aeronau-
tical Laboratories, Wright-Patterson Air Force Base, Ohio 45433-6553.
Mr. Melvin L. Buck (FIMG) managed the program for the Air Force Wright
Aeronautical Laboratories. That part of the program with which this
report is concerned was conducted from May 1984 through August 1987.

The data acquisition system used in the experimental program was
acquired under Grant AFOSR-85-0075, and the water tunnel was
constructed under Amendment A to that grant.

The authors wish to thank Mr. Melvin Buck and Dr. Tony Fiore for
their support and encouragement. The authors also wish to acknowledge
the interest, encouragement and contributions of Dr. James Wilson of
the Air Force Office of Scientific Research.

iii

Accession For		
NTIS GRA&I	☑	
DTIC TAB	☐	
Unannounced	☐	
Justification		
By		
Distribution/		
Availability Codes		
	Avail and/or	
Dist	Special	
A-1		

TABLE OF CONTENTS

TABLE OF CONTENTS (Continued)

LIST OF FIGURES

LIST OF FIGURES (Continued)

LIST OF FIGURES (Continued)

LIST OF FIGURES (Concluded)

LIST OF TABLES

NOMENCLATURE

C_D Drag coefficient; Equation 10

d_o Roughness element base diameter

$d(y)$ Local roughness element diameter

D Pipe diameter

f Friction factor; Equations 2 and 7

k Roughness element height

k' Projected height of conical roughness elements

k^+ Nondimensional roughness height; ku^*/ν

k_s Equivalent sandgrain roughness

L Roughness element spacing

ℓ_m Prandtl mixing length; Equation 8a

$N(y)$ Number of elements at y-location

P Pressure

Q Volumetric flowrate

r Radial coordinate

R Pipe radius

R^+ Nondimensional R; Ru^*/ν

R_τ Roughness parameter; τ_R/τ_T

Re Reynolds number based on test section diameter

Re_d Reynolds number based on local roughness element diameter; Equation 9

Re_{k_s} Roughness Reynolds number; $k_s u^*/\nu$

T Temperature

$u(y)$ Velocity at y-location

u^* Friction velocity; $u_{ave}\sqrt{f/2}$

u_{ave} Average velocity in pipe

V Voltage

y Coordinate normal to the surface

y^+ Nondimensional y; yu^*/ν

Z Zero voltage shift

Greek

β_x Blockage factor

β_y Blockage factor

xii

NOMENCLATURE (Concluded)

δ	Uncertainty in a measured quantity
ΔP	Pressure drop
ΔX	Pressure tap spacing
μ	Dynamic viscosity
μ_T	Eddy viscosity
ν	Kinematic viscosity
ρ	Density
τ_R	Apparent wall shear stress due to form drag on elements
τ_T	Total wall shear stress
τ_w	Wall shear stress

Subscripts

B	Bias error
P	Precision error
w	Values at the wall

SECTION I
INTRODUCTION

Skin friction and heat transfer can be significantly larger for
turbulent flow over a rough surface as compared to an equivalent
turbulent flow over a smooth surface. Many surfaces of engineering
interest are rough in the aerodynamic sense. Examples of systems for
which surface roughness is an important concern are reentry vehicles,
missiles, stores carried externally on high performance aircraft,
ships' hulls, turbines, heat exchangers, piping networks and
atmospheric flows. In light of this broad applicability, there is a
significant engineering interest in the development of accurate
predictive models for fluid mechanics and heat transfer in turbulent
flow over rough surfaces.

1. BACKGROUND

Given the geometry of an object immersed in a flowfield, a speci-
fication of the freestream flow conditions, and a geometrical descrip-
tion of the roughness of the system surfaces, an analyst or designer
would like to at least predict the surface shear distribution, the heat
transfer distribution and the total drag. In the past, most of the
research effort was to develop computational methods for various
geometries with smooth surfaces, and the roughness problem has received
relatively little attention. However, many systems of engineering
interest have surfaces which are aerodynamically rough. Therefore, if
the flow parameters mentioned above are to be predicted, computational
procedures to model the effects of rough surfaces must be developed and
proven by comparison with well-documented data sets.

Schlichting (1936) experimentally investigated the fluid dynamics
of this type of problem. He related his skin friction results on a
range of well-described rough surfaces to the previous results obtained
by Nikuradse (1933) for sand-roughened pipes through definition of an
equivalent sandgrain roughness, k_s. In subsequent surface roughness
effects investigations, workers used these results of Schlichting and

1

the equivalent sandgrain roughness concept to analyze their experimental data and to develop analytical models for use in predictive methods. Over the years, several correlations (Dvorak, 1969; Simpson, 1973; Dirling, 1973) were developed which produced a value of k_s for a rough surface when certain geometrical descriptors were known. These correlations were all intimately tied to the original k_s results of Schlichting.

Over the past decade or so, a predictive approach called the discrete element method, which does not use the equivalent sandgrain roughness concept, has been used with varying degrees of rigor by several groups of researchers (Adams and Hodge, 1977; Finson and Wu, 1979; Finson and Clark, 1980; Lin and Bywater, 1980; Finson, 1982; Coleman, Hodge and Taylor, 1983; Taylor, Coleman and Hodge, 1985). Such approaches rely on empirical input to calibrate the roughness models.

Up until the present time, the experimental results of Schlichting (1936) have remained the only data sets which included the effects of well-defined roughness element shape, size and spacing on skin friction. However, during a recently completed research program (Coleman, Hodge and Taylor, 1983) we discovered that Schlichting had made erroneous assumptions during his data reduction which had significant effects on the data which he reported. The reevaluation of Schlichting's data (Coleman, Hodge and Taylor, 1984) showed that his skin friction results were too large by amounts ranging up to 73 percent and that his reported values of k_s were too high by amounts ranging from 26 percent to 555 percent. These findings caused some consternation since practically all work since the 1930's on surface roughness effects relied significantly on either the skin friction or k_s results as originally reported by Schlichting.

As described in detail in the journal article (Coleman, Hodge and Taylor, 1984), Schlichting tested fully developed flow in a rectangular channel of 40-mm height and 170-mm width. The top wall was rough, and the bottom and side walls were smooth. Schlichting made two assumptions which significantly affected the originally reported values of friction coefficient. He neglected the contribution of the shear stresses on the smooth side walls to the pressure drop in the channel thus overestimating the apparent shear on the rough wall. When he used

2

the law-of-the-wall to recover a friction coefficient, he used an
arbitrary choice of effective wall location for the rough wall which
bore no relationship to the effective location required to attain the
assumed value of the slope in the logarithmic region of the velocity
profiles. The corrected values recommended in the reference were
determined from Schlichting's pressure drop measurements and with the
shear on the side walls taken into account.

In the research program mentioned above, a discrete element pre-
diction approach for two-dimensional, nonisothermal turbulent boundary
layer flow over a rough surface was derived from first principles
(Taylor, Coleman and Hodge, 1985). Any such approach requires empiri-
cal input to calibrate the roughness model (much as empirical informa-
tion was necessary to calibrate the turbulence models used in all
Reynolds-averaged turbulent flow calculations). In the discrete ele-
ment approach, experimental data were required to calibrate both a
roughness element drag coefficient (C_D) model and a roughness element
Nusselt number (Nu_d) model. The corrected data of Schlichting for
surfaces with spherical, spherical segment and conical roughness ele-
ments of various size and spacing was used for the initial calibration
of the C_D model. One heat transfer data set from the series of experi-
ments at Stanford University (Healzer, 1974; Pimenta, 1975; Coleman,
1976) on a rough surface comprised of spheres of a single size packed
in the most dense array was used for the initial calibration of the Nu_d
model.

From these research efforts, there evidently exists a critical
need for accurate, precise, comprehensive data sets on both the heat
transfer and the fluid dynamics in turbulent flow over well-defined
rough surfaces. This research program was designed to investigate the
effects of surface roughness element size, spacing and shape on fric-
tion factor in fully developed flow over a wide range of Reynolds
numbers.

3

SECTION II

EXPERIMENTAL APPARATUS

This section presents a description of the experimental apparatus.
The data reduction equation is presented, and the instrumentation and
measurement procedures are discussed along with the uncertainties
associated with the measurements. The qualification of the test rig is
then presented.

1. DESCRIPTION

The closed-loop water tunnel, shown in Figure 1, has been con-
structed to experimentally investigate the effects of surface roughness
on friction factors in fully developed pipe flow. The system can be
operated over a range of pipe Reynolds numbers from about 10,000 to
600,000.

The pump and motor for the tunnel are located on a spring-mounted
concrete base to isolate induced vibrations. The inlet and outlet of
the pump are connected to flexible hoses in a further attempt to iso-
late the pump and motor vibrations from the rest of the system.

After exiting the pump the water enters a 2.44-m (8-foot) long,
50-mm (2-inch) diameter clear PVC pipe. In this clear section the flow
can be visually inspected to insure that there is no swirl superimposed
on the flow (early in this investigation a honeycomb flow straightener
was used but then abandoned; this is discussed later). This inspection
was done as the air was bled from the tunnel after initially filling it
with water. That is, during the first few minutes the circulating
water contained air bubbles. The flow did not exhibit any swirl as the
air bubbles passing through the clear section moved linearly with no
superimposed angular motion.

Connected to the clear PVC pipe is one of the 2.44-m (8-foot) long
test sections, shown in Figure 2. Each section has a nominal diameter
of 50-mm (2-inch) and is made of two fiberglass halves. In each half,
molded silicone sheet test surfaces are glued into the test section. So
that the pressure drop can be measured, there are 12 pressure taps
evenly spaced at 203.2-mm (8-inches) along the test section. These

4

Turbine Meters

Clear Inlet
Section

Test Section

Honeycomb

Pump

Filters

Dump

Make-up
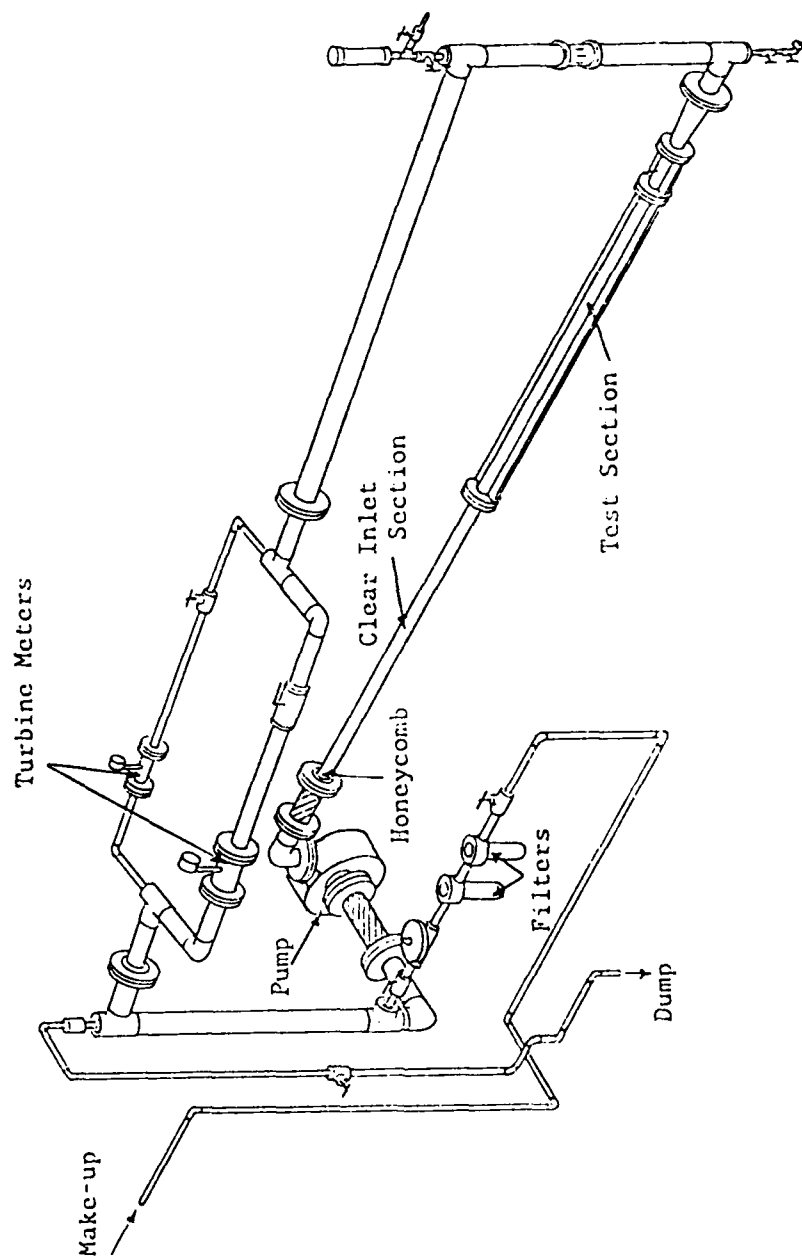
Figure 1. Schematic of Water Tunnel Facility.

5
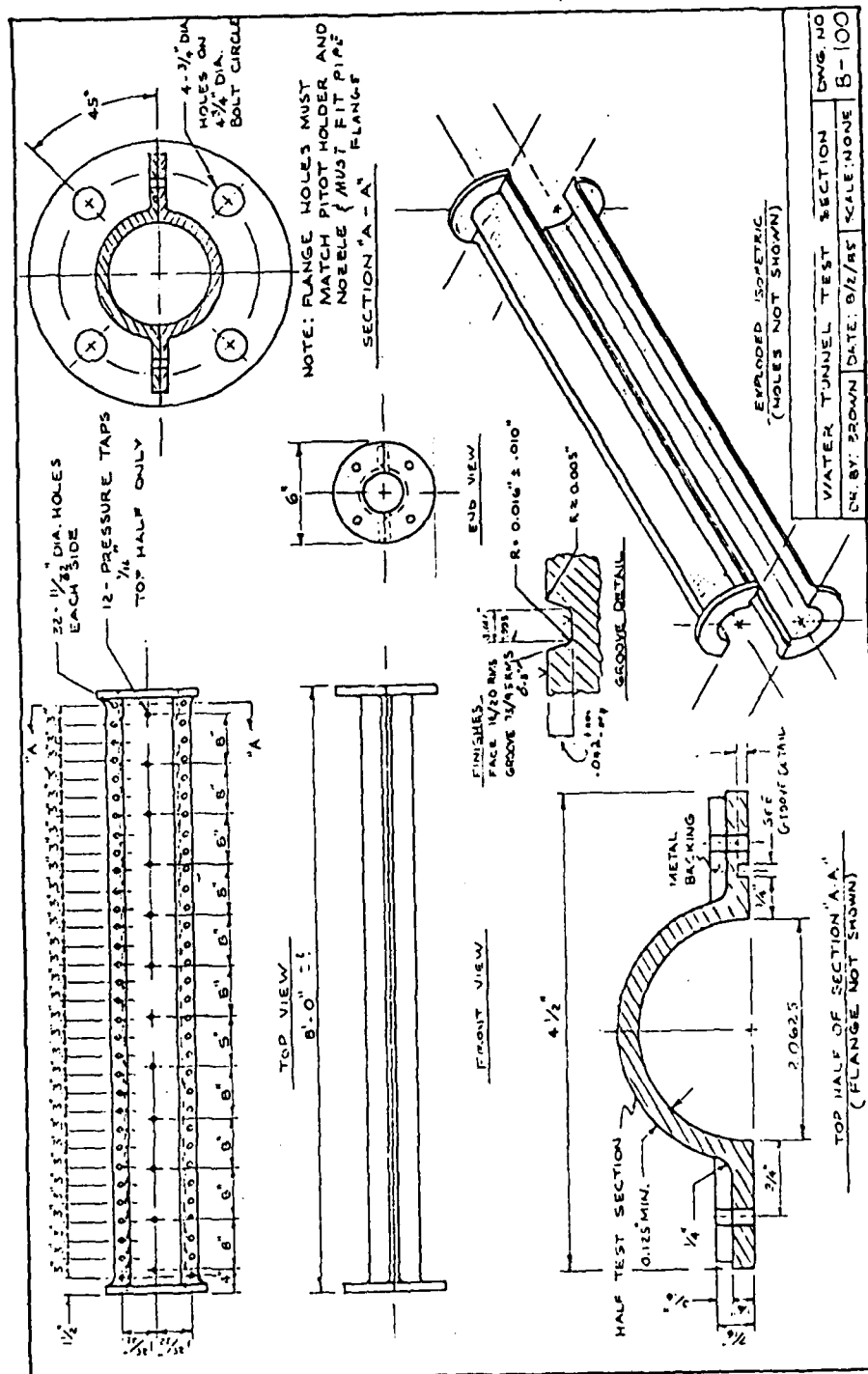
Figure 2. Water Tunnel Test Section.

taps are brass tubing with an outside diameter of 1.59-mm (1/16-inch) and an inside diameter of 0.79-mm (1/32-inch). Using a specially designed guide and cutter, techniques were developed so that very repeatable holes were cut in the silicone sheets to finish the pressure taps. With the pressure tap holes cut, the two halves were bolted together and the test section was ready to be placed in the water loop.

The silicone skins mentioned above are the means by which a rough surface is created for each test section. These skins are precision molded 203-mm (8-inch) by 81-mm (3.2-inch) silicone sheets. The desired roughness pattern, say hemispheres spaced four diameters apart, is molded on the skin at the same time that the skin is molded. This process allows a large number of roughness elements to be precisely and easily attached to the test section wall. All skins used in this project were manufactured according to the procedures described by Holden (1983).

After exiting the test section, the flow passes through one of two turbine meters. The turbine meters measure the volumetric flowrate of the water. The meters are valved manually and chosen depending on the desired Reynolds number range.

The flow then returns to the inlet of the pump; however, since the temperature of the water tends to increase from the pump work, a portion of the flow is dumped and cooler make-up water is added. The make-up water passes through a pressure regulator and a 50-micron particulate filter before entering the system.

2. DATA REDUCTION EQUATION

The wall shear stress for steady incompressible fully-developed pipe flow can be written as

$$\tau_w = \frac{\Delta P}{4} \frac{D}{\Delta X} \quad . \tag{1}$$

The friction factor is defined as

$$f = \frac{\tau_w}{\rho u_{ave}^2 / 2} \quad . \tag{2}$$

7

Recalling that for pipe flow the average velocity is $u_{ave} = 4Q/\pi D^2$, substitution of equation (1) into (2) yields the data reduction equation for this experiment:

$$f = \frac{\pi^2}{32} \frac{\Delta P}{\rho} \frac{D^5}{\Delta X} \frac{1}{Q^2} \ .$$

(3)

3. INSTRUMENTATION AND MEASUREMENT PROCEDURE

The measuring devices used in this investigation were a thermistor, two turbine meters, and three differential pressure transducers. The thermistor, a temperature sensitive resistor, was used to measure the water temperature so that the water density and viscosity could be determined. The turbine meters output a square wave signal whose frequency is proportional to the volumetric flowrate. A 25-mm (1-inch) diameter turbine meter covered the lower range of Reynolds numbers, 10,000 to 100,000; while the upper range, 100,000 to 600,000, was covered by a 75-mm (3-inch) diameter turbine meter. The differential pressure transducers output a dc voltage which is proportional to the pressure difference between a pair of pressure taps 406.4-mm (16-inches) apart on the test section. Three transducers were used to cover the range of pressure drops encountered in this investigation. The details of the calibration of these transducers are given in Appendix A.

In addition to these measuring devices, a Scanivalve fluid switch wafer was used to switch the differential pressure measurement from one pair of pressure taps to another pair. Also, the pump speed (and thus the Reynolds number) was controlled by an eddy current clutch between the 11.2-kW (15-hp) electric motor and the water pump.

The thermistor, turbine meters, pressure transducers, fluid switch, and eddy current clutch were all linked to a Hewlett Packard 3054A Automatic Data Acquistion/Control System (ADACS) and Hewlett Packard 9000 model 220 microcomputer. .

The procedure used to obtain a data point (f and Re) was as follows. Considering Re = $\rho D u_{ave}/\mu$ and equation (3) for f, five measurements are required: water temperature, to obtain ρ and μ; test section

8

diameter, D; flow rate, Q; pressure drop, ΔP; and pressure tap spacing, ΔX. The temperature and the flow rate are measured using the thermistor and turbine meters discussed above. The diameters of the test sections were measured and are reported in Appendix C. The pressure drop is determined by measuring the pressure difference between two static taps spaced $\Delta X = 406.4$-mm (16-inches) apart. The 2.44-m (8-foot) test section was divided into 10 of these ΔX's by plumbing the Scanivalve fluid switch to place across the differential pressure transducer tap 1 vs. 3, tap 2 vs. 4, tap 3 vs. 5, etc.

Although fully developed smooth wall pipe flow exists at the junction of the inlet section and the test section, slight misalignments might cause an entry effect. In addition, the flow requires several diameters to adjust to the test section roughness. Therefore, the first two ΔP's (the first 500-mm or 10 diameters) are not used in determining friction factors. Using the remaining downstream ΔP's, eight values of f are then computed and averaged to give the reported value. The Reynolds number is actually the average of the one computed before the pressure scan and the one computed after the scan. These two values are separated by about 5 minutes and differed only by a small amount (< 2 percent).

4. UNCERTAINTIES

The uncertainties associated with the measurements made are as follows:

temperature	$\pm 0.2°C$ ($\pm 0.36°F$)
flowrate	± 1.25 percent
pressure drop	± 1.5 percent
diameter	± 0.74 percent
length ΔX	± 0.05 mm (0.002 inch)

The resulting uncertainty in the friction factor is ± 4.7 percent. The uncertainty in the diameter is the major cause of the uncertainty in the friction factor. This is caused by the dependence of the friction factor on the fifth power of the diameter as shown in equation (3). The uncertainty in the Reynolds number is ± 1.5 percent. The data points plotted in the figures correspond approximately in size to the measurement uncertainty in the friction factor at ± 4.7 percent. There is,

9

however, no implied reference to the uncertainty in the Reynolds num-
bers in the size of the plotted data points. A more detailed uncer-
tainty analysis is presented in Appendix B.

5.   TEST RIG QUALIFICATION

To qualify this experimental apparatus, a bare wall test section
and a test section with smooth silicone skins were run repeatedly so
that the smooth wall data generated by this water tunnel might be
compared to existing smooth wall data.

An excellent source of smooth wall pipe data is the exhaustive
compilation of data prepared and presented by Drew, Koo, and McAdams
(1932). The results of their survey (plotted as 4 times the friction
factor, f) are given in Figure 3. In all, 1328 data points were re-
ported, with all but a few falling within a ± 5 percent band. They
reported the best line through the friction factor data to be

$$f = 0.00140 + \frac{0.125}{Re^{0.32}} \, , \tag{4}$$

which yields essentially the same smooth wall line as the Swamee-Jain
correlation, Hodge (1985):

$$f = \frac{0.25/4}{[\log(5.74/Re^{0.9})]^2} \, . \tag{5}$$

The bare wall data generated by the Mississippi State University
(MSU) water tunnel are plotted in Figure 4 and given in Appendix C in
Table C-1. These data fall within the ± 5 percent data scatter exhib-
ited in the compilation of Drew, et al. (1932). This close agreement
with such a large volume of smooth wall data indicates the validity of
the MSU instrumentation and data reduction procedures, thus moving the
experimental program through the qualification phase and into the
production phase of this research project.

The runs plotted in Figure 4 and the other runs presented in this
work include replications made on different days as well as
replications made with the test section reversed. That is, the exit
end of the test section was made the entrance end for the reverse run.

10

Figure 3. Compilation of Smooth Pipe Friction Data as Presented
by Drew, Koo, and McAdams (1932).

11
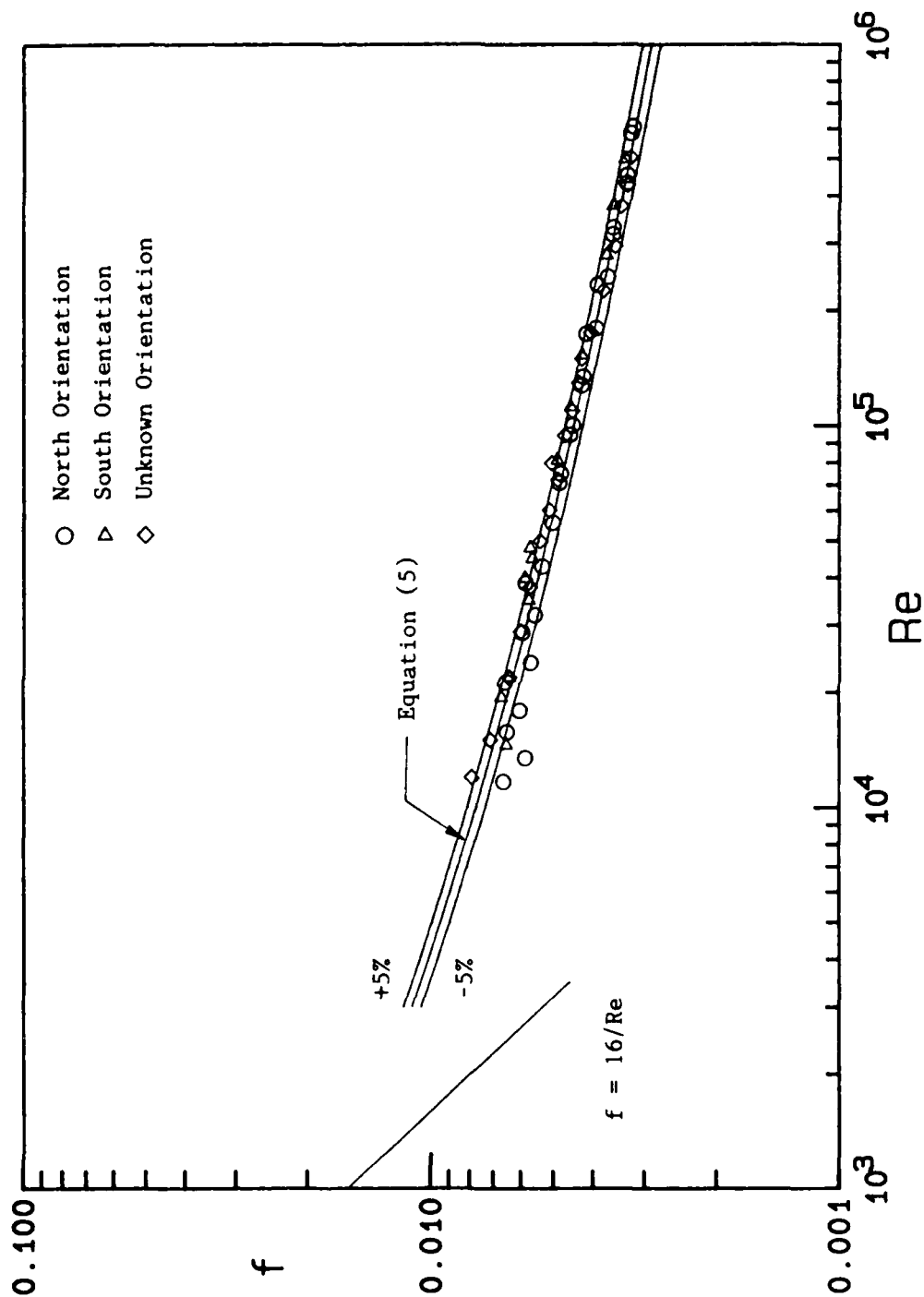
Figure 4. Friction Factor Data for the Smooth Bare Wall Test Section.

One of these orientations was arbitrarily labeled north while the other was labeled south. With the flow entrance noted as north, friction factor data was taken for a series of Reynolds numbers. The section was then reversed, the flow entrance now being south; data was taken at Reynolds numbers that would fall between those of the northern replication. No preference should be assumed for the north or south designations.

The data generated using the test section with the smooth silicone skins are plotted in Figure 5 and given in Table C-2. The data of these replications fall above the ± 5 percent band of the Swamee-Jain smooth wall line. This is not surprising since the addition of the glue and the silicone sheets to the test section produced a surface that was not as smooth as the surface finish of the bare fiberglass section. Also, seams resulted at the joints between two silicone sheets. This created small transverse ridges every 203-mm (8-inches) down the test section. The effects of this added roughness on the friction factors is more pronounced at the higher Reynolds numbers as seen in Figure 5.

Unfortunately only two replications (both north) using the smooth skin test section could be made. The skins were destroyed when the honeycomb flow straightener previously mentioned came dislodged and passed through the test section. From this point, the flow was visually inspected for swirl during each start-up as mentioned above and a flow straightener was no longer used.

The data obtained using the bare wall section and the smooth skin section are presented together in Figure 6. Although the friction factors at the higher Reynolds numbers of the smooth skin section fall above the bare wall data, the two sets belong to the same family of data.
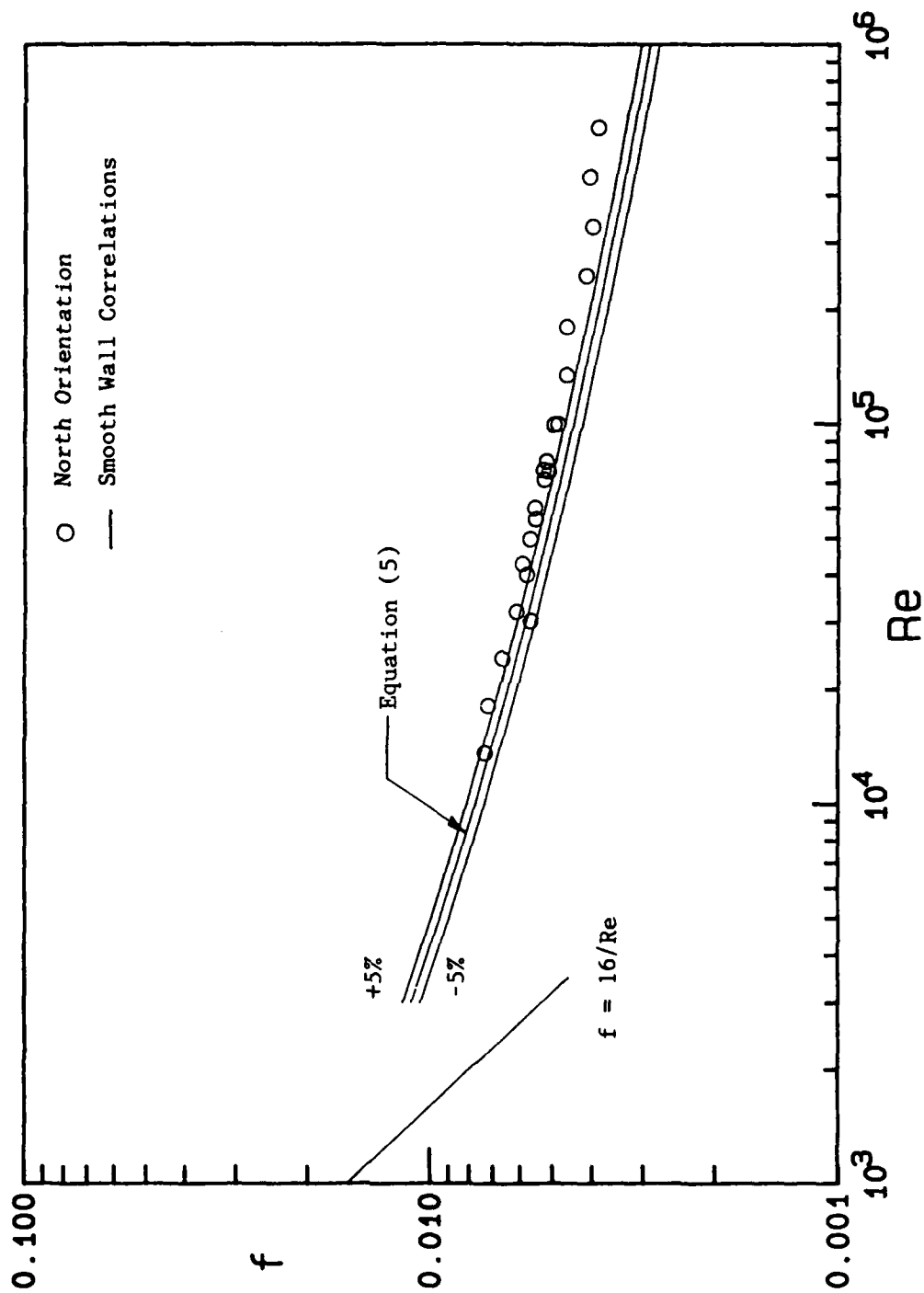
Figure 5. Friction Factor Data for Test Section with Smooth Molded Silicone Skins.

14
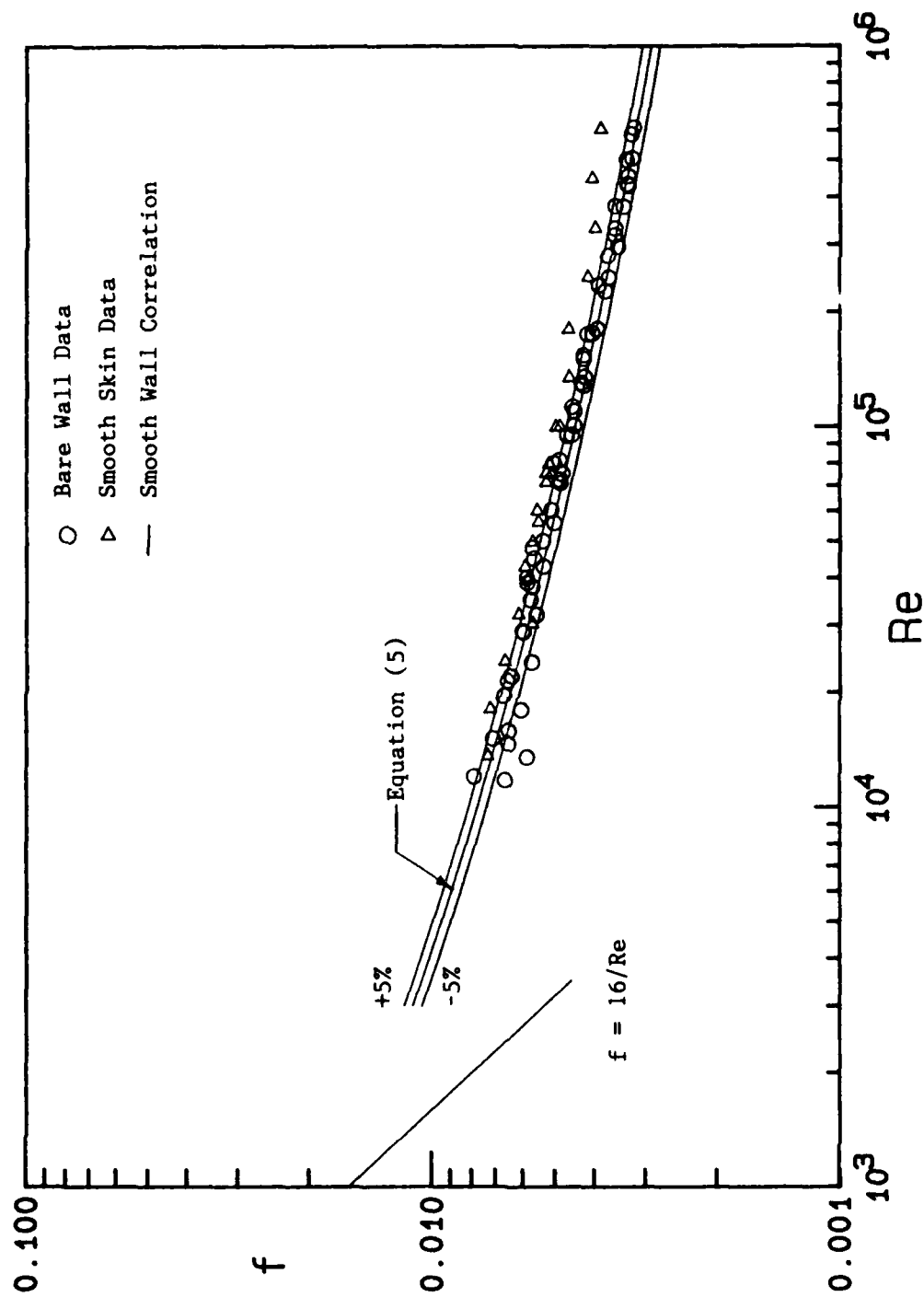
Figure 6. Comparison of Smooth Bare Wall and Smooth Silicone Skin Friction Factor Data.

15

SECTION III
UNIFORM ROUGHNESS RESULTS

This section presents the experimental friction factor data sets
generated at MSU for nine different uniform roughness geometries. The
discrete element roughness model developed by Taylor, Coleman, and
Hodge (1984, 1985) is introduced, and the resulting equations are
presented. The friction factor predictions obtained from the discrete
element model are then compared to the MSU experimental data.

The general shapes of the hemispherical and conical roughness
elements used in this experimental program are shown in Figure 7.
The nominal and measured values of the geometrical parameters used in
describing these uniformly rough surfaces are presented in Table 1.
These parameters characterize the test surfaces discussed in this
section. The descriptors A-1, B-2, etc. assigned to each surface as
given in Table 1 are used merely out of convenience since actually
three parameters (element shape, size, and spacing) distinguish the
surfaces tested.

1. LARGE HEMISPHERES

Three surfaces with large hemispherical roughness elements were
tested. Each surface was made up of hemispheres with a nominal base
diameter d_O = 2.54 mm (0.100 inch) and a nominal height k = 1.27 mm
(0.050 inch). The roughness elements of the three surfaces were spaced
2, 4, and 8 base diameters apart, respectively. Figure 8 contains
individual plots of the three large hemispherical element data sets
demonstrating the effects of the north and south replications previ-
ously discussed. The curves in the plots represent the laminar and
turbulent friction factor relations for smooth pipes. They are
included in most plots in this report for reference.

The data set for surface A-1 (L/d_O = 2) is presented in tabular
form in Table C-3, and is plotted in Figure 8a. It contains 66 data
points taken during three replications. The north and south
replications blend well, indicating that this test section has no
direction dependency.

16
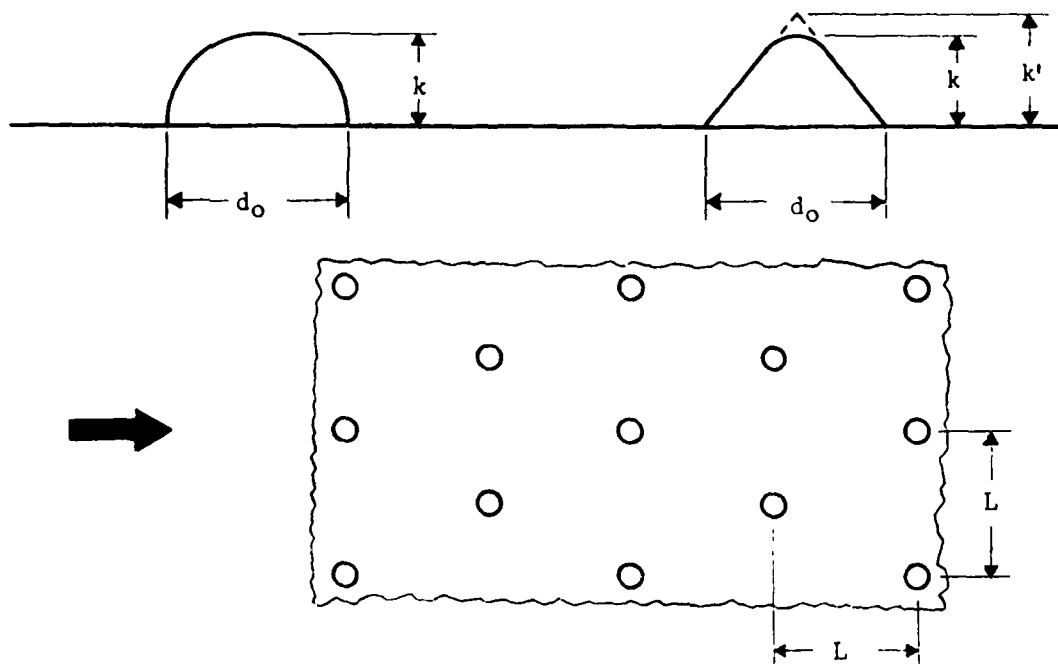
Figure 7.   Surface Roughness Geometry.

TABLE 1. Nominal and Measured Geometries of the Uniform Rough Surfaces

Surface	Test Section Diameter (mm)	Base diameter d_o (mm)		Element spacing L (mm)		Element height k (mm)		Projected height k' (mm)	
		nominal	measured	nominal	measured	nominal	measured	measured	nominal
Large Hemispheres									
A-1	51.46	2.54	2.55	5.08	5.10	1.27	1.25	--	--
A-2	51.46	2.54	2.55	10.16	10.20	1.27	1.25	--	--
A-3	51.54	2.54	2.55	20.32	20.25	1.27	1.15	--	--
Cones									
A-4	51.31	2.54	2.50	5.08	5.05	1.27	1.30	1.52	1.52
A-5	51.40	2.54	2.55	10.16	10.10	1.27	1.30	1.52	1.52
A-6	51.46	2.54	2.50	20.32	20.25	1.27	1.25	1.52	1.52
Small Hemispheres									
B-1	51.88	1.27	1.25	2.54	2.50	0.64	0.65	--	--
B-2	51.54	1.27	1.25	5.08	5.05	0.64	0.60	--	--
B-3	51.63	1.27	1.30	10.16	10.10	0.64	0.55	--	--

a) Surface A-1 L/d_o = 2

b) Surface A-2 L/d_o = 4

c) Surface A-3 L/d_o = 8

Figure 8.   Friction Factor Data from the Large Hemispherical
            Roughness Elements (d_o = 2.54 mm). Orientation:
            North - o, South - ▷; Smooth Wall Correlations — .

19

The data set for surface A-2 ($L/d_o = 4$) is presented in Figure 8b and also tabulated in Table C-4. This data set includes 52 data points taken in two replications. This test section also appears not to have a direction dependency as the north and south replications agree very well.

The data set for surface A-3 ($L/d_o = 8$) is tabulated in Table C-5 and plotted in Figure 8c. It contains 60 data points taken during four replications. Unlike the two previously discussed surfaces, the A-3 data shows a sensitivity to test section orientation. The friction factors produced by the northern replications are about 10 percent greater (at the larger Reynolds numbers) than those of the southern replications. This general trend was observed to a lesser degree for the sparsest element density ($L/d_o = 8$) of both the cones and the small hemispheres. As was shown in Figure 4, the bare wall test section did not exhibit this behavior. Unfortunately no southern replications were made using the smooth silicone surface before it was destroyed.

The silicone surfaces of all of the test sections were carefully inspected to insure that none of the individual roughness elements were obstructing a pressure tap. This particular test section did not appear to be any different from the other test sections. Although not fully explained, this phenomenon was very repeatable. The A-3 data plotted in Figure 8c is made up of two northern replications, each taken 1 month apart, and two southern replications, each also taken 1 month apart; there is no discernable difference between the northern replications and none between the southern replications.

The relative magnitudes of the friction factors for the three large hemisphere spacings can be seen in Figure 9. At the larger Reynolds numbers, the A-1 ($L/d_o = 2$) data are about 5 times greater than the smooth wall correlation values, the A-2 ($L/d_o = 4$) data about 2.7 times, and the A-3 ($L/d_o = 8$) data about 1.5 times. The A-1 surface produced the largest friction factors of this experimental study.

Figure 10 shows, for the three surfaces with large hemisphere roughness, the variation of nondimensional roughness height, k^+, with Re, where $k^+ = ku^*/\nu$, and u^* is the friction velocity, $u_{ave}\sqrt{f/2}$. This nondimensional value is a measure of the height of the element in the inner region coordinates commonly used in turbulent flow analyses.

20
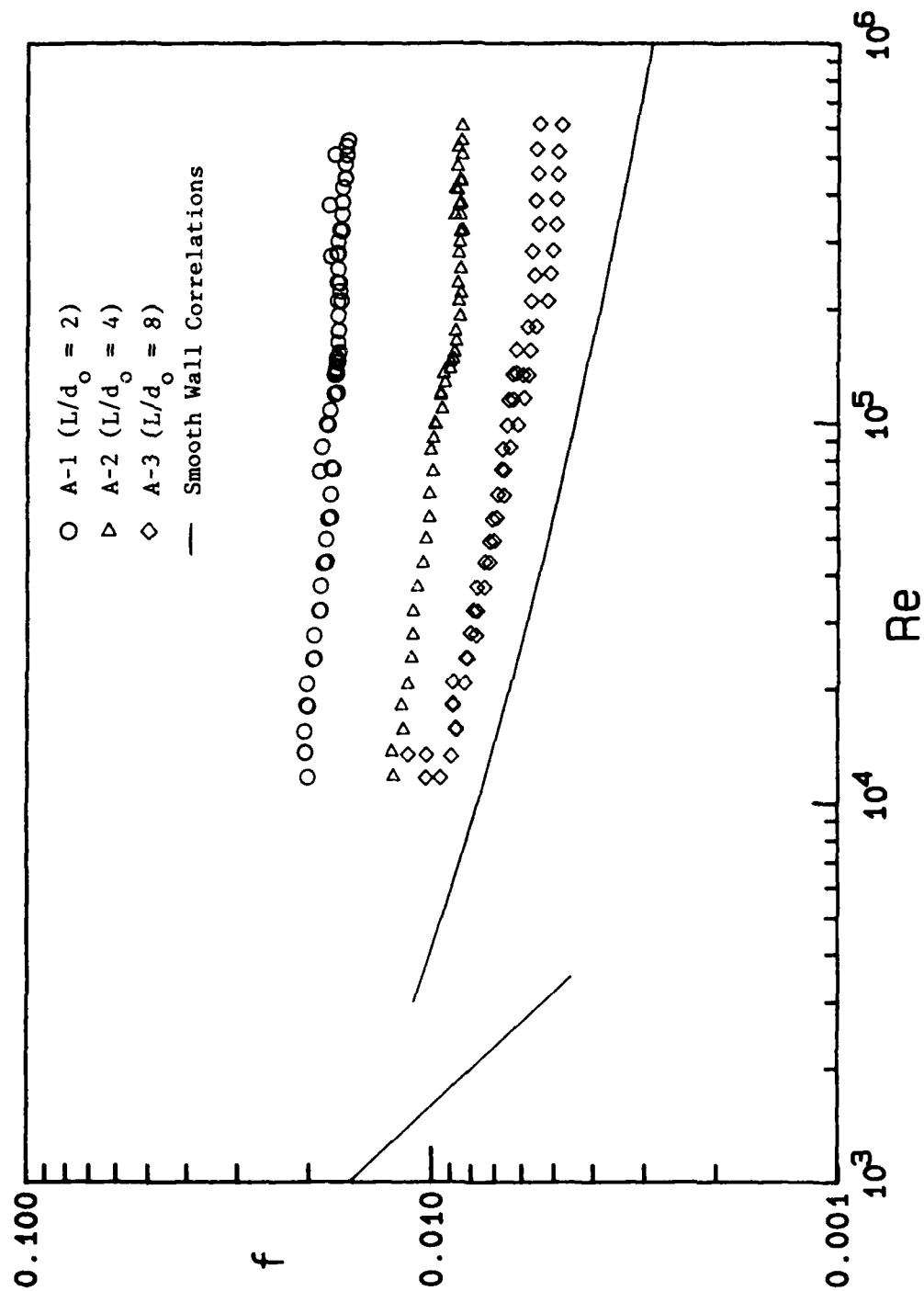
Figure 9. Comparison of Friction Factor Data from the Large Hemispherical
Roughness Elements (d_o = 2.54 mm).

21

Figure 10. Nondimensional Roughness Height versus Pipe Reynolds Number for the Three Surfaces with Large Hemispherical Roughnesses.

Figure 10 shows that for the A-3 surface k^+ varies between 20 and 750 and for the A-1 surface between 30 and 1250. The thickness of the viscous sublayer for flow over smooth surfaces is usually taken to be $y^+ = 5$ in these nondimensional inner region coordinates.

2. CONES

Three surfaces with truncated conical roughness elements were tested. Each of these surfaces was made up of truncated cones with a nominal base diameter $d_o = 2.54$-mm (0.100-inch) and a nominal height $k = 1.27$-mm (0.050-inch). The roughness elements of the three surfaces were spaced 2, 4, and 8 base diameters apart, respectively. Figure 11 contains individual plots of data sets from the three conical element surfaces with the replications for the north and south test section orientations distinguished from one another.

The data set for surface A-4 ($L/d_o = 2$) is presented in Table C-6 and in Figure 11a. This data set includes 32 data points taken during two replications. The north and south replications are in very good agreement indicating that this test section did not have a sensitivity to orientation.

The data set for surface A-5 ($L/d_o = 4$) is tabulated in Table C-7 and plotted in Figure 11b. It contains 30 data points taken in two replications. The data from this test section did not exhibit any direction dependency.

The data set for surface A-6 ($L/d_o = 8$) is presented in Table C-8 and plotted in Figure 11c. This data set includes 33 data points taken during two replications. Orientation effects, though present, are much smaller in magnitude than those demonstrated by the large hemispherical roughnesses.

The relative magnitude of the friction factors for the three conical spacings are plotted in Figure 12. At the larger Reynolds numbers, the A-4 ($L/d_o = 2$) data are approximately 5 times greater than the smooth wall correlation values, the A-5 ($L/d_o = 4$) data about 2.6 times, and the A-3 ($L/d_o = 8$) data about 1.6 times.

Figure 13 shows the nondimensional roughness height, k^+, versus pipe Reynolds number. This figure shows that for the A-6 surface, k^+ varies between 20 and 725 and for the A-4 surface between 30 and 1200.

23
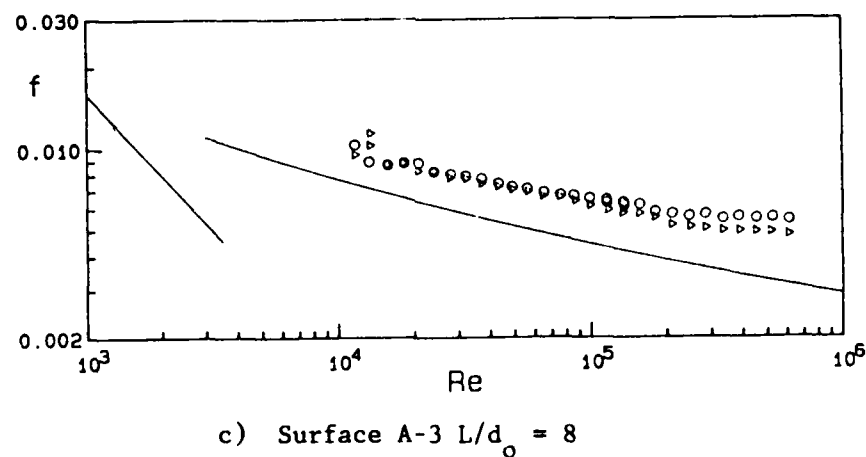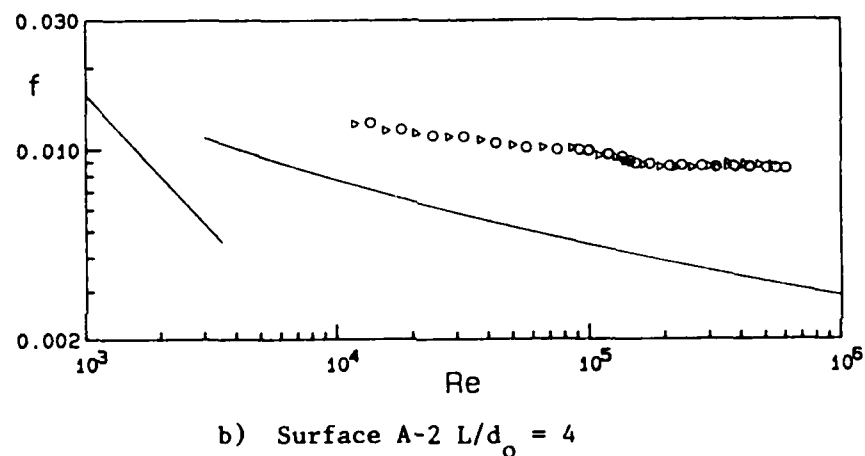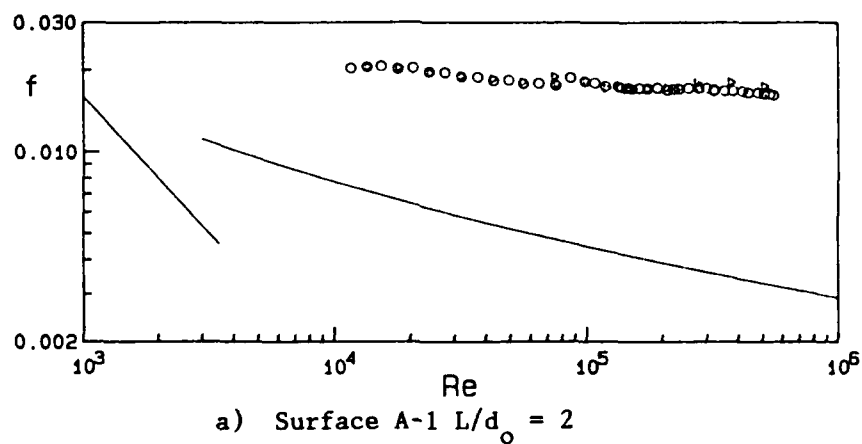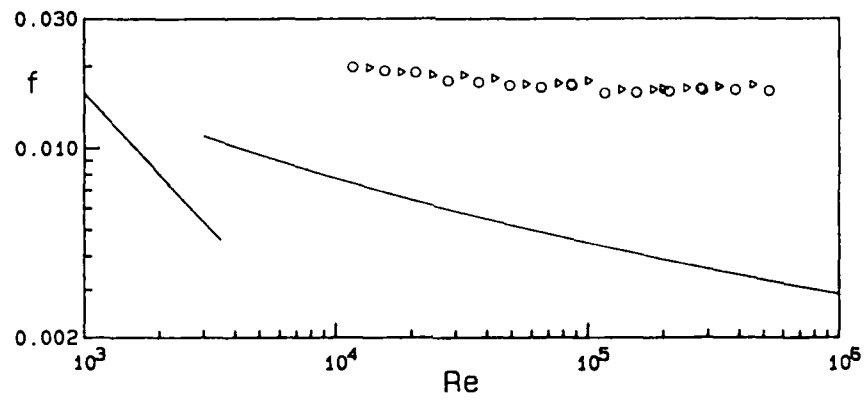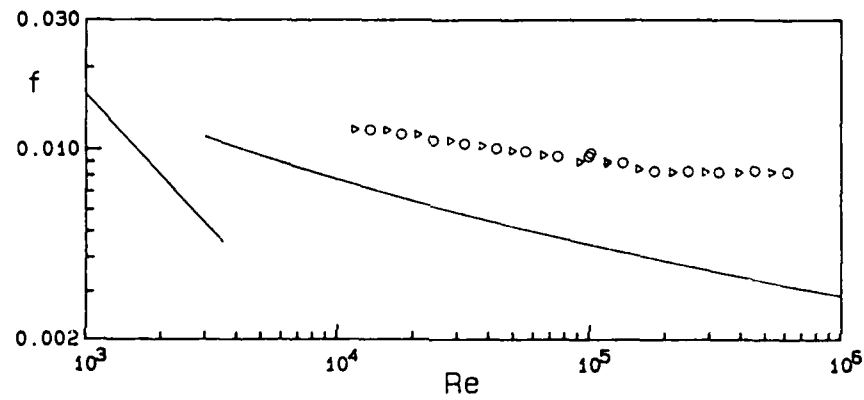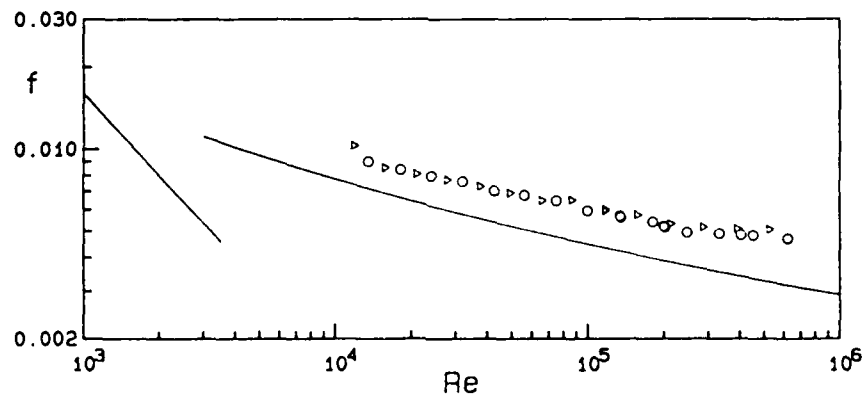
Figure 11. Friction Factor Data from the Conical Roughness Elements (d_o = 2.54 mm). Orientation: North - o, South - ▷; Smooth Wall Correlations —.

24
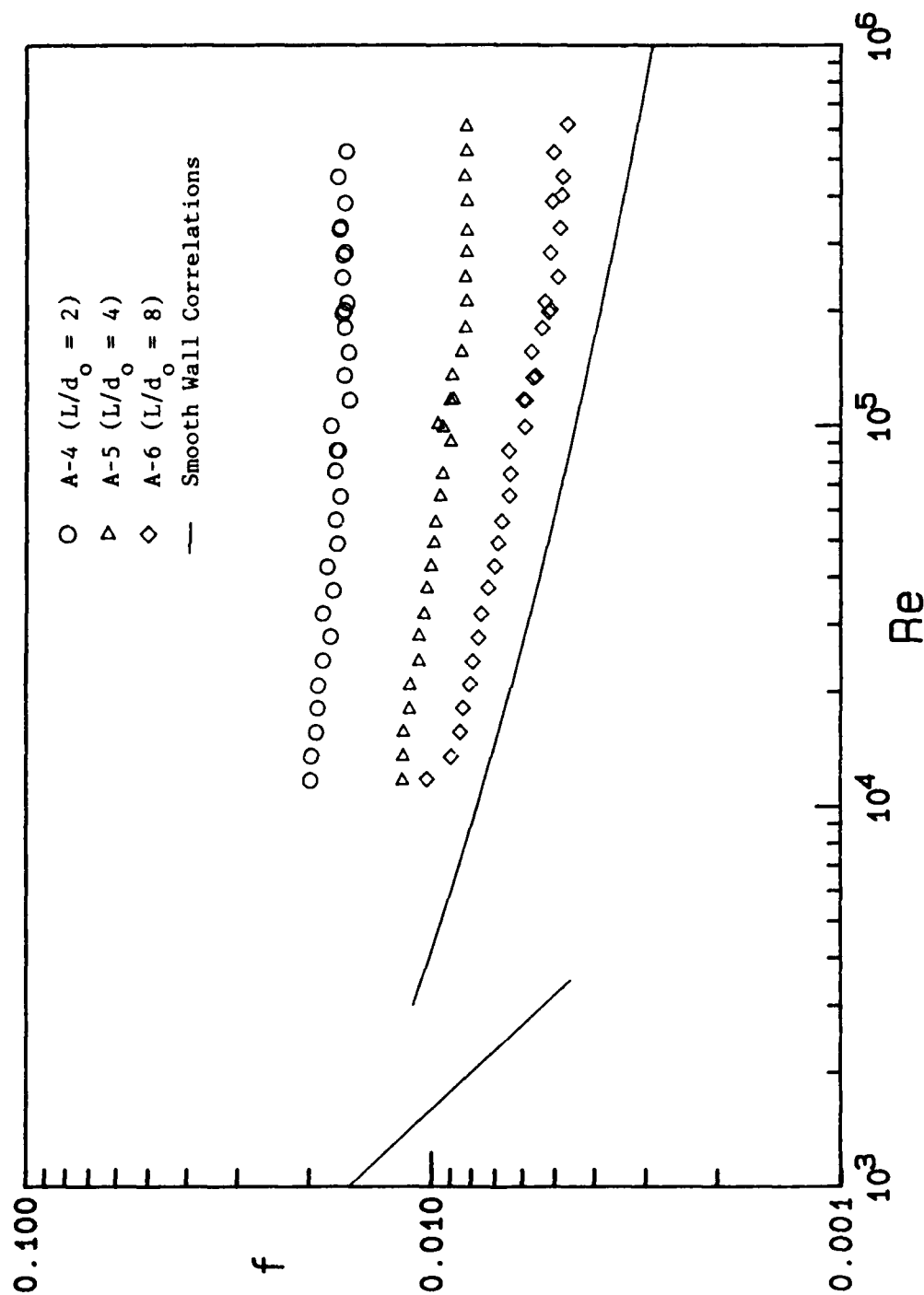
Figure 12. Comparison of Friction Factor Data from the Conical Roughness Elements (d_o = 2.54 mm).

3. SMALL HEMISPHERES

Three surfaces with small hemispherical roughness elements were tested. Each of these surfaces was made up of hemispheres with a nominal base diameter $d_o = 1.27$ mm (0.050 inch) and a nominal height $k = 0.64$ mm (0.025 inch). The roughness elements of the three surfaces were spaced 2, 4, and 8 base diameters apart, respectively. Figure 14 contains individual plots of data sets from the three small hemispherical element surfaces with the replications for the north and south test section orientations distinguished from one another.

The data set for surface B-1 ($L/d_o = 2$) is given in Table C-9 and is plotted in Figure 14a. This data set includes 29 data points taken during two replications. The data from this test section do not show any sensitivity to orientation.

The data set for surface B-2 ($L/d_o = 4$) is tabulated in Table C-10 and plotted in Figure 14b. It contains 31 data points taken in two replications. The north and south replications blend very well; and so, this test section did not have any orientation dependency.

The data set for surface B-3 ($L/d_o = 8$) is given in Table C-11 and is plotted in Figure 14c. There are 30 data points taken during two replications included in this data set. This surface does however exhibit a difference between the northern and southern replications, as was the case with the two other $L/d_o = 8$ surfaces (A-3 and A-6). The northern replication produced friction factors approximately 10 percent greater (at the higher Reynolds numbers) than those of the southern replication.

The relative magnitude of the friction factors for the three small hemisphere spacings can be seen in Figure 15. At the larger Reynolds numbers, the B-1 ($L/d_o = 2$) data are about 4.5 times greater than the smooth wall correlation values, the B-2 ($L/d_o = 4$) data about 2.3 times, and the B-3 ($L/d_o = 8$) data about 1.4 times. The B-3 surface produced the smallest friction factors of the rough surfaces tested in this experimental study.
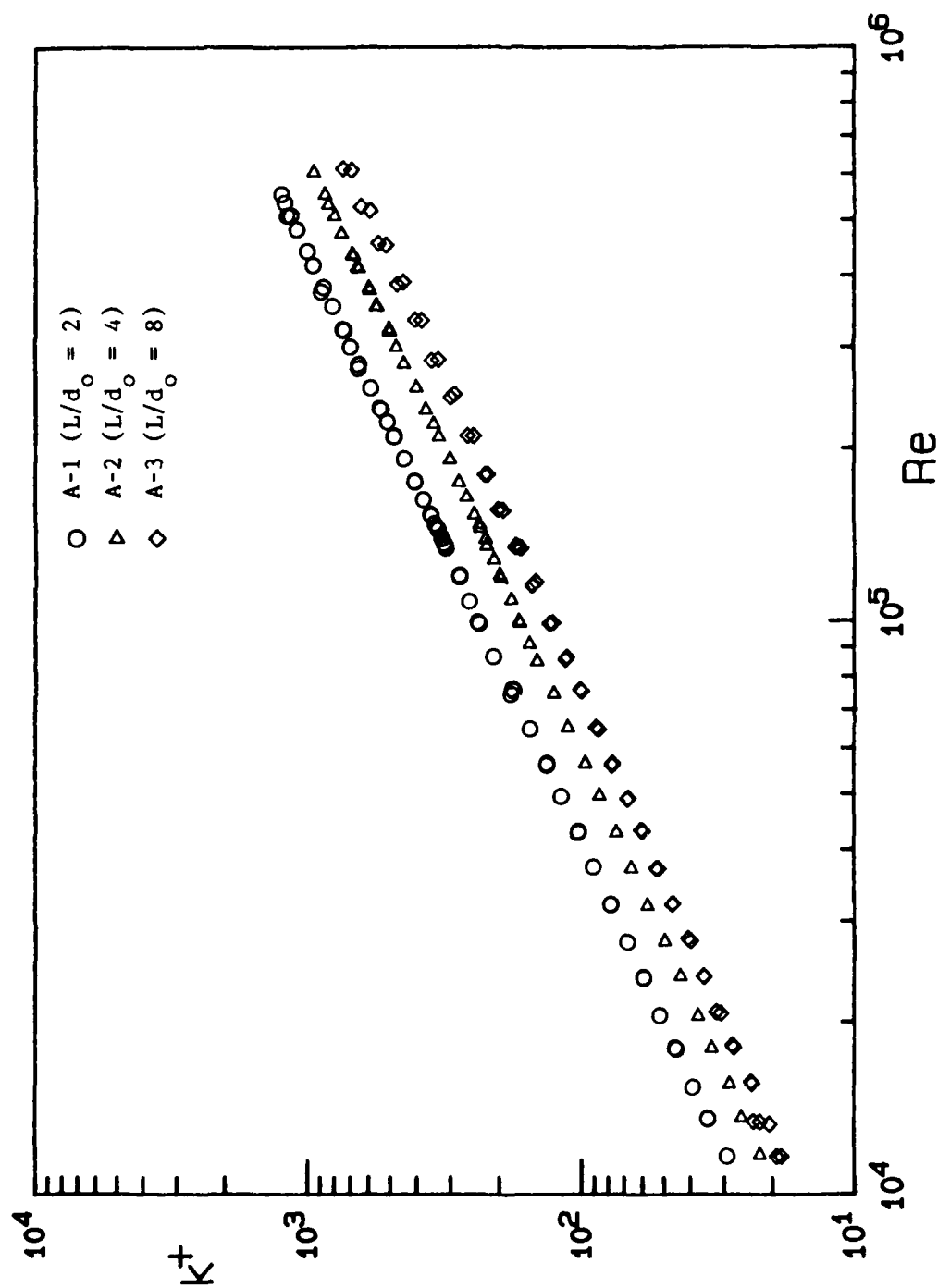
26
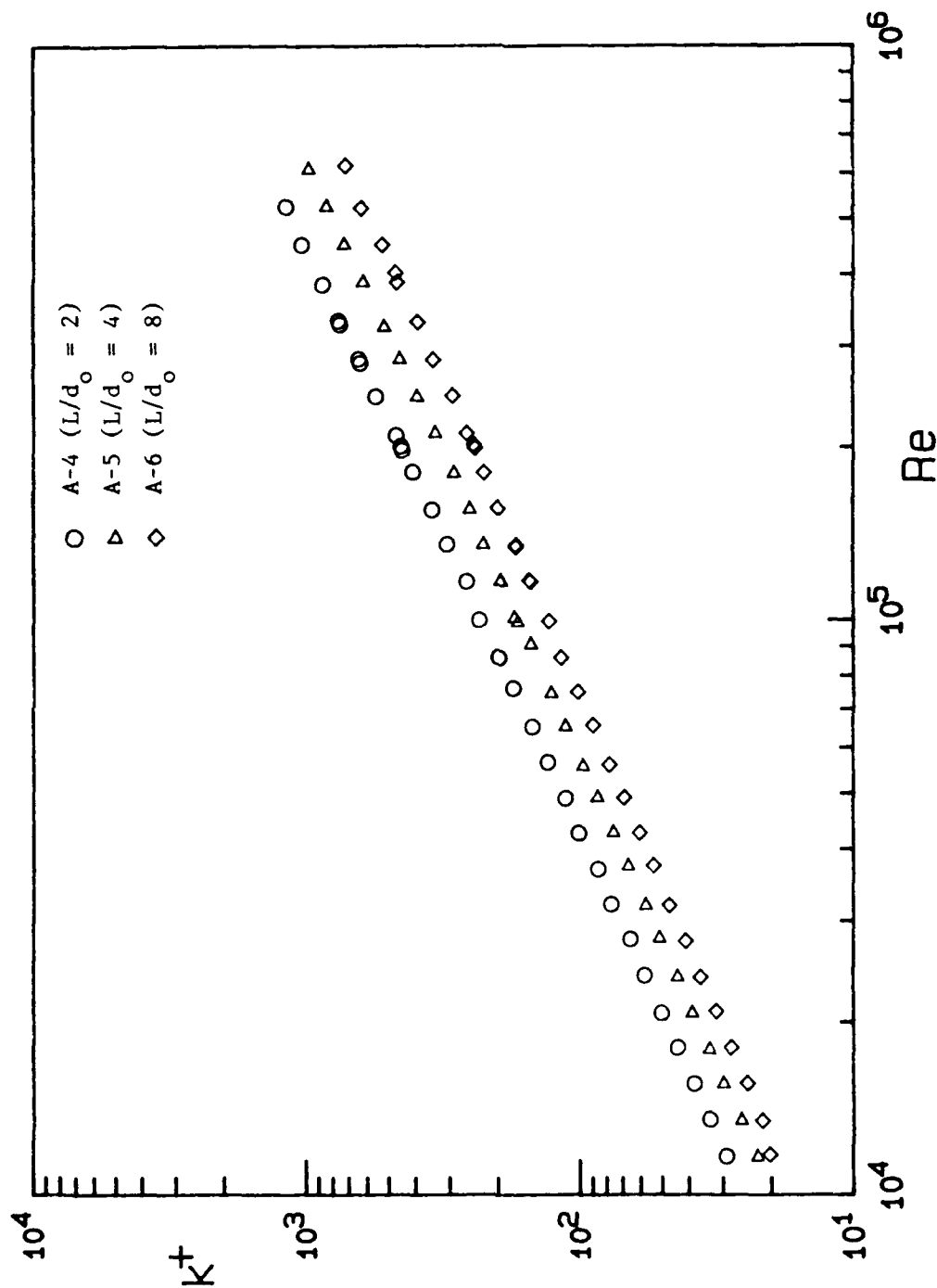
Figure 13. Nondimensional Roughness Height versus Pipe Reynolds Number for the Three Surfaces with Conical Roughnesses.

27
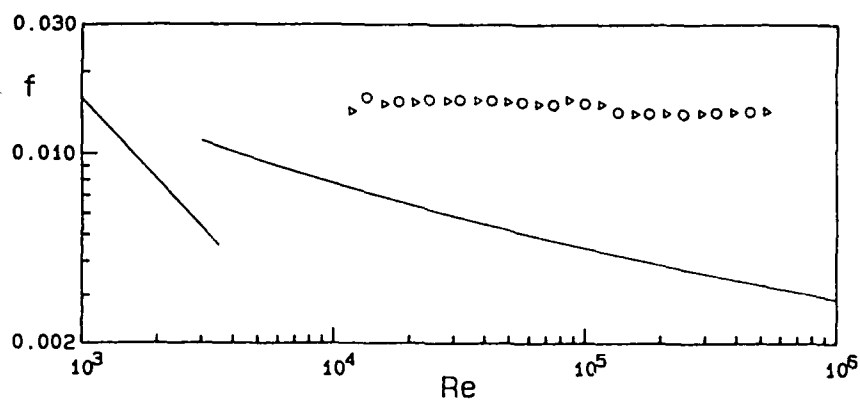
a) B-1 (L/d$_o$ = 2)
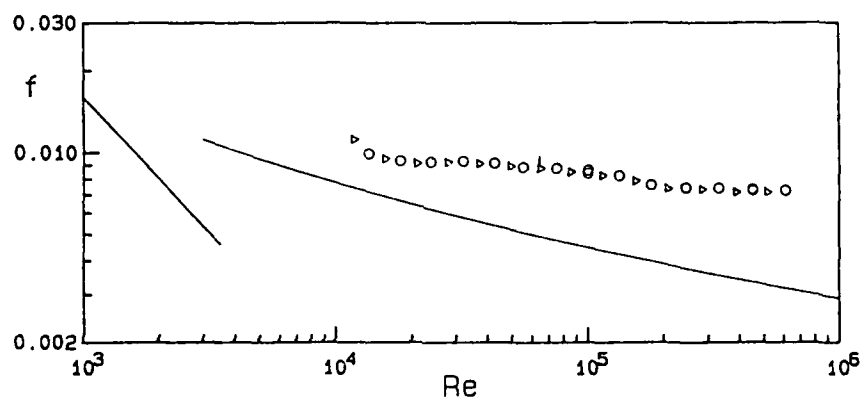
b) B-2 (L/d$_o$ = 4)
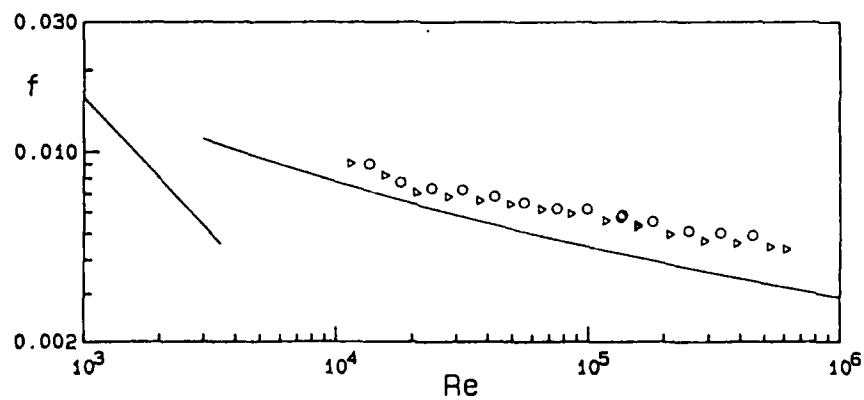
c) B-3 (L/d$_o$ = 8)

Figure 14.   Friction Factor Data from the Small Hemisphere
Roughness Elements (d$_o$ = 1.27 mm).   Orientation:
North - o, South - ▷; Smooth Wall Correlation —.

28
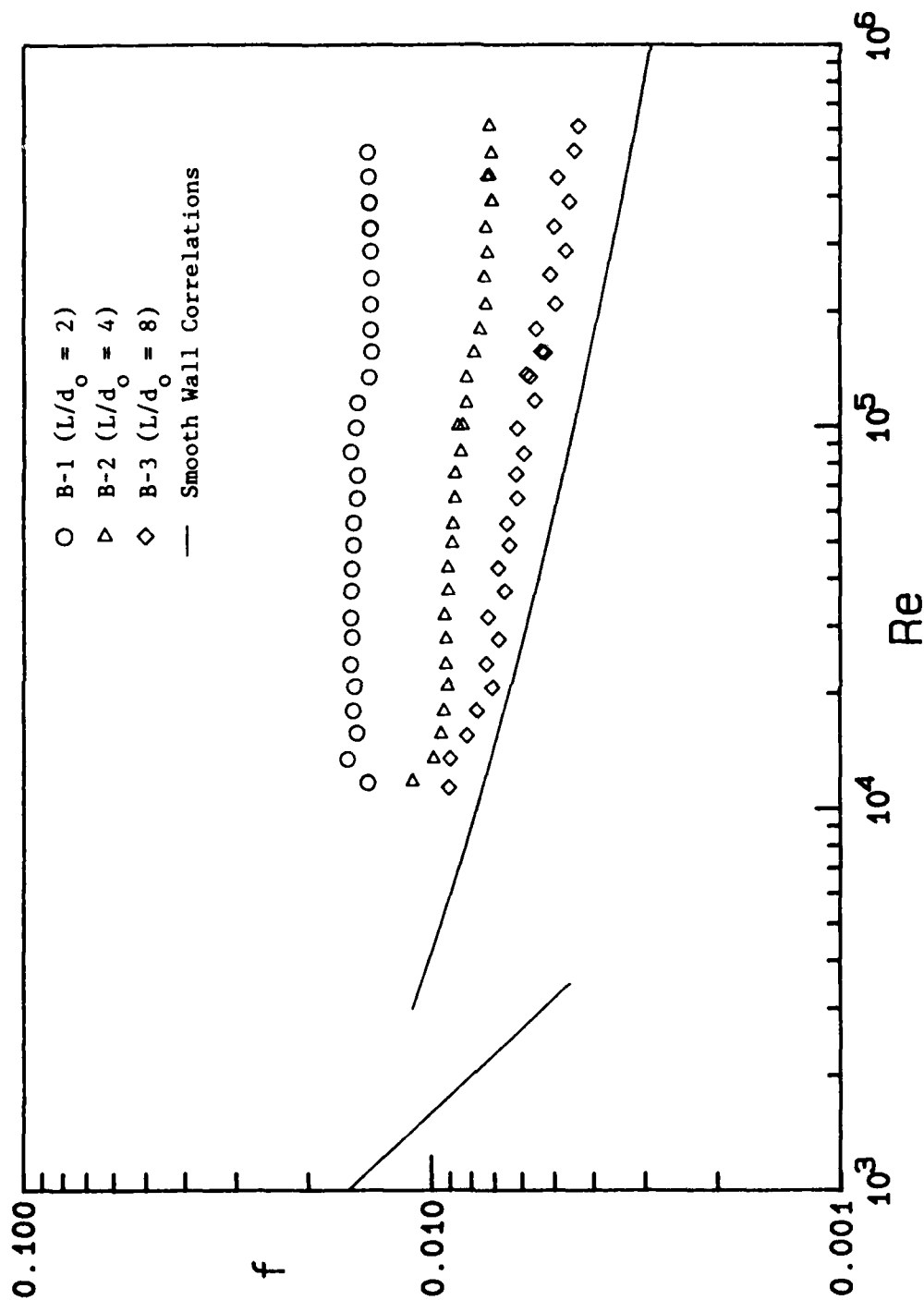
Figure 15. Comparison of Friction Factor Data from the Small Hemispherical Roughness Elements (d_o = 1.27 mm).

29

Figure 16 shows a graph of nondimensional height k^+, versus pipe Reynolds number. From the figure it is seen that for the B-3 surface k^+ varies between 10 and 300 and for the B-1 surface between 15 and 575.

4. FURTHER COMPARISONS

It is interesting to make some further comparisons between the surfaces with different geometries (large hemispheres versus cones, large versus small hemispheres, etc.).

The friction factors for the surfaces with large hemispherical elements and for the surfaces with conical elements are plotted in Figure 17 for the roughness spacings of 2, 4, and 8 base diameters. The hemispherical elements produced slightly larger friction factors, though at the higher Reynolds numbers the values associated with each surface are essentially the same within the data uncertainty. This result is somewhat surprising to the authors. While the large hemispheres and the cones have essentially the same height and aspect ratio (d_o/k), their projected areas differ by 35 percent. Figure 18 shows a comparison of a large hemispherical element and a conical element. The projected area for the large hemisphere is 2.50-mm^2 (0.0039-inch^2) and that for the cone is 1.85-mm^2 (0.0029-inch^2).

The friction factors for the large and small hemispherical roughness elements for the three spacings of 2, 4, and 8 base diameters are compared in Figure 19. The $L/d_o = 2$ data for the large hemispheres are about 15 percent greater than the small hemisphere values, and the $L/d_o = 4$ data about 20 percent greater. The wide data scatter at the higher Reynolds numbers exhibited by the two $L/d_o = 8$ surfaces is due to the difference between the northern and southern replications of both surfaces, as discussed above.

It is also interesting to examine the influence of roughness size on the friction factor without the superimposed effects of the element density (the number of elements per unit area). This is shown in Figure 20 where the friction factors for the $L/d_o = 2$ large hemispherical surface are compared with those of the $L/d_o = 4$ small hemispherical surface. These two surfaces have the same element density since the roughness elements have different base diameters. The friction factors

30
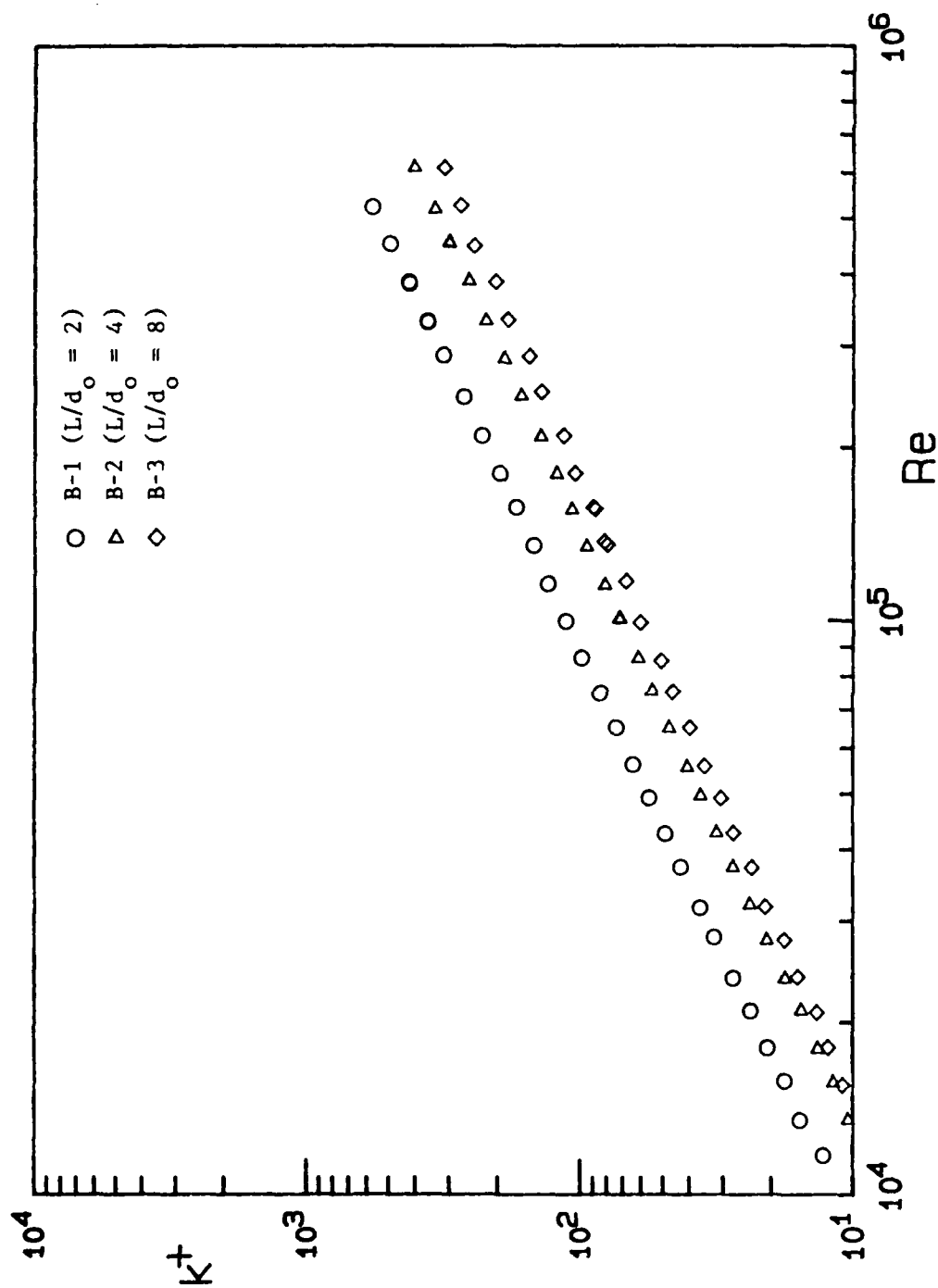
Figure 16: Nondimensional Roughness Height versus Pipe Reynolds Number for the Three Surfaces with Small Hemispherical Roughnesses.

31
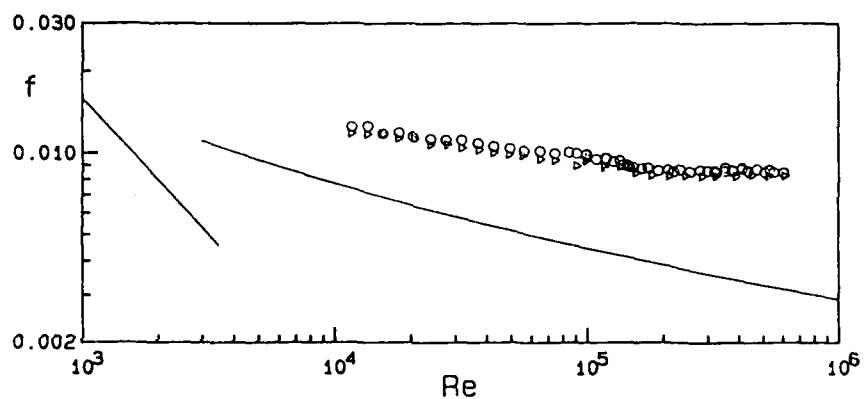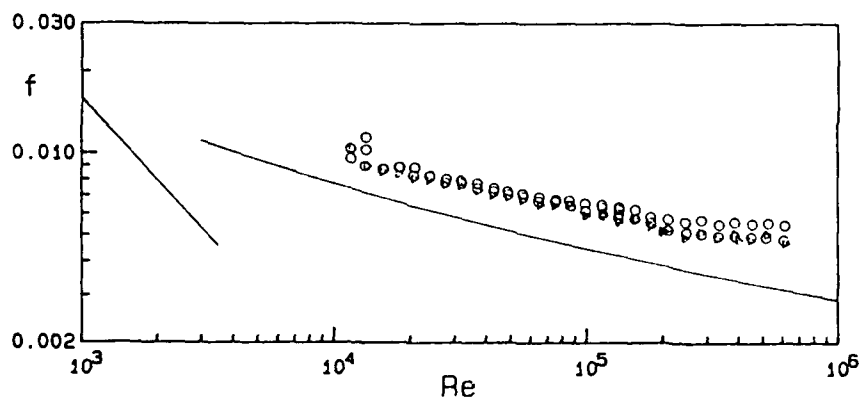
Figure 17. Comparison of the Data from the Surfaces with Large Hemispheres and Cones for the Same Value of L/d_o. Large Hemispheres - o, Cones - ▷; Smooth Wall Correlations —.

32
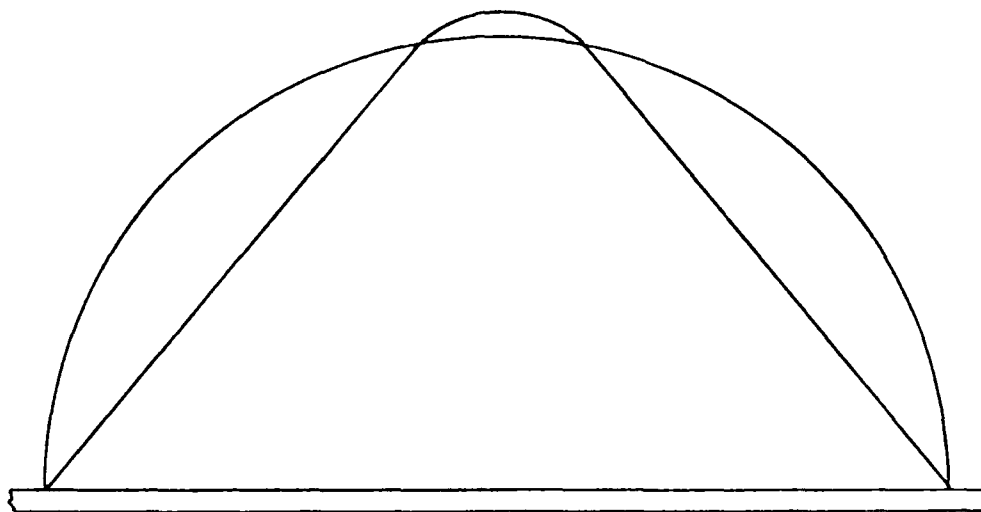
Figure 18. Comparison of the Projected Area of a Large
Hemisphere and a Conical Roughness Element.
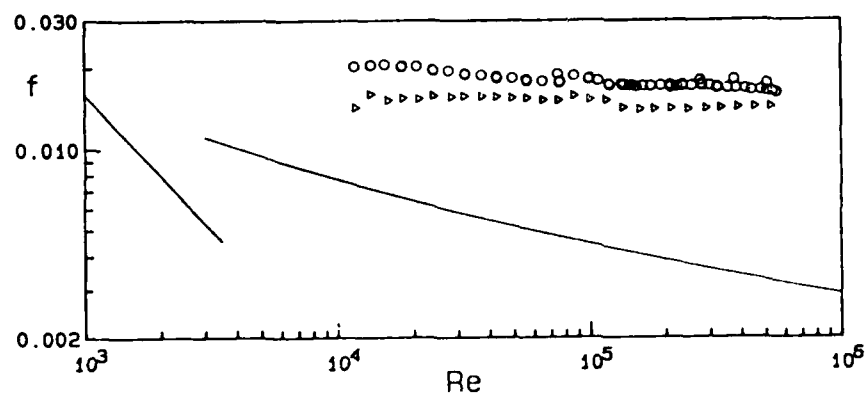
a) $L/d_o = 2$
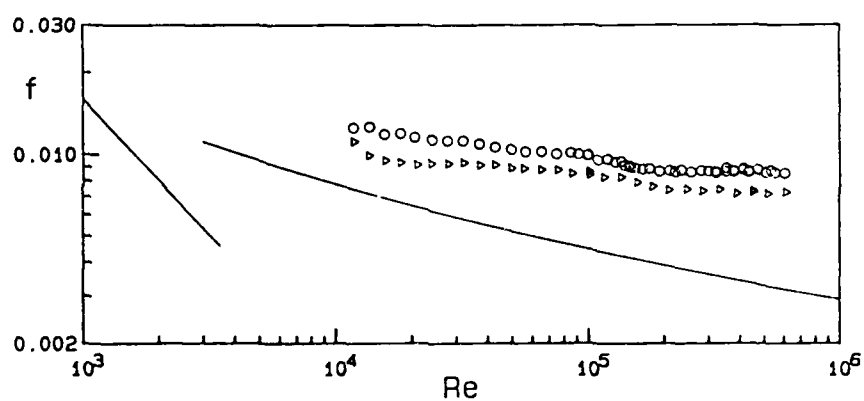
b) $L/d_o = 4$
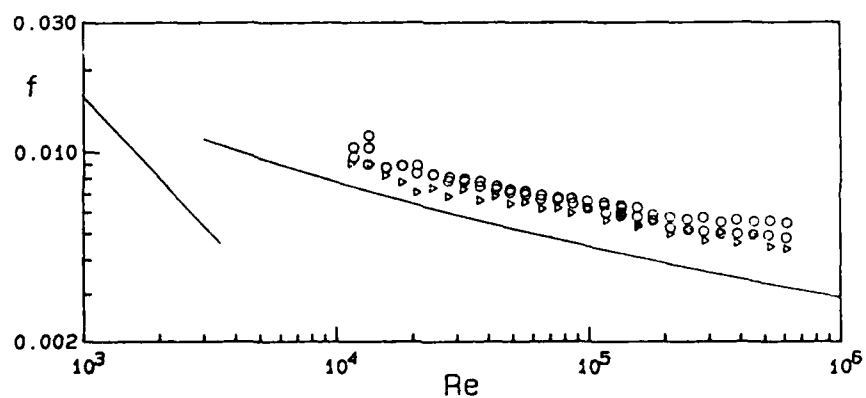
c) $L/d_o = 8$

Figure 19. Comparison of the Data from the Surfaces with Large Hemispheres and Small Hemispheres for the Same Value of L/d_o. Large Hemispheres - o, Small Hemispheres ▷; Smooth Wall Correlations —.

34

for the large hemispheres are about 2.3 times greater than those for the small hemispheres. This effect is also shown in the figure for the $L/d_o = 4$ large hemisphere data and the $L/d_o = 8$ small hemisphere data. In this instance the large hemisphere friction factor data are about 2 times greater than the small hemisphere data.

5.   THE DISCRETE ELEMENT MODEL

The discrete element model presented in this work is formulated for roughness elements with three-dimensional shapes (as opposed to transverse ribs, for example) for which the element cross section can be approximated as circular at every height, y. The physical effects of roughness on the flow field are modeled by considering the blockage effect of the roughness elements and the drag forces which the roughness elements exert on the fluid. In the following, attention is restricted to roughness elements of uniform shape and spacing. The case of axisymmetric fully developed internal flow in a pipe of radius R as presented below is a simplified extension of the equations for steady (Reynolds-averaged), two-dimensional turbulent boundary layer flow over a rough surface as derived by Taylor, Coleman, and Hodge (1984, 1985). The momentum equation is

$$0 = \frac{\mu}{R-y} \frac{d}{dy} \left[r\beta_y \left(1 + \frac{\mu_T}{\mu}\right) \frac{du}{dy} \right] - \beta_x \frac{dP}{dx} - \frac{1}{2} \rho C_D \frac{u^2 d(y)}{(R-y)L^2/R} \quad , \qquad (6)$$

where $\beta_x = \beta_y = 1 - (\pi d^2(y)/4L^2)$.

The parameters β_x, β_y, and d(y) were determined solely from the roughness element geometry given in Table 1 with no empirical input required. For the uniform arrays previously discussed the cross-sectional diameter, d(y), is the same for all of the elements at a given y-location.

As in Taylor, et al. (1984, 1985), the "wall shear stress" is defined as the sum of the shear and drag forces on the wall in the mean flow direction divided by the plan area of the wall. The corresponding friction factor can then be written as

35
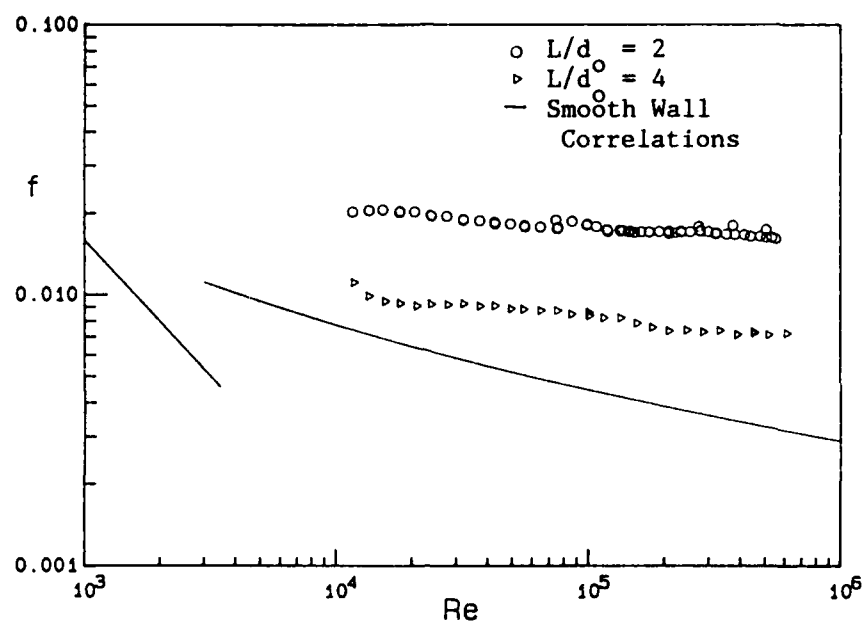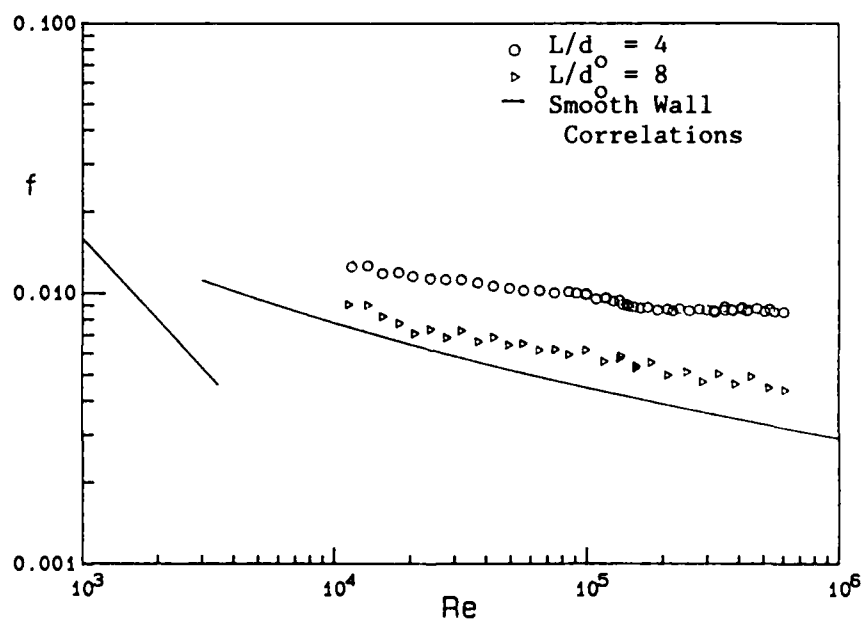
Figure 20.   Comparison of Fraction Factor Data from the
Large and Small Hemispherical Roughness for
the Same Element Densities. d_o = 2.54 mm - o,
d_o = 1.27 mm - ▷.

36

$$f = \frac{(\beta_y)_w \, \mu \, \frac{du}{dy}\Big|_w + \frac{1}{2}\int_0^k \frac{1}{(R-y)L^2/R}\,(\rho d C_D u^2)\,dy}{\frac{1}{2}\,\rho u_{ave}^2} \quad . \tag{7}$$

To solve equation (6) an eddy viscosity turbulence model for μ_T and a roughness model for C_D were required. Turbulence closure was achieved using the Prandtl mixing length formulation with van Driest damping as suggested by Kays and Crawford (1980). That is, near the wall

$$\mu_T = \rho \ell_m^2 \left|\frac{du}{dy}\right| \tag{8a}$$

where

$$\ell_m = 0.40y\left[1 - \exp(-y^+/26)\right]$$

and

$$\mu_T = 0.40 \, \mu R^+/6 \tag{8b}$$

in the core region. The boundary between expressions 8a and 8b is taken to be where they give the same value of μ_T. This model was not modified to include roughness effects since the physical effects of the roughness on the flow are included explicitly in the differential equations.

Taylor, et al. (1984, 1985) chose to formulate the C_D model as a function of the local element Reynolds number

$$Re_d = \frac{u(y)d(y)}{\nu} \tag{9}$$

which includes roughness element size and shape information through $d(y)$. This model is given by

37

$$\log C_D = -0.125 \log(Re_d) + 0.375 \quad ; \; Re_d < 6 \times 10^4$$
$$C_D = 0.6 \qquad\qquad\qquad\qquad ; \; Re_d \geq 6 \times 10^4 \quad . \qquad (10)$$

For the conditions covered in this experimental program, the largest predicted value of Re_d was about 17,000 as calculated for the densest spacing of the large hemispheres.

With the closure models formulated, equation (6) was solved using an iterative, implicit finite difference technique. Details of this procedure are presented by Taylor, et al. (1984).

6. DISCRETE ELEMENT MODEL PREDICTIONS

The following is a comparison between the experimental friction factor data generated at MSU and the friction factors calculated using the discrete element model of Taylor, et al. (1984, 1985). We should emphasize that no empirical information from data taken using the rough surfaces in this program was input into the discrete element model. Rather, the only information required for these discrete element predictions was the measured roughness geometry of the surfaces (presented in Table 1), the pipe diameter, the fluid properties, and the water flowrate.

The comparison of the predictions with the friction fa tr data of the large hemispherical roughnesses is shown in Figure 21. Inspection of the figure shows very good agreement for the three element spacings. The predicted values of friction factor are slightly high over most of the range of data for surfaces A-1 and A-2 (L/d_o = 2 and 4, respectively). The measurement uncertainty of $\pm$ 4.7 percent associated with the experimental friction factors is approximately represented by the size of the data point symbols in the figures presented in this work. This reference shows that the maximum disagreement between the predicted and measured friction factors is 10 percent. The prediction of the friction factor data for surface A-1 trails off slightly at the very low range of reported Reynolds numbers. This was typical behavior of the predictions for the densest element spacing, $L = 2d_o$, of the surfaces presented in this work.

38
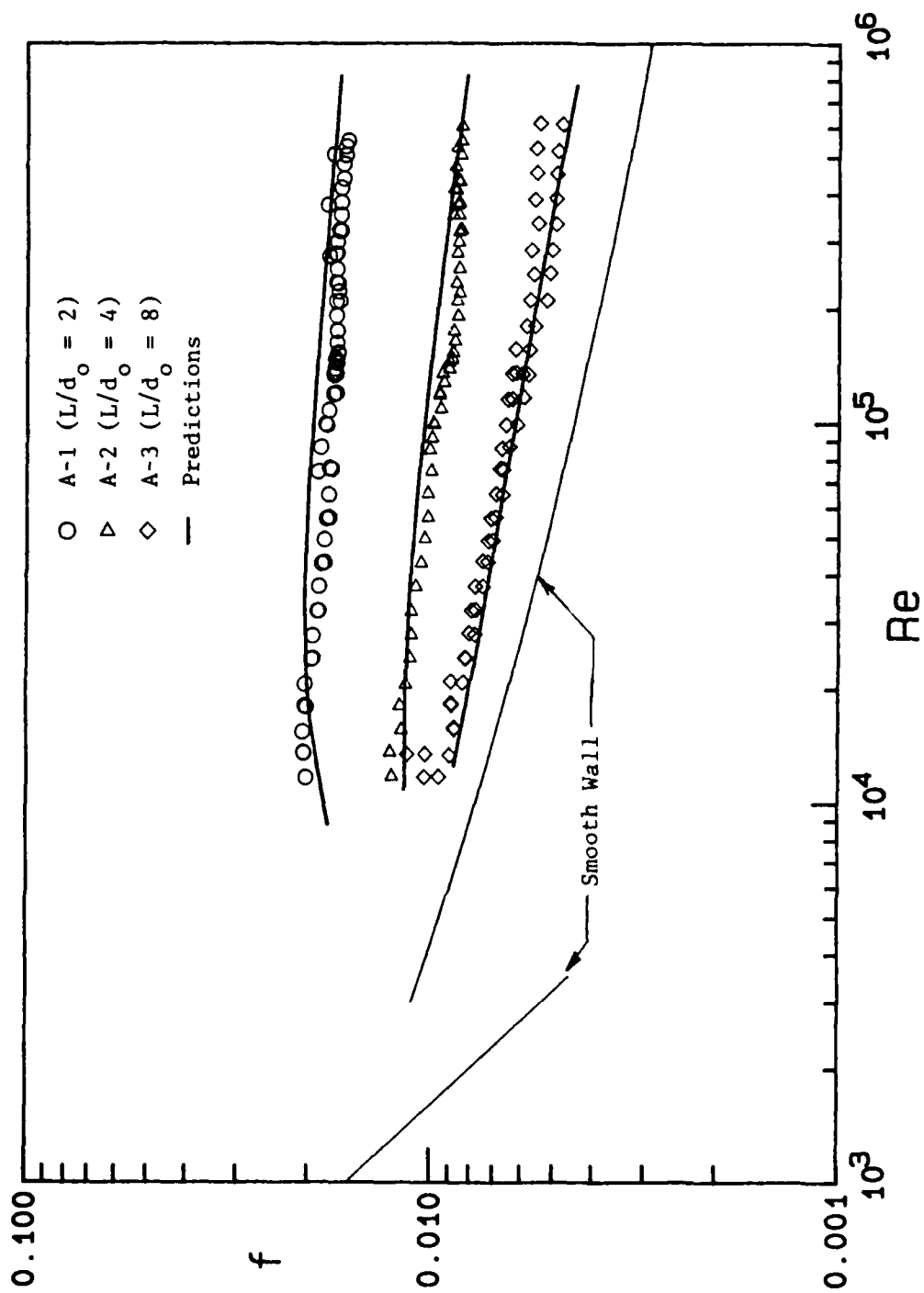
Figure 21. Comparison of the Large Hemispherical Data with Predictions.

39

Figure 22 shows the comparison between the predicted and the measured friction factor data of the conical roughness elements. The agreement is excellent. The predicted trend for surface A-4 ($L/d_o = 2$) tends to trail off at the low end of reported Reynolds numbers.

The friction factor data from the small hemispherical elements is compared to the discrete element predictions in Figure 23. Overall the agreement is again excellent. The trend predicted for surface B-1 ($L/d_o = 2$) at the lowest Reynolds numbers behaves like that for surfaces A-1 and A-4 shown in Figures 21 and 22, respectively.

Figure 24 shows predictions and friction factor data for the A-2 (large hemisphere, $L/d_o = 4$) and the A-5 (cone, $L/d_o = 4$) surfaces. This comparison is made as a follow-on to the surprising observation in Figure 17 that the friction factor data for the hemisphere roughness and the cone roughness were essentially the same. Inspection of Figure 24 reveals that the cone predictions are somewhat lower than the hemisphere predictions; however, the difference between the predictions is of the order of the uncertainty of the data.

7. TRANSITIONALLY AND FULLY ROUGH FLOWS

For pipe flow the traditional definition of a fully rough flow is one for which the friction factor is no longer a function of Reynolds number, but is only a function of the roughness. For boundary layer flows and other developing flows, this definition is no longer applicable and some other character of the roughness must be used to delimit aerodynamically smooth, transitionally rough, and fully rough flows.

In the past, the value of the so-called roughness Reynolds number,

$$Re_{k_s} = u^* k_s / \nu \tag{11}$$

was used. However the equivalent sandgrain roughness, k_s, is a somewhat contrived single-length-scale roughness discriptor, which has been abandoned in the discrete element approach.

An alternate candidate suggested by Taylor, et al. (1985) is

$$R_\tau = \tau_R / \tau_T \quad , \tag{12}$$

40
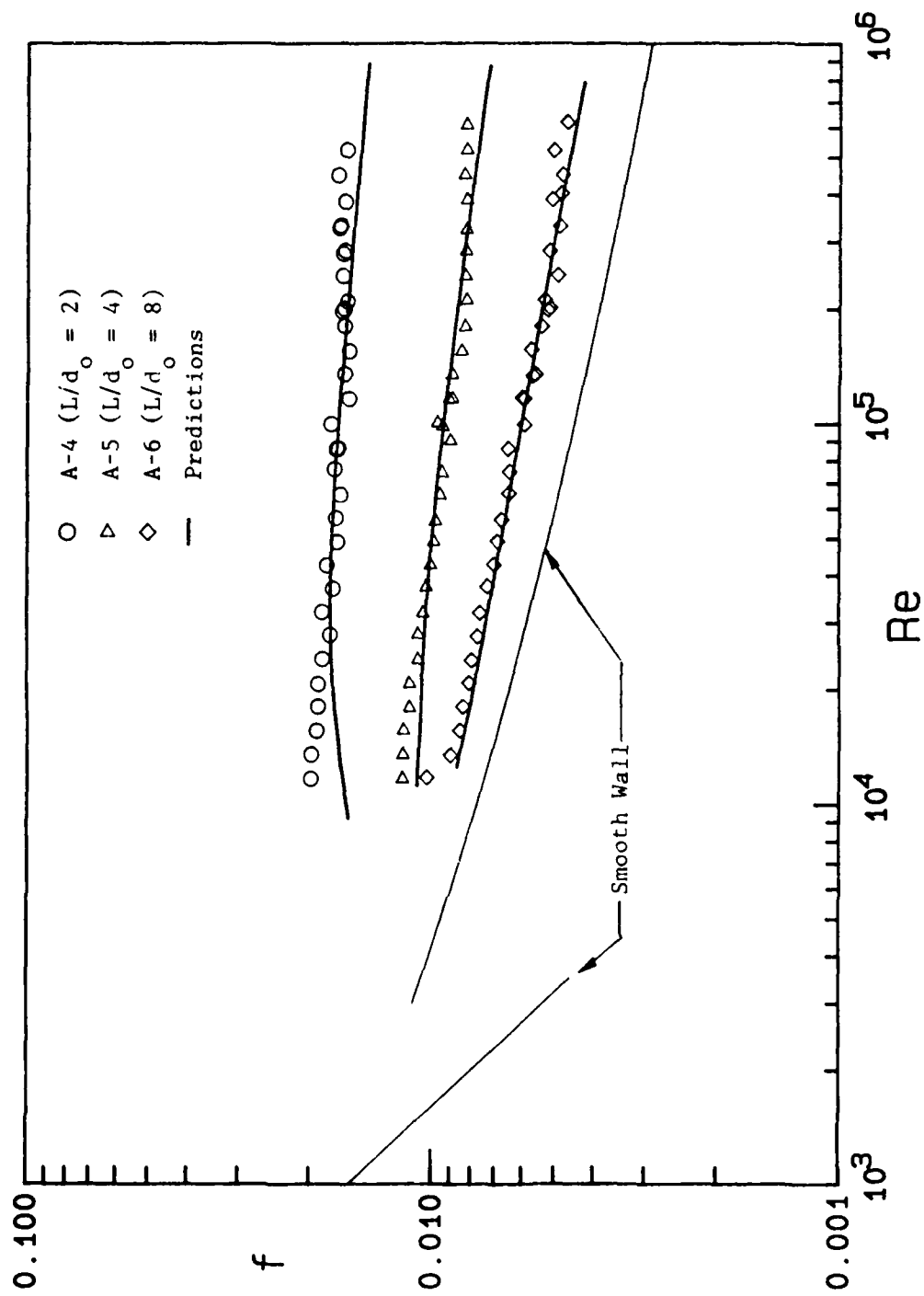
Figure 22. Comparison of the Conical Data with Predictions.

41
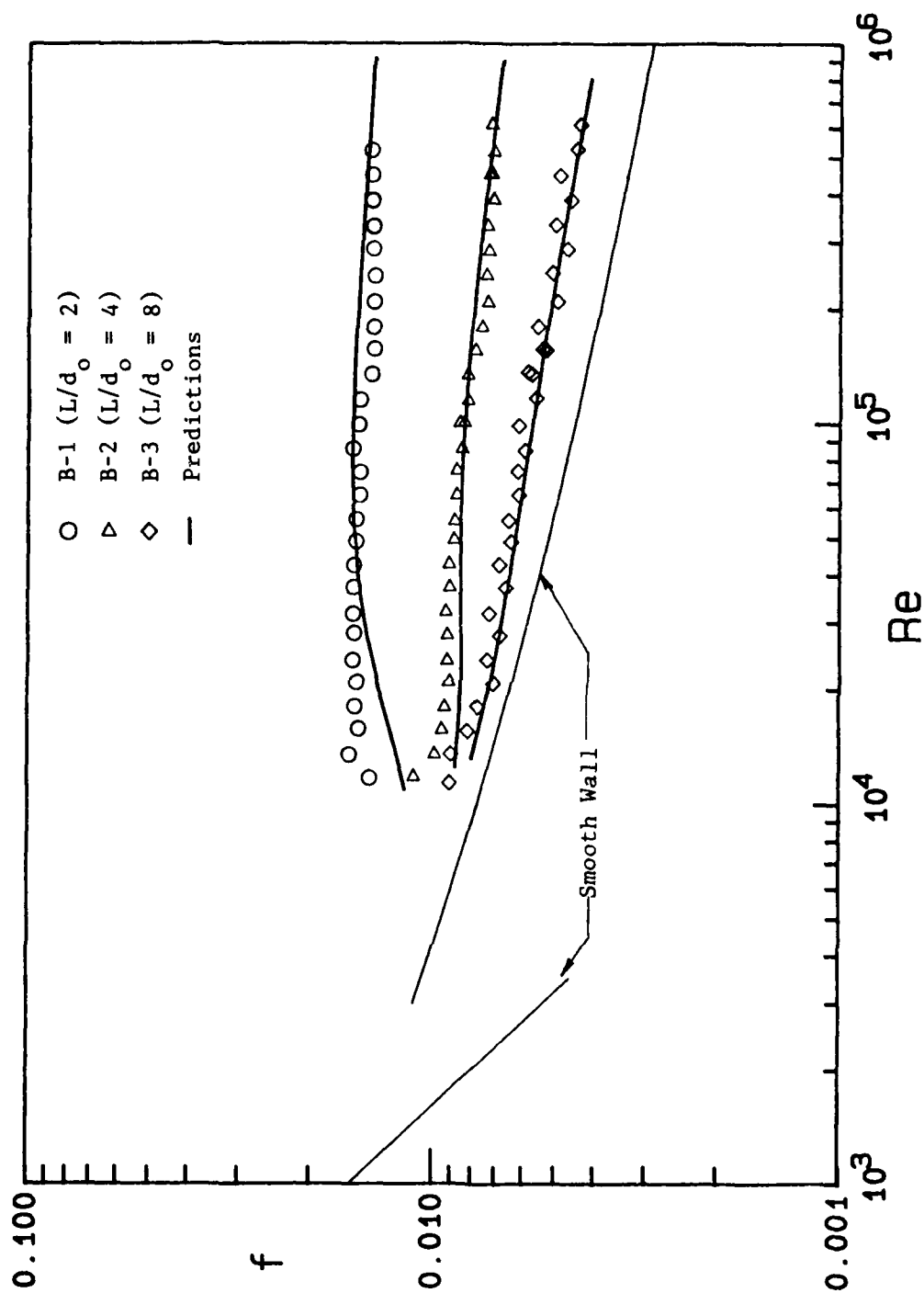
Figure 23. Comparison of the Small Hemispherical Data with Predictions.

42
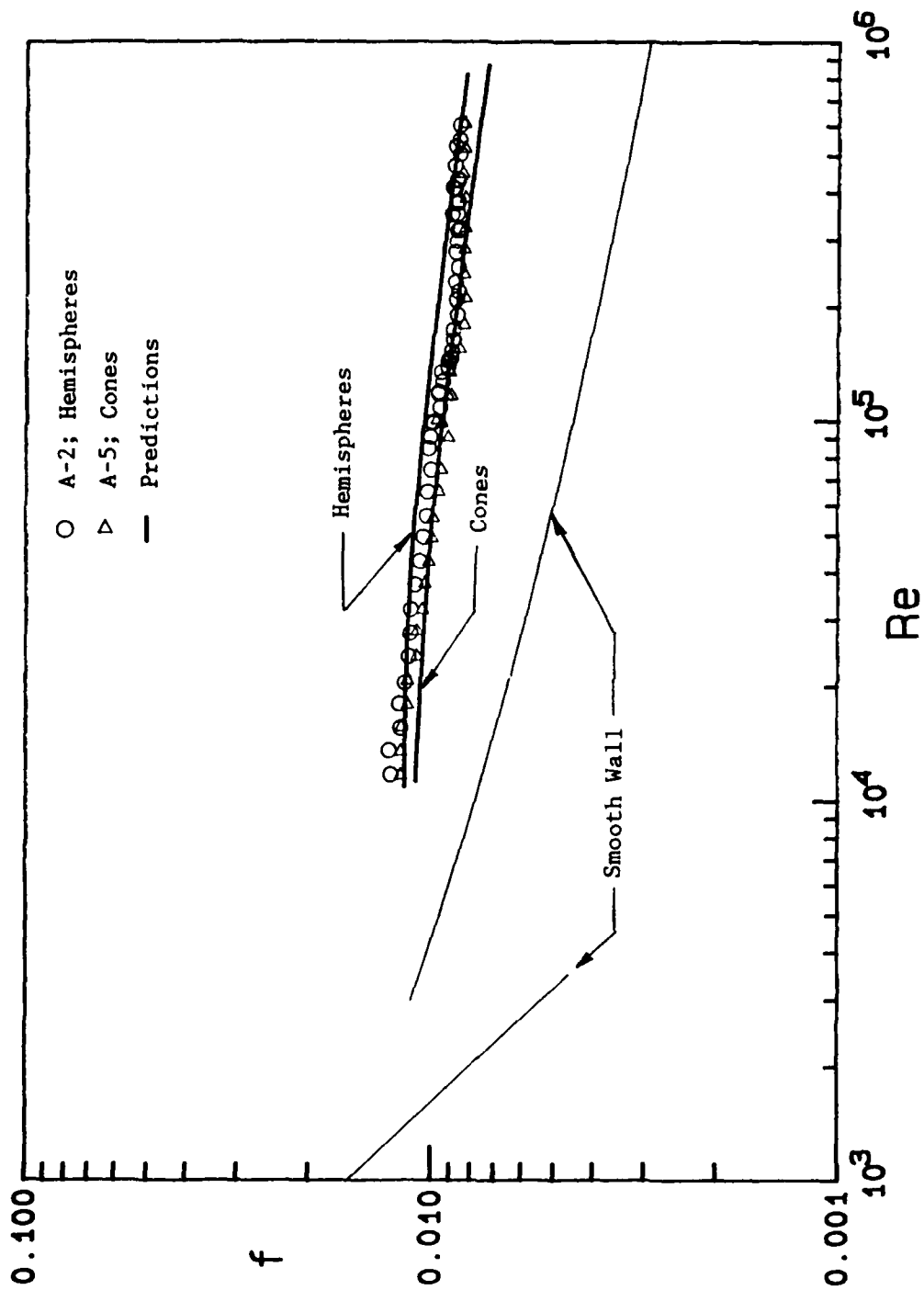
Figure 24. Comparison of the Predictions for the Cones and Large Hemispheres at $L/d_o = 4$.

43

the ratio of the apparent wall shear stress due to form drag on the
roughness elements to the total wall shear stress. They proposed,
based on data available at the time, that

$$R_\tau < 0.05 - 0.10, \text{ aerodynamically smooth}$$
$$0.05 - 0.10 < R_\tau < 0.80 - 0.90, \text{ transitionally rough}$$
$$R_\tau > 0.80 - 0.90, \text{ fully rough.}$$

The values of R_τ calculated from the predictions presented earlier
are shown in Figures 25, 26, and 27 for the surfaces with large
hemispheres, cones and small hemispheres, respectively. Based on these
calculations and the friction factor data presented earlier, the
authors suggest that a value of $R_\tau \approx 0.60$ might be considered an
appropriate boundary between the transitionally and fully rough
regimes.
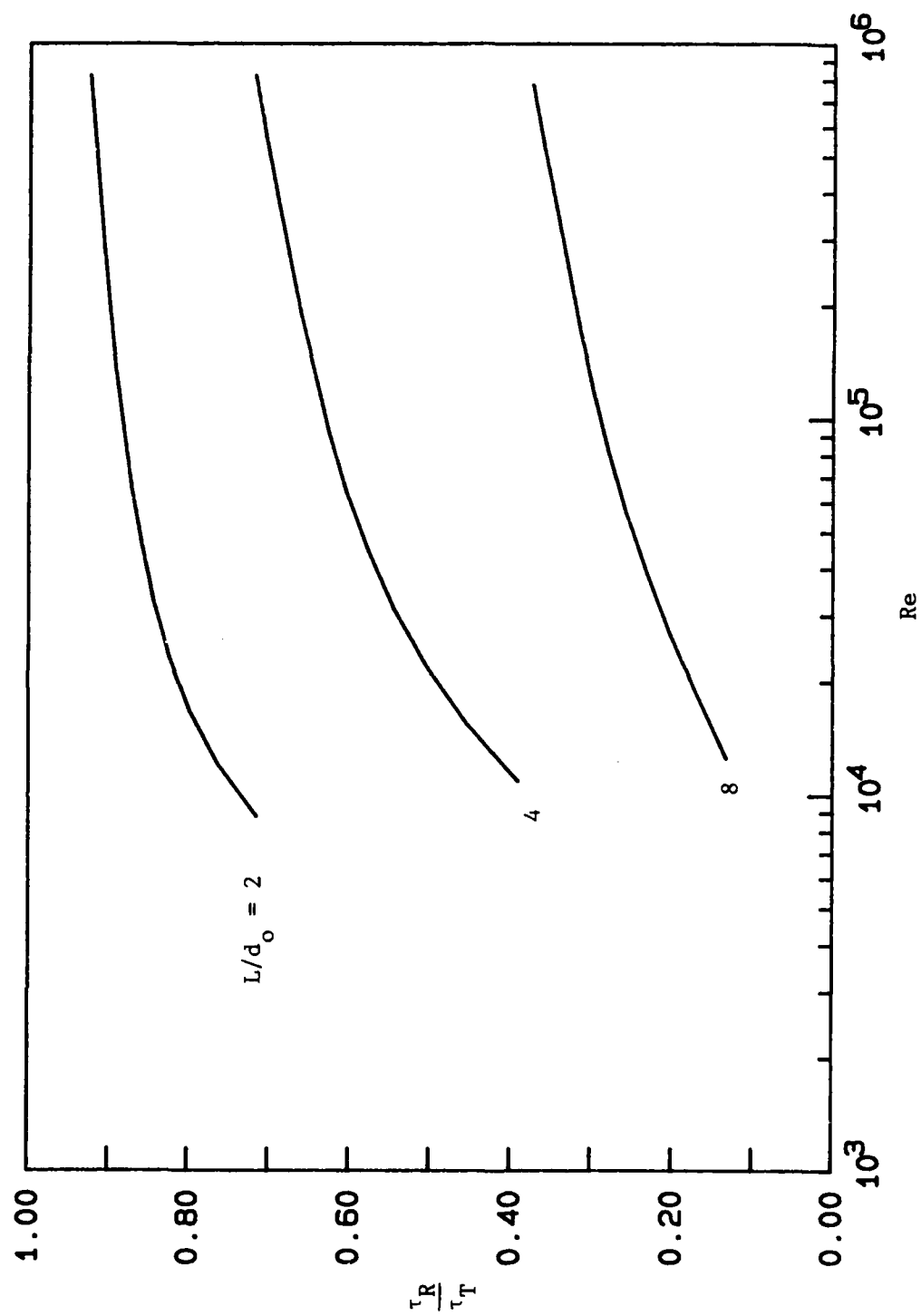
Figure 25. Roughness Parameter R_τ, Computed for the Surfaces with Large Hemispheres.

45
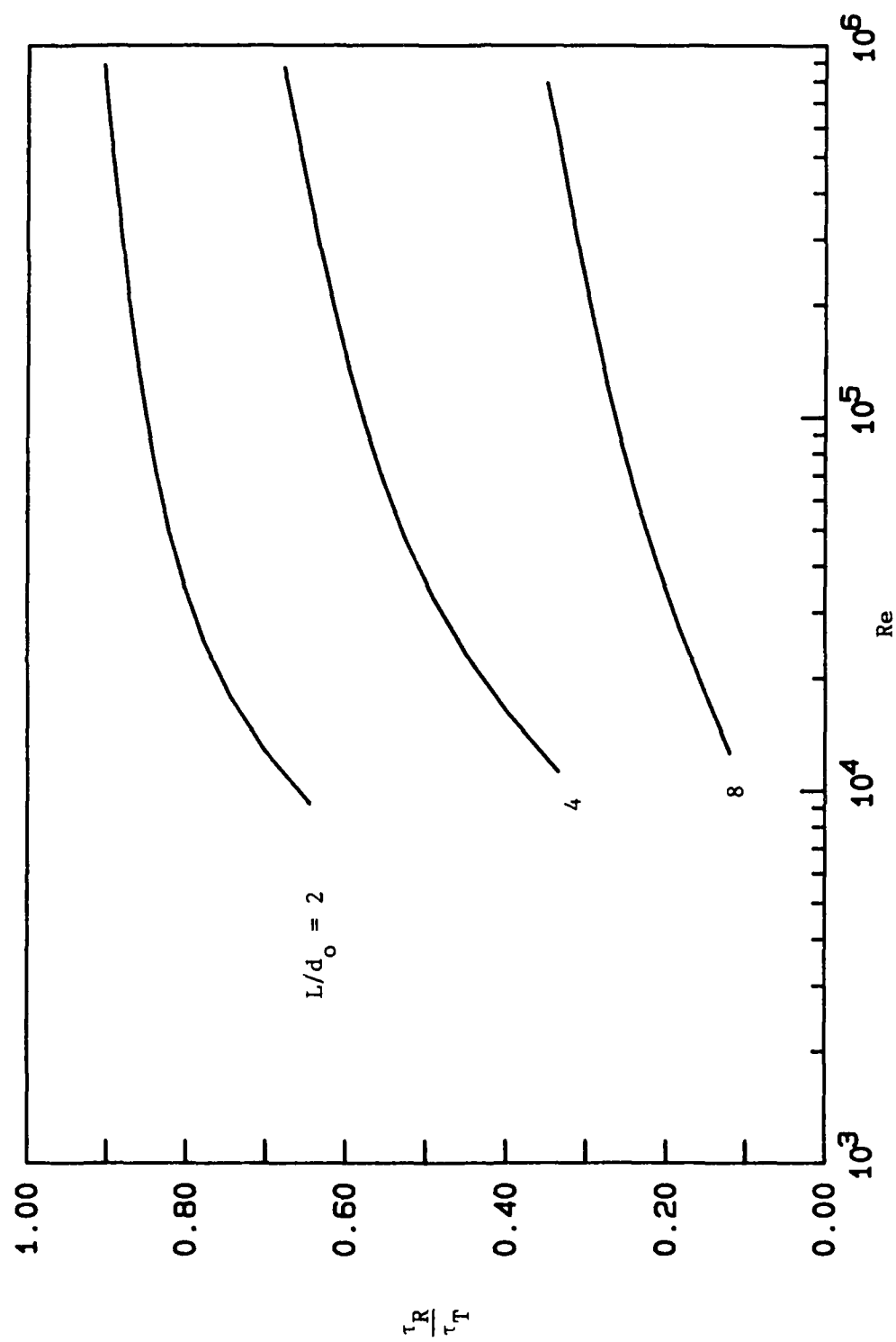
Figure 26. Roughness Parameter, R_τ, Computed for the Surfaces with Cones.

46
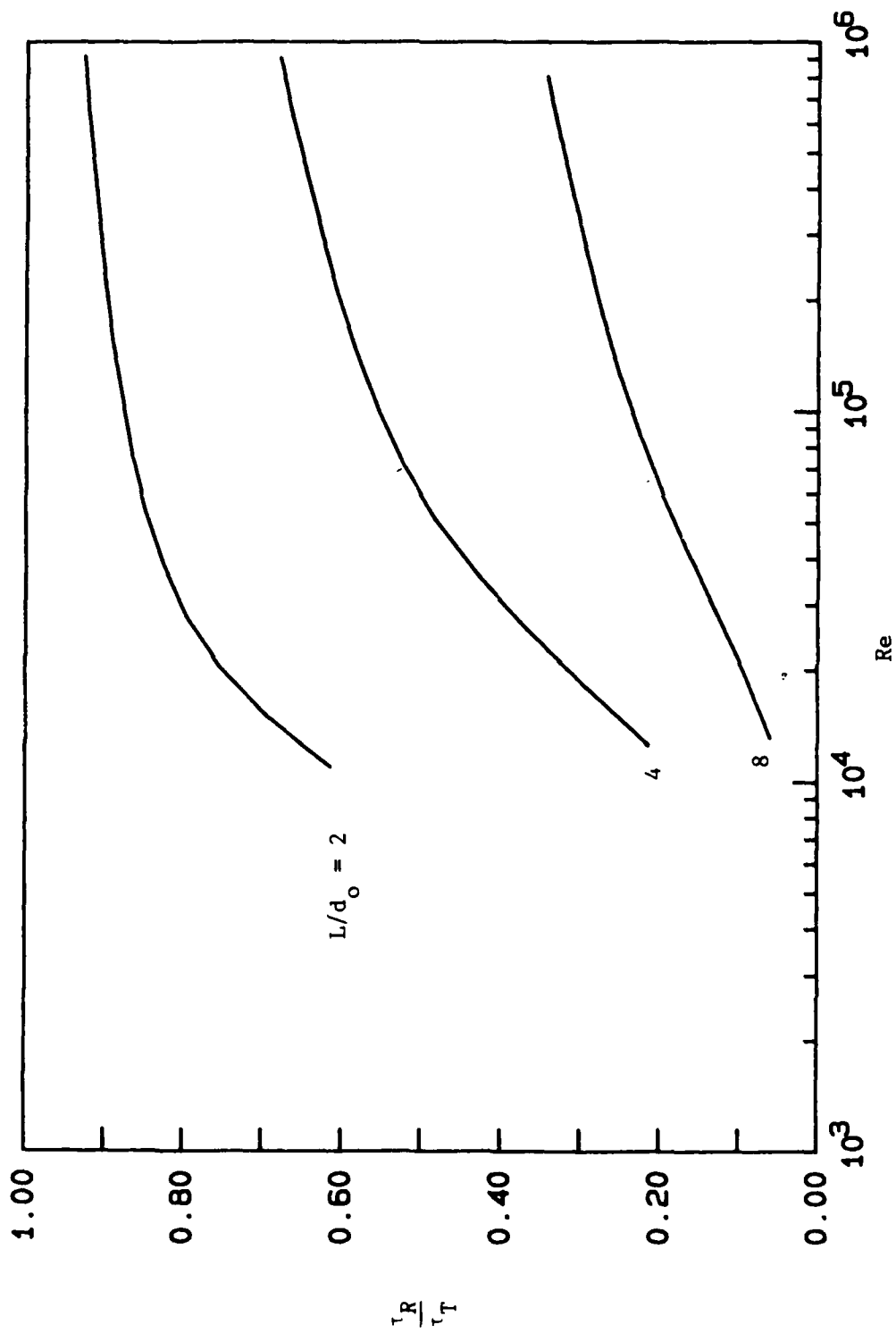
Figure 27. Roughness Parameter, R_τ, Computed for the Surfaces with Small Hemispheres.

47

SECTION IV

PSEUDORANDOM ROUGHNESS RESULTS

This section presents the experimental friction factor data
generated at MSU for two pseudorandom roughness geometries. The imple-
mentation of the discrete element model for the pseudorandom roughness
geometries of this section is discussed. The friction factor predic-
tions obtained from the discrete element model are then compared to the
experimental data.

The general shapes and geometrical parameters of the hemispherical
and conical roughness elements that make up the two nonuniform surfaces
discussed in this section are the same as presented in Figure 7. The
nominal and measured values of these geometrical parameters used in
describing these two surfaces are presented in Table 2.

1. MIXTURE 1

The surface of Mixture 1 was made up of large hemispheres and
cones. Both of these roughness elements had a nominal base diameter
d_0 = 2.54-mm (0.100-inch) and a nominal height k = 1.27-mm
(0.050-inch). The roughness elements were spaced 4 base diameters
apart. Figure 28 illustrates the configuration of the large
hemispheres and cones that make up the surface of Mixture 1.

The data set for Mixture 1 is presented in Table C-12 and plotted
in Figure 29. It contains 32 data points taken during two
replications. This test section does not appear to have a direction
dependency as the north and south replication agree very well.

2. MIXTURE 2

The surface of Mixture 2 was made up of large hemispheres and
cones, and small hemispheres and cones. The large hemispheres and
cones had the same nominal base diameters and heights as those of
Mixture 1 given above. The small hemispheres and cones had a nominal
base diameter d_0 = 1.27-mm (0.050-inch) and a nominal height k =
0.64-mm (0.025-inch). The elements were spaced 10.16-mm (0.400-inch)
apart. The element spacing can not be given in terms of element base

48

TABLE 2. Nominal and Measured Geometries of the Nonuniform Rough Surfaces

Surface	Test Section Diameter (mm)	Base diameter d_o (mm)		Element spacing L (mm)		Element height k (mm)		Projected height k' (mm)
		nominal	measured	nominal	measured	nominal	measured	nominal
Mixture 1:	51.46			10.16	10.10			
hemispheres		2.54	2.50			1.27	1.20	--
cones		2.54	2.55			1.27	1.30	1.52
Mixture 2:	51.61			10.16	10.15			
Large Hemispheres		2.54	2.50			1.27	1.25	--
Large Cones		2.54	2.50			1.27	1.32	1.52
Small Hemispheres		1.27	1.25			0.64	0.65	--
Small Cones		1.27	1.30			0.64	0.60	0.76

49

Figure 28. Rough Surface Configuration for Hemisphere/Cone
Mixture with d_o = 2.54 mm, Mixture 1.

50
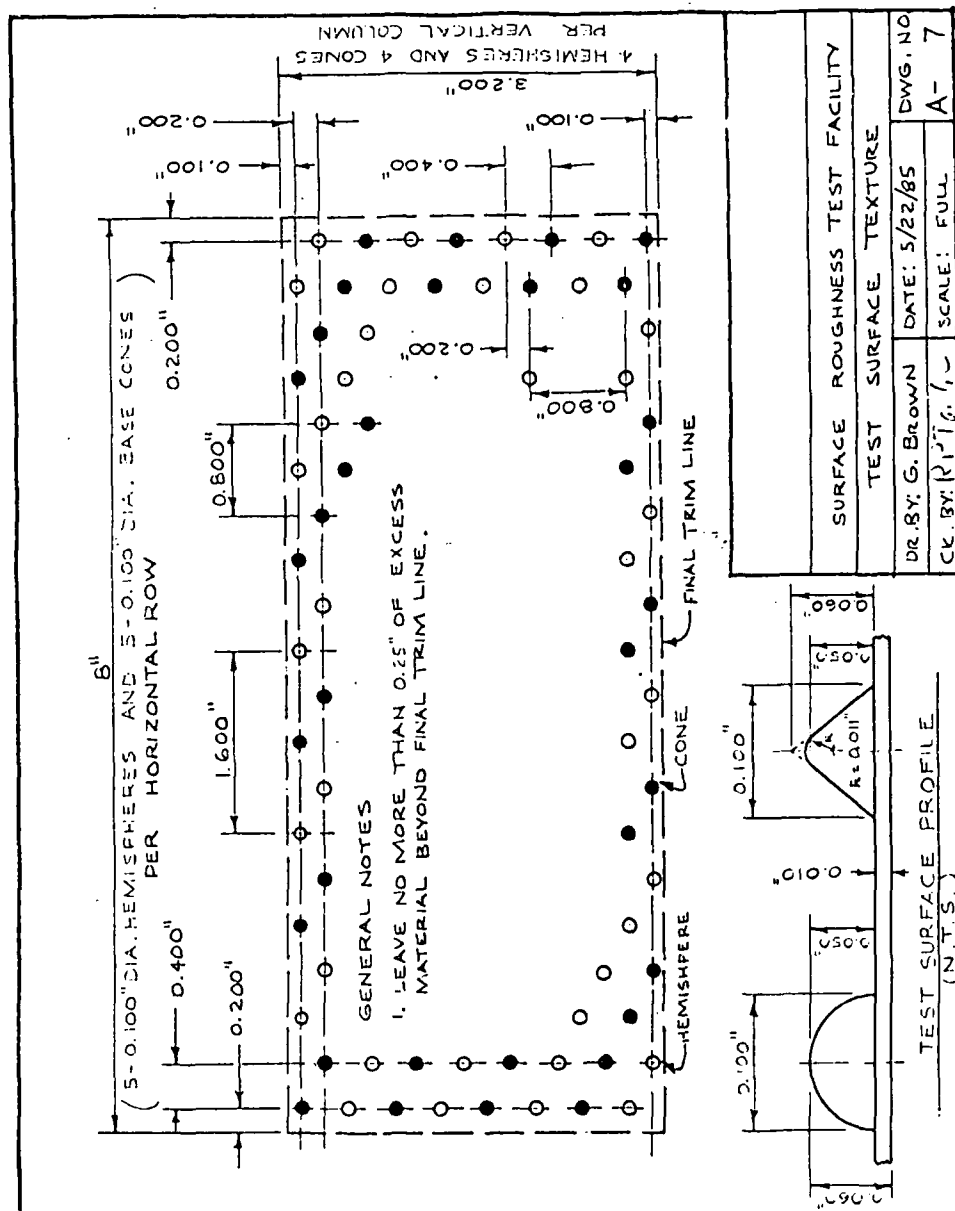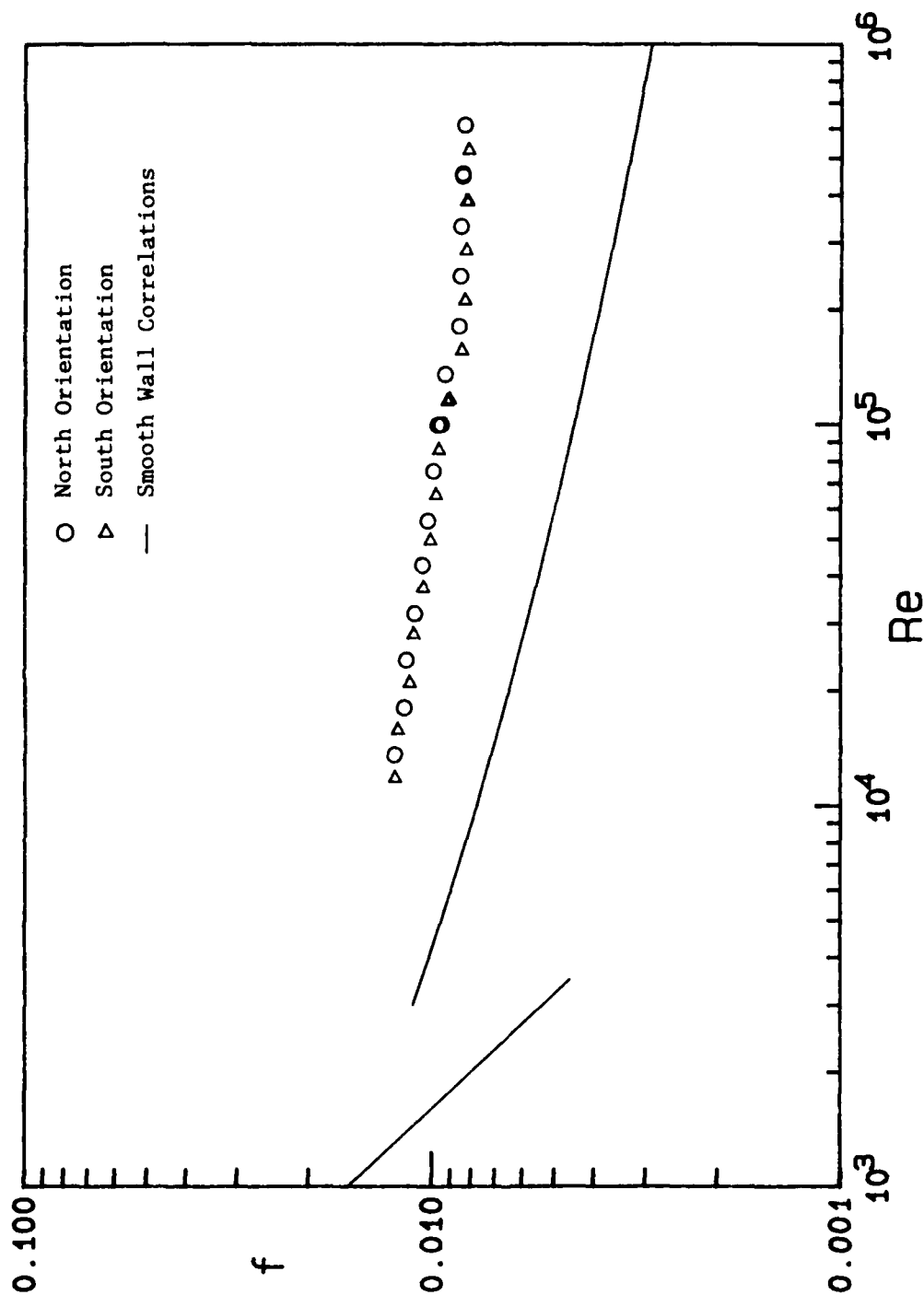
Figure 29. Friction Factor Data for Mixture 1.

51

diameter as two different element base diameters are present on this surface. Figure 30 illustrates the roughness element configuration of this surface.

The data set for Mixture 2 is presented in Figure 31 and also given in Table C-13. This data set includes 31 data points taken in two replications. This test section does not appear to have any direction dependency as the replications of the north and south orientations agree within the data scatter.

3. DISCRETE ELEMENT MODEL FOR RANDOM ROUGH SURFACES

An adaptation of the discrete element model has been proposed by Taylor, et al. (1985) for three-dimensional (as opposed to rib-type) roughness of random shape, height and spacing.

Equation (6) is reformulated as

$$0 = \frac{\mu}{R-y} \frac{d}{dy} \left[r\beta_y \left(1 + \frac{\mu_T}{\mu}\right) \frac{du}{dy} \right] - \beta_x \frac{dP}{dx}$$

$$- \frac{1}{2} \frac{\rho u^2}{(R-y)L^2/R} \sum_{i=1}^{N(y)} C_{Di} d_i(y) \, , \tag{13}$$

where

$$\beta_x = \beta_y = 1 - \frac{\pi}{4(R-y)L^2/R} \sum_{i=1}^{N(y)} d_i^2(y)$$

The parameter $N(y)$ is the number of elements which penetrate a level y in a given wall area L^2; $d_i(y)$ is the diameter associated with each of these elements. The area L^2 must be large enough to contain a statistically representative sample of the surface. The other parameters are defined as they were in equation (6).

The friction factor is defined in a form similar to equation (7)

52

Figure 30. Rough Surface Configuration for Hemisphere/Cone
Mixture with d_o = 2.54 mm and 1.27 mm, Mixture 2.

53
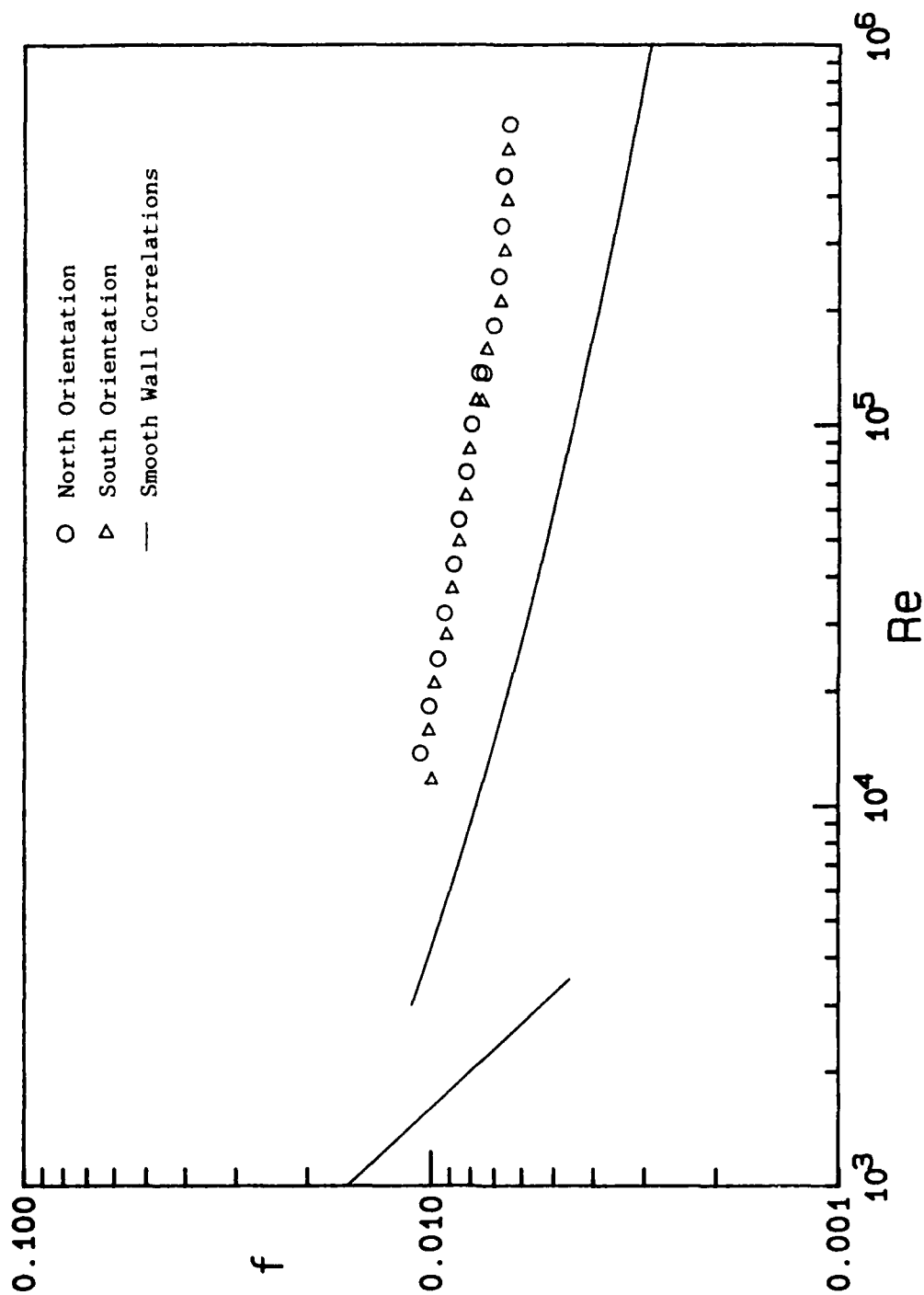
Figure 31. Friction Factor Data for Mixture 2.

54

$$f = \frac{\left(\beta_y \mu \dfrac{du}{dy}\right)_w + \dfrac{1}{2} \displaystyle\int_0^k \dfrac{\rho}{(R-y)L^2/R} u^2 \left(\sum_{i=1}^{N(y)} C_{Di} d_i\right) dy}{\dfrac{1}{2} \rho u_{ave}^2} \; . \qquad (14)$$

This model should apply to any surface for which the surface can be described as a collection of isotropic elements. In the following this model is applied to the nonuniform surfaces of Mixture 1 and Mixture 2 to test its capabilities of accounting for the variation of size and shape.

4.   PREDICTIONS FOR THE PSEUDORANDOM ROUGHNESS CASES

The experimental friction factor data for the pseudorandom rough surfaces and the friction factors calculated using the discrete element model are compared in Figures 32 and 33. The comparison of the predictions with the friction factor data of Mixture 1 is shown in Figure 32. The agreement is excellent over the entire range of Reynolds numbers tested. Similarly, the comparison of the predictions with the friction factor data of Mixture 2 is shown in Figure 33, and again the agreement over the entire range of Reynolds numbers is excellent.

The values of the roughness parameter, R_τ, calculated from the predictions are shown in Figure 34 for the surfaces of Mixture 1 and Mixture 2.
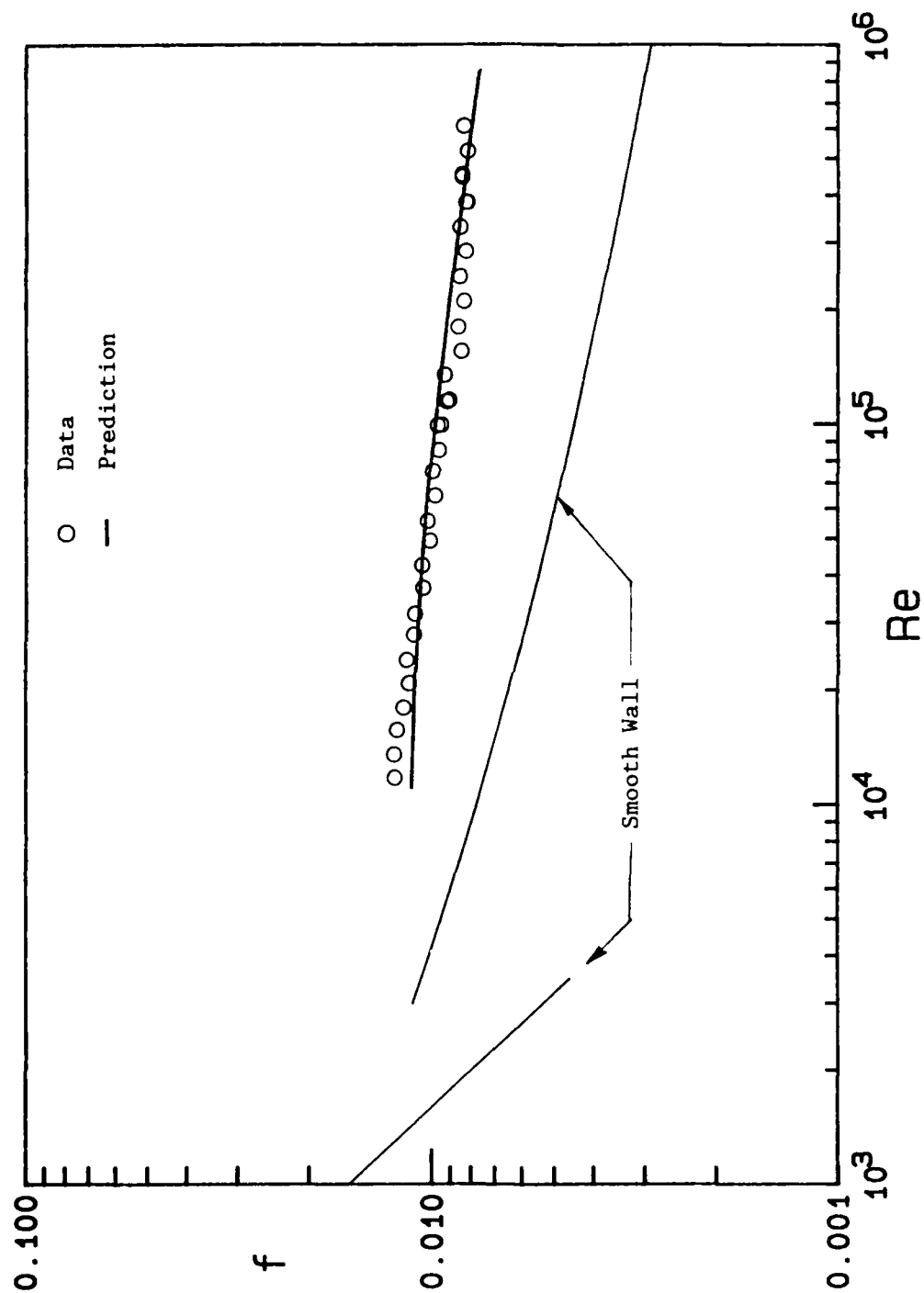
Figure 32. Comparison of Friction Factor Data and Predictions for Mixture 1.

56
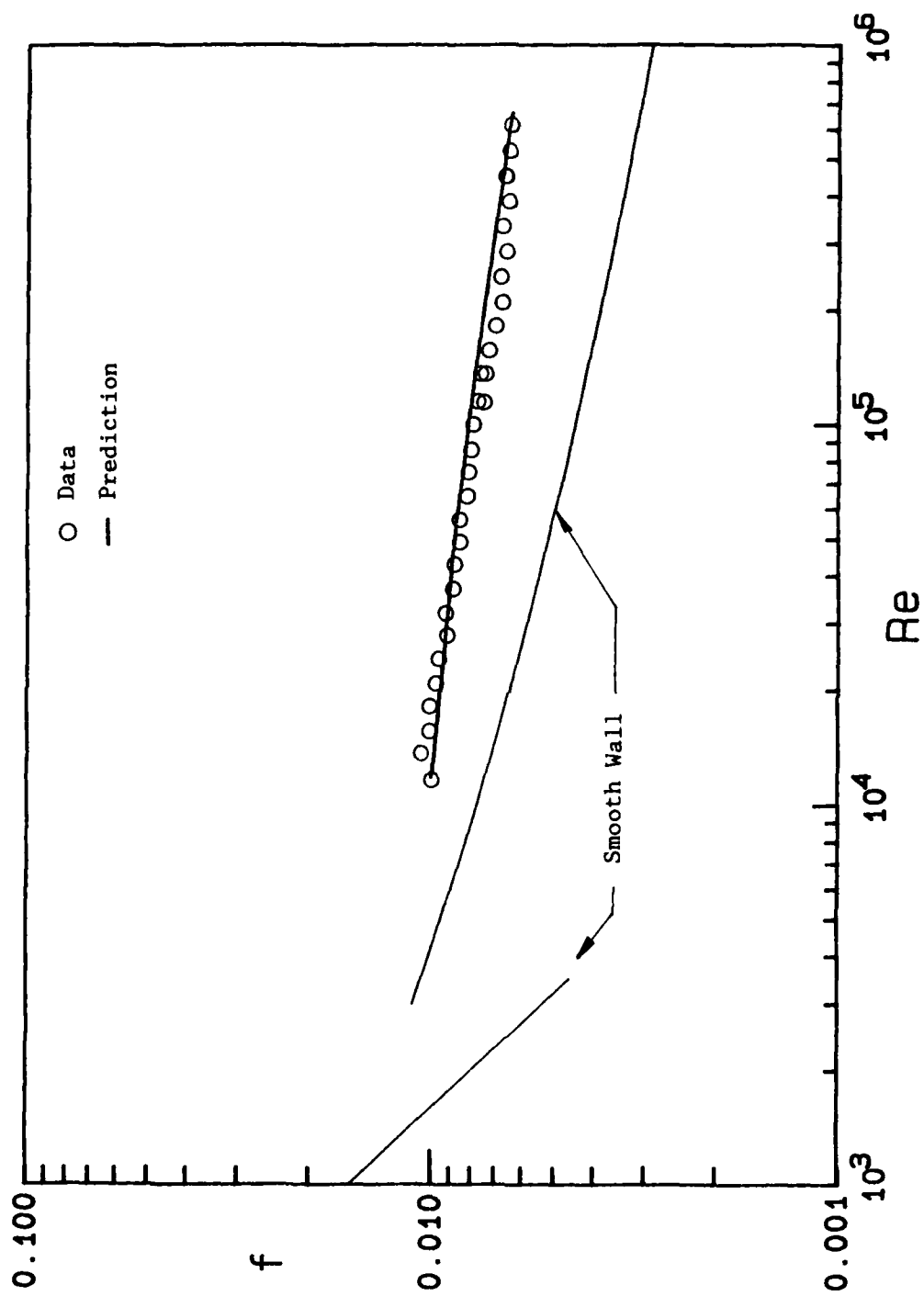
Figure 33. Comparison of Friction Factor Data and Predictions for Mixture 2.
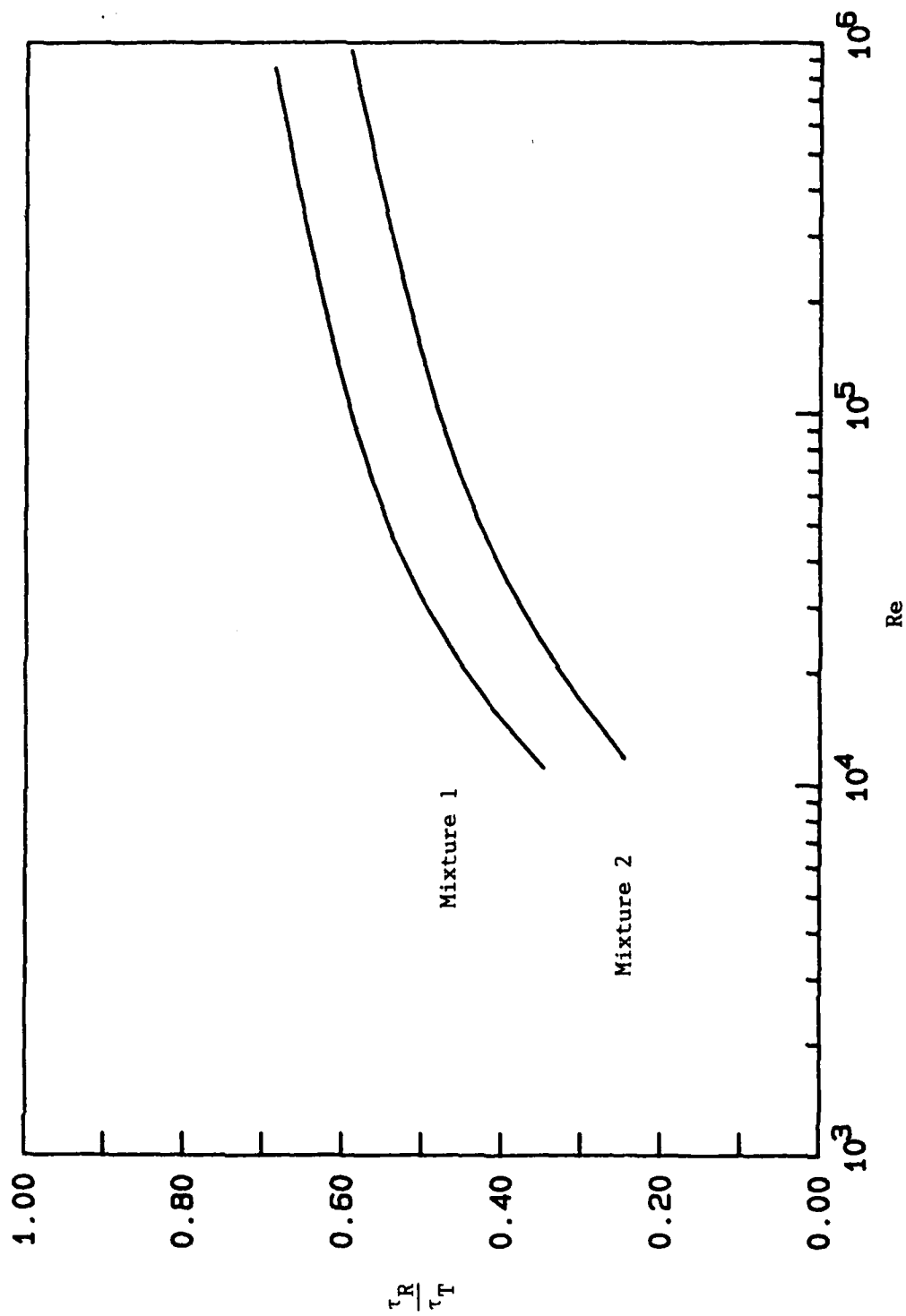
Figure 34. Roughness Parameter, R_τ, Computed for the Surfaces with Mixed Roughness Elements.

SECTION V

CONCLUSIONS AND RECOMMENDATIONS

As stated in the introduction, the objective of this project was to obtain comprehensive data sets which investigate the effects of surface roughness element size, spacing and shape on friction factor in fully developed flow over a wide range of Reynolds numbers. The motivation for this project is the fact that the only other comprehensive data set, Schlichting (1936), was in error as shown by Coleman et al (1984). In particular Schlichting's friction factors were in error as much as 73 percent. Such data sets are necessary for the calibration and verification of predictive models.

This objective has been accomplished. Friction factor data were collected for 12 surfaces. One of these cases was a smooth surface, nine were uniform rough surfaces, and two were nonuniform or pseudorandom rough surfaces. The data for each of these surfaces was collected at test section Reynolds numbers which ranged from 10,000 to 600,000. This combination covered the entire range of aerodynamically smooth, transionally rough, and fully rough flows. Some particular observations are given below.

The discrete element model as calibrated with the corrected Schlichting data, Coleman et al (1984), predicted friction factors which were in very good agreement with the data for all of the surfaces in this project. These computations were true predictions since they were based solely on surface geometry descriptions and previous model calibrations. Of particular interest is the excellent agreement of the predictions with the data for the two nonuniform surfaces.

One surprising outcome of the friction factor data analysis was the fact that the hemispherical roughness and the conical roughness with the same spacing and aspect ratio had the same friction factors. This result was surprising to the authors because the projected frontal area of a hemisphere is 35 percent larger than that of a cone.

No direct comparisons (in the sense of friction coefficient data plotted on the same figure in the same coordinates) are possible between the data from this research program and the corrected or

59

uncorrected data of Schlichting. Geometric similarity is lacking between the pipe and channel configurations, and no defensible definition of a rough wall hydraulic diameter can be made for the rectangular channel with 1 rough and 3 smooth walls. The results from the predictions with the discrete element method do indicate, in an indirect manner, that the data from this research program and the corrected data of Schlichting are in agreement.

Based on the results of this project, it is recommended that friction factor data be taken for surfaces with well documented random roughness. Here well documented means complete statistical description. Also, it is recommended that the computational development be continued to extend the discrete element model to prediction of flow over randomly rough surfaces.

REFERENCES

Adams, J. C. and Hodge, B. K. (1977), "The Calculation of
Compressible Transitional Turbulent and Relaminarizational Boundary
Layers over Smooth and Rough Surfaces Using an Extended Mixing-Length
Hypothesis," AIAA Paper 77-682.

Coleman, H. W. (1976), "Momentum and Energy Transport in the
Accelerated Fully Rough Turbulent Boundary Layer," Ph.D. Dissertation,
Mech. Eng. Dept., Stanford Univ.

Coleman, H. W., Hodge, B. K. and Taylor, R. P. (1983), "General-
ized Roughness Effects on Turbulent Boundary Layer Heat Transfer,"
AFATL-TR-83-90.

Coleman, H. W., Hodge, B. K. and Taylor, R. P. (1984), "A
Reevaluation of Schlichting's Surface Roughness Experiment," Journal of
Fluids Engineering, Vol. 106. pp. 60-65.

Dirling, R. B., Jr. (1973), "A Method for Computing Rough Wall Heat
Transfer Rates on Reentry Nose Tips," AIAA Paper No. 73-763.

Drew, T. B., Koo, E. C. and McAdams, W. H. (1932), "The Friction
Factor for Clean Round Pipes," Transactions of the AIChE, Vol. 28, pp.
56-72.

Dvorak, F. A. (1969), "Calculation of Turbulent Boundary Layers
on Rough Surfaces in Pressure Gradients," AIAA Journal, Vol. 7, pp.
1751-1759.

Finson, M. L. and Wu, P. K. S. (1979), "Analysis of Rough Wall
Turbulent Heating with Applications to Blunted Flight Vehicles," AIAA
Paper 79-008.

Finson, M. L. and Clark, A. S. (1980), "The Effect of Surface
Roughness Character on Turbulent Reentry Heating," AIAA Paper 80-1459.

Finson, M. L. (1982), "A Model for Rough Wall Turbulent Heating
and Skin Friction," AIAA Paper 82-0199.

Healzer, J. M. (1974), "The Turbulent Boundary Layer on a Rough,
Porous Plate: Experimental Heat Transfer with Uniform Blowing," Ph.D.
Dissertation, Mech. Eng. Dept., Stanford Univ.

Hodge, B. K. (1985), Analysis and Design of Energy Systems,
Prentice-Hall, Inc., Englewood Cliffs, New Jersey.

Holden, M. S. (1983), "Studies of Surface Roughness Effects in Hypersonic Flow," Calspan Report No. 7018-A-2, Advanced Technology Center, Buffalo, NY.

Kays, W. M. and Crawford, M. E. (1980), Convective Heat and Mass Transfer, 2nd edition, McGraw-Hill, New York, NY.

Nikuradse, J. (1933), "Stromungsgesetze in Rauhen Rohren," VDI-Forchungsheft 361. (Also Laws of Flow in Rough Pipes. NACA TM 1292.)

Pimenta, M. M. (1975), "The Turbulent Boundary Layer: An Experimental Study of the Transport of Momentum and Heat with the Effect of Roughness," Ph.D. Dissertation, Mech. Eng. Dept., Stanford Univ.

Schlichting, H. (1936), "Experimentelle Untersuchungen Zum Rauhigkeits-Problem," Ingenieur-Archiv., Vol. VII, No. 1, pp. 1-34. (Also Experimental Investigation of the Problem of Surface Roughness, NACA TM 823).

Simpson, R. L. (1973), "A Generalized Correlation of Roughness Density Effects on the Turbulent Boundary Layer," AIAA Journal, Vol. 11, pp. 242-244.

Taylor, R. P., Coleman, H. W., and Hodge, B. K. (1984), "A Discrete Element Prediction Approach for Turbulent Flow Over Rough Surfaces," Mechanical and Nuclear Engineering Department, Mississippi State University, Report TFD-84-1.

Taylor, R. P., Coleman, H. W. and Hodge, B. K. (1985), "Prediction of Turbulent Rough-Wall Skin Friction Using a Discrete Element Approach," Journal of Fluids Engineering, Vol. 107, No. 2, pp. 251-257.

APPENDIX A

PRESSURE TRANSDUCER CALIBRATION

This appendix presents the procedures used to calibrate the three differential pressure transducers used in this experimental study. The curvefits obtained from these calibrations are presented along with an estimate of the uncertainty associated with these curvefits.

1. LOW-RANGE TRANSDUCER

The 0- to 0.522-kPa (0.08-psi) Validyne differential pressure transducer, Model P305D, was calibrated with a Meriam water micromanometer, Model 34 FB2TM, accurate to ± 0.0254-mm (± 0.001-inch) of H_2O. A U-tube manometer filled with increasing amounts of water was used as the constant pressure source.

The calibration data consisted of 12 data points which were curvefit with a linear expression. This curvefit expression is

$$P = 0.1103(V-Z)$$

where

P is the pressure in kPa,

V is the transducer voltage signal in volts, and

Z is the transducer zero voltage shift in volts.

A composite plot of the calibration data and the resulting curvefit is given in Figure A-1. The best estimate of the uncertainty associated with the curvefit is ± 1.0 percent at a 95 percent confidence level.

2. MID-RANGE TRANSDUCER

The 0- to 8.62-kPa (1.25 psi) Validyne differential pressure transducer, Model P305D, was calibrated using the water micromanometer arrangement discussed above and a mercury filled U-tube manometer. The micromanometer was used to take calibration data over the lower 30 percent of the transducer's range; while the upper 70 percent of the range was covered using the mercury manometer. A charged air tank with a pressure regulator was used as the constant pressure source during

63
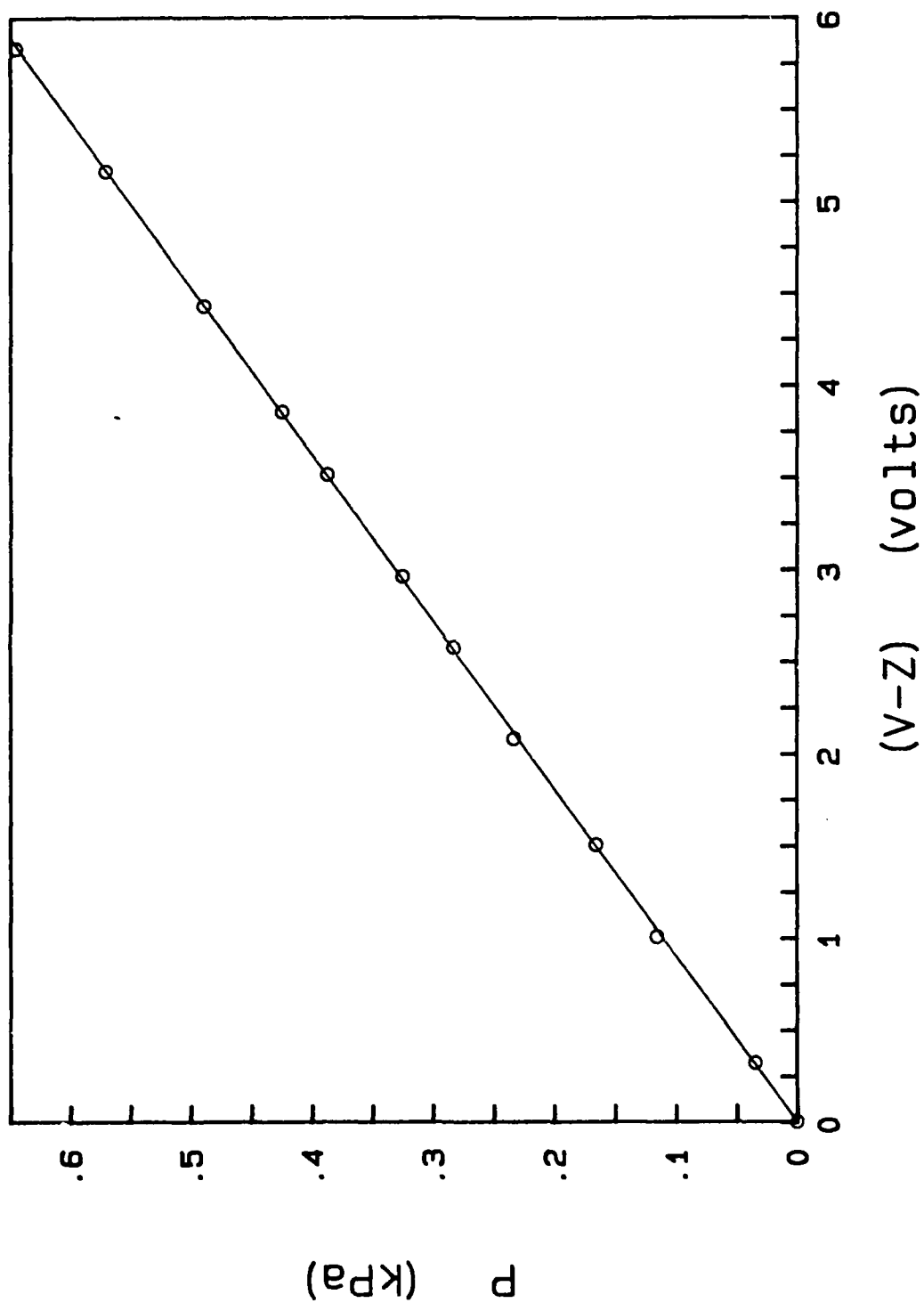
Figure A-1. Plot of the Calibration Data and the Calibration Curve for the Low-Range Pressure Transducer.

the calibration. A cathetometer was used to measure the change in height of the mercury column to the nearest 0.05-mm (0.002-inch). The corresponding pressure was then converted from mm Hg to kPa.

A piece-wise quadratic curve gave the best curvefit results. One curve used just micromanometer data for an output voltage signal less than 0.5 volts, and the other curve used micromanometer and mercury manometer data for an output voltage signal equal to or greater than 0.5 volts. The first curve was based on 9 data points, and the second was based on 63 data points. The curvefit expressions are

$$P = -0.08501(V-Z)^2 + 1.84779(V-Z), \quad V < 0.5 \text{ volts}$$
$$P = -0.00241(V-Z)^2 + 1.72678(V-Z), \quad V \geq 0.5 \text{ volts}$$

where

P is the pressure in kPa,

V is the transducer voltage signal in volts, and

Z is the transducer zero voltage shift in volts.

A composite plot of the calibration data and the resulting curvefits is given in Figure A-2. The best estimate of the uncertainty associated with the curvefits is ± 1.5 percent at a 95 percent confidence level.

3. HIGH-RANGE TRANSDUCER

The 0- to 55.16-kPa (8.0-psi) Validyne differential pressure transducer, Model P305D, was calibrated using the mercury filled U-tube manometer arrangement and procedure discussed above. The calibration data consisted of 29 data points which were curvefit with a linear expression. The curvefit expression is

$$P = 11.4505(V-Z)$$

where

P is the pressure in kPa,

V is the transducer voltage signal in volts, and

Z is the transducer zero voltage shift in volts.

A composite plot of the calibration data and the resulting curvefit is given in Figure A-3. The best estimate of the uncertainty associated with the curvefit at a 95 percent confidence level is ± 1.0 percent.
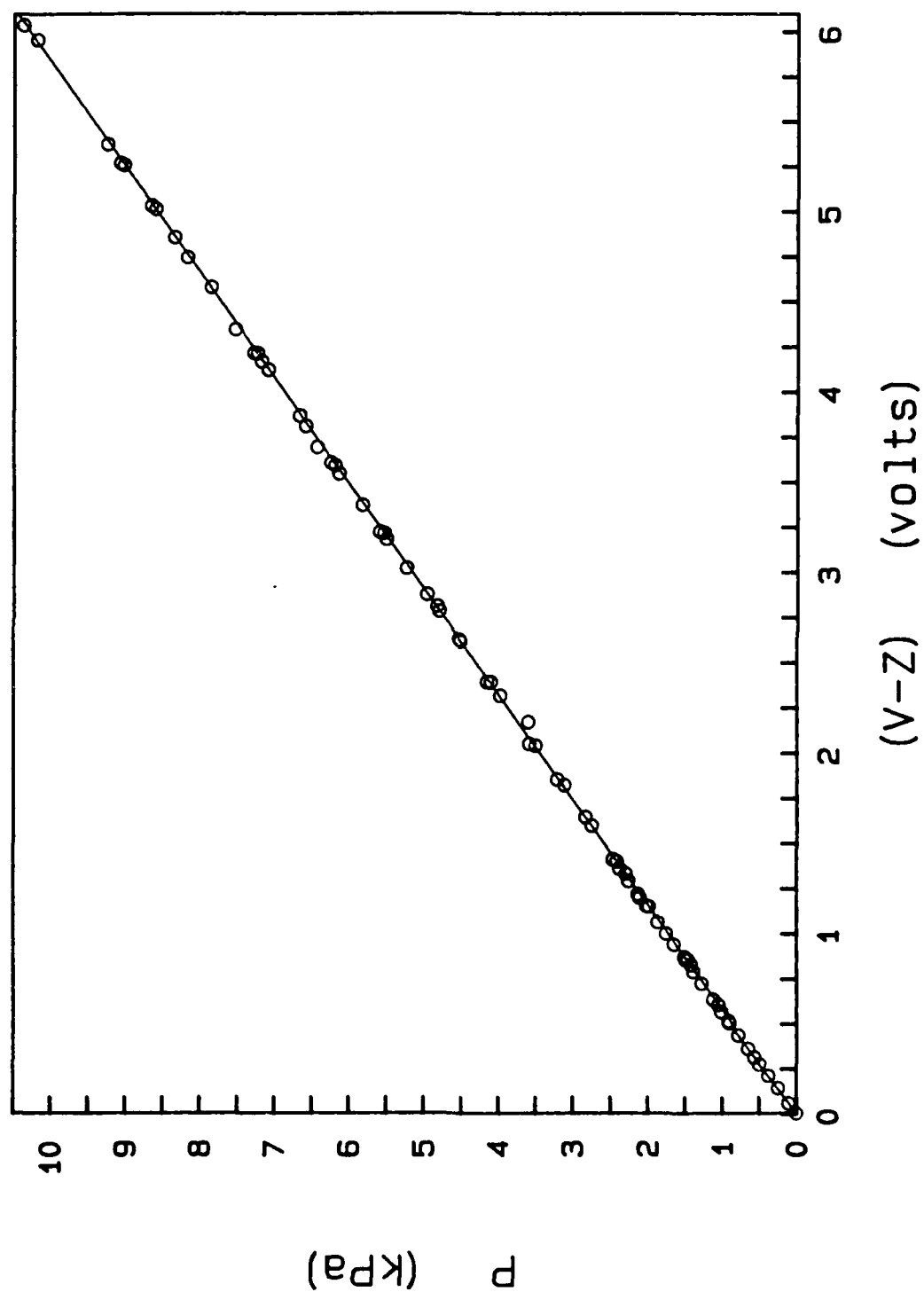
Figure A-2. Plot of the Calibration Data and the Calibration Curve for the Mid-Range Pressure Transducer.
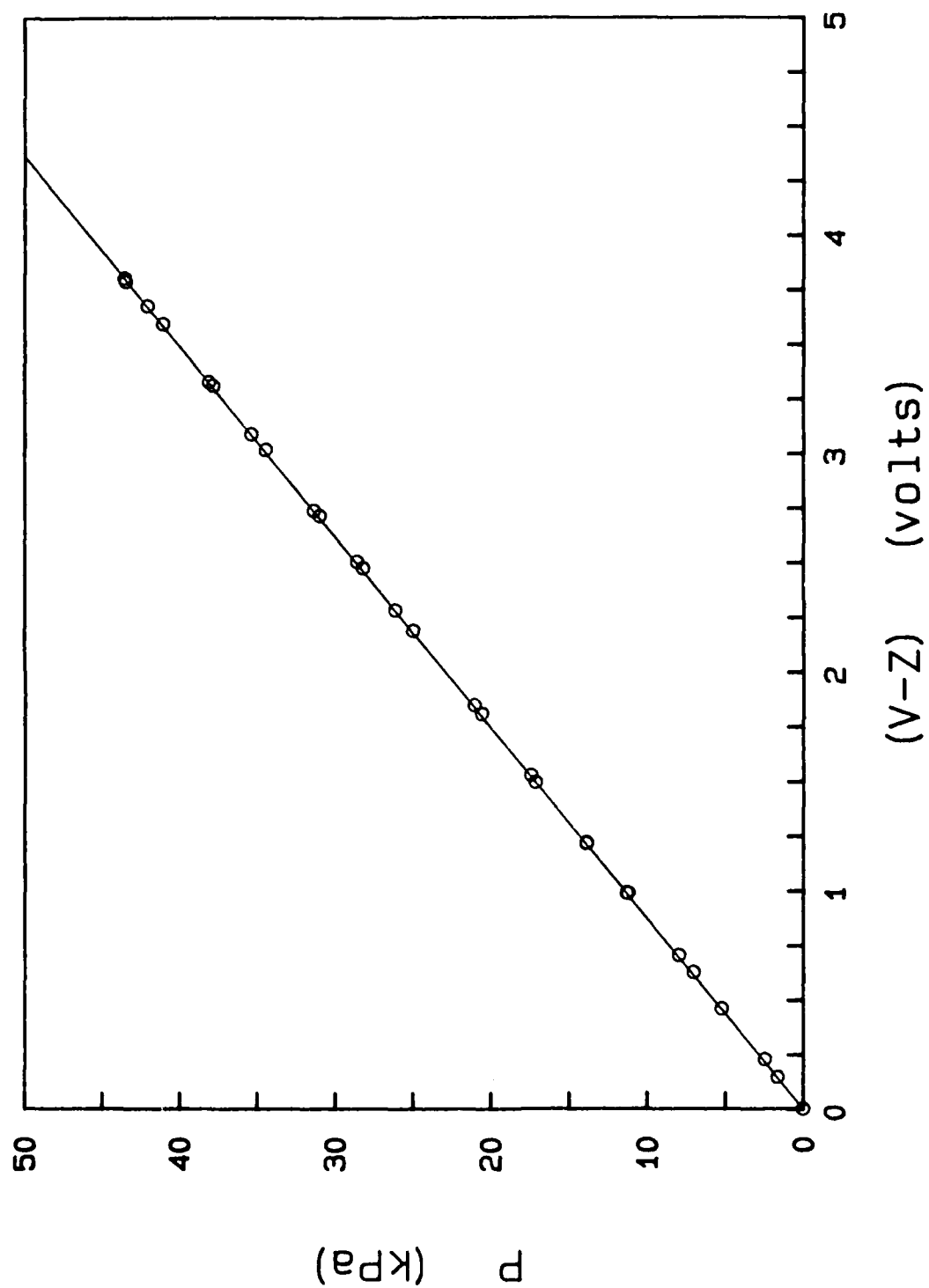
Figure A-3. Plot of the Calibration Data and the Calibration Curve for the High-Range Pressure Transducer.

APPENDIX B

UNCERTAINTY ANALYSIS

This appendix presents the best estimate of the error associated
with the friction factor and with the Reynolds numbers. It presents in
detail the uncertainties associated with each measured quantity and how
those uncertainties combine to affect the final estimated error.

The data reduction equation for this experiment is

$$f = \frac{\pi^2}{32} \frac{\Delta P}{\rho} \frac{D^5}{\Delta X} \frac{1}{Q^2} . \tag{B-1}$$

The uncertainty in the friction factor is given by

$$(\delta f)^2 = \left(\frac{\partial f}{\partial \Delta P} \delta \Delta P\right)^2 + \left(\frac{\partial f}{\partial \rho} \delta \rho\right)^2 + \left(\frac{\partial f}{\partial D} \delta D\right)^2 + \left(\frac{\partial f}{\partial \Delta X} \delta \Delta X\right)^2 + \left(\frac{\partial f}{\partial Q} \delta Q\right)^2. \tag{B-2}$$

After taking the required partial derivatives and rearranging terms,
the expression for the uncertainty in the friction factor becomes

$$\left(\frac{\delta f}{f}\right)^2 = \left(\frac{\delta \Delta P}{\Delta P}\right)^2 + \left(\frac{\delta \rho}{\rho}\right)^2 + 25 \left(\frac{\delta D}{D}\right)^2 + \left(\frac{\delta \Delta X}{\Delta X}\right)^2 + 4 \left(\frac{\delta Q}{Q}\right)^2 . \tag{B-3}$$

The propagation of the individual uncertainties in equation (B-3)
is carried out according to the 1986 ANSI/ASME Standard on Measurement
Uncertainty, PTC 19.1.

1.   PRESSURE DIFFERENCE UNCERTAINTY

The pressure difference is measured with a transducer that outputs
a dc voltage which is proportional to the pressure drop in the test
section. There is an error in the pressure measurement associated with
the pressure transducer and there is also an error from the ADACS's
accuracy in measuring a voltage. The total error in the pressure meas-
urement is therefore,

$$\left(\frac{\delta\Delta P}{\Delta P}\right)^2 = \left(\frac{\delta\Delta P}{\Delta P}\right)^2_{\text{transducer}} + \left(\frac{\delta\Delta P}{\Delta P}\right)^2_{\text{ADACS}} \quad . \tag{B-4}$$

The pressure transducers were calibrated to ± 1.5 percent of reading (the details of the calibration are given in Appendix A). This transducer uncertainty is a bias error. The ADACS is set up to measure the pressure drop 100 times, and then to use the mean value of the pressure drop in the data reduction equation. The precision error becomes negligible with this many readings of the pressure drop.

The uncertainty in the ADACS's voltage measurement is ± 0.007 percent of the reading plus ± 0.0002 percent per °C deviation from a room temperature of 23°C (73°F). Assuming that the control room in which the ADACS is located is maintained at 26°C (78°F), the total uncertainty in the ADACS reading is ± 0.0076 percent of the voltage measurement. While this error can be assumed to be all bias error, it is negligible when compared to the bias error associated with the pressure transducer.

And so,

$$\left(\frac{\delta\Delta P}{\Delta P}\right)_B = \pm 1.5 \text{ percent,}$$

$$\left(\frac{\delta\Delta P}{\Delta P}\right)_P \cong \pm 0.0 \text{ percent .}$$

2. DENSITY UNCERTAINTY

The density of the water is a function of the water temperature. A standard curvefit expression from the American Chemical Society, CRC Handbook of Chemistry and Physics (1979), for water density is:

$$\rho(\text{kg/m}^3) = \frac{a + bT + cT^2 + dT^3 + eT^4 + fT^5}{1 + gT} \tag{B-5}$$

where

$$a = 999.83952,$$
$$b = 16.941576,$$
$$c = -7.90070401 \times 10^{-3},$$
$$d = -46.1704610 \times 10^{-6},$$
$$e = 105.5630200 \times 10^{-9},$$
$$f = -280.542530 \times 10^{-12}$$
$$g = 16.87985000 \times 10^{-3}, \text{ and}$$
$$T \text{ is in } °C.$$

The uncertainty in the water density is

$$(\delta\rho)^2 = \left(\frac{\partial\rho}{\partial T} \delta T\right)^2, \qquad (B-6)$$

and the required partial derivative is

$$\frac{\partial\rho}{\partial T} = \frac{(1+gT)(b+2cT+3dT^2+4eT^3+5fT^4)-(a+bT+cT^2+dT^3+eT^4+fT^5)G}{(1+gT)^2}. \qquad (B-7)$$

The value of the partial derivative evaluated at a nominal water temperature of 27°C (80°F) is -0.2751 kg/m^3-°C. And now all that is needed to calculate the uncertainty in the density is the uncertainty in the temperature, δT.

However, the temperature of the water is measured with a thermistor; and therefore, the temperature is a function of resistance. The uncertainty in the temperature is a function of the uncertainty in the thermistor, the uncertainty in the resistance to temperature curvefit, and the uncertainty in the ADACS's resistance reading, or

$$(\delta T)^2 = (\delta T)^2_{\text{thermistor}} + (\delta T)^2_{\text{curvefit}} + (\delta T)^2_{\text{ADACS}}. \qquad (B-8)$$

The manufacturer of the thermistor gives the uncertainty in the thermistor reading as ± 0.2°C (± 0.36°F), and gives the uncertainty in the supplied curvefit as ± 0.02°C (± 0.036°F). The temperature uncertainty due the resistance, R, reading of the ADACS is

70

$$(\delta T)^2_{ADACS} = (\frac{\partial T}{\partial R} \delta R)^2 . \tag{B-9}$$

The functional relationship between resistance and temperature is

$$T = \frac{a}{\ell nR - b} - c \tag{B-10}$$

where

a = 5844.7364,

b = -5.7061806

c = 55.670391,

and T is in °C and R is in ohms.

The required partial derivative is

$$\frac{\partial T}{\partial R} = \frac{-a}{R(\ell nR - b)^2} . \tag{B-11}$$

Substituting the partial derivative into equation (B-8) yields

$$(\delta T)^2_{ADACS} = (\frac{-a}{(\ell nR - b)^2} \frac{\delta R}{R})^2 . \tag{B-12}$$

The uncertainty in the resistance value is ± 0.01 percent. A nominal value of the water temperature is 27°C (80°F) which corresponds to a resistance of 45,563 ohms. The uncertainty in the ADACS's temperature reading is then

$$(\delta T)_{ADACS} = \pm 0.036°C (\pm 0.065°F).$$

The error in the thermistor reading (± 0.20°C) was assumed to consist of both bias and precision errors of ± 0.19°C and ± 0.06°C, respectively. While the errors in the curvefit and the ADACS's resistance reading were both taken as bias errors, these errors could be calibrated out assuming that the appropriate standards were available.

71

However, in light of the relative magnitudes of the three bias errors there is no need for calibrating out the errors in the curvefit of the ADACS's resistance reading.

Therefore

$$(\delta T)_B = (0.19^2 + 0.02^2 + 0.036^2) \quad \text{or}$$
$$(\delta T)_B = \pm 0.19°C \ (\pm 0.34°F),$$

and

$$(\delta T)_P = \pm 0.06°C \ (\pm 0.10°F).$$

Now that the uncertainty in the temperature is known, the uncertainty in the density can be calculated from equation (B-6),

$$(\delta \rho)_B^2 = (0.2751 \ kg/m^3\text{-}°C \times 0.19°C)^2$$
$$(\delta \rho)_B = 0.0523 \ kg/m^3 \ (0.0336 \ lb_m/ft^3)$$

and

$$(\delta \rho)_P^2 = (0.2751 \ kg/m^3\text{-}°C \times 0.06°C)^2$$
$$(\delta \rho)_P = 0.0165 \ kg/m^3 \ (0.0103 \ lb_m/ft^3).$$

Assuming that a nominal water temperature is 27°C (80°F), the corresponding density is 96.79 kg/m³ (62.22 lb_m/ft³); and so the density uncertainties in percentage form are

$$\left(\frac{\delta \rho}{\rho}\right)_B = \pm 0.054 \text{ percent} \quad \text{and} \quad \left(\frac{\delta \rho}{\rho}\right)_P = \pm 0.017 \text{ percent} \ .$$

3.   TEST SECTION DIAMETER UNCERTAINTY

The diameters of the test sections were measured directly using a micrometer. Twelve measurements (six from each end of the test section) were taken from each of the twelve test sections. Based on these 144 measurements, an average diameter was 51.51-mm (2.028-inches). The precision error associated with the diameter measurement based on two standard deviations was 0.005-mm (0.0002-inch).

The bias error was estimated as 0.381-mm (0.015-inches), and is due to the variations in the thicknesses of the silicone skins along the length of the test section. These variations are present because of inconsistencies in the skins themselves and because of the method by which the skins are glued to the test section wall. Since the skins are made of silicone, they are very pliable and can be inadvertently stretched when being bonded to the test section. Any misalignment of individual roughness elements from skin to skin is assumed to average out and have a negligible effect.

And so the errors in the diameter expressed in percentage form are

$$\left(\frac{\delta D}{D}\right)_B = \pm\ 0.74 \text{ percent} \quad \text{and} \quad \left(\frac{\delta D}{D}\right)_P = \pm\ 0.01 \text{ percent} \quad .$$

4. ΔX UNCERTAINTY

The distance between pressure taps is the ΔX quantity in the data reduction equation. The taps were drilled in the test section at 203.20-mm (8.000-inches) apart using a carefully machined steel jig with predrilled holes. The bias error in the distance between the taps was estimated as ± 0.025-mm (± 0.001-inch); this bias error dominates the precision error, and so the precision error is negligible. The uncertainties in percentage form are

$$\left(\frac{\delta\Delta X}{\Delta X}\right)_B = \pm\ 0.013 \text{ percent} \quad \text{and} \quad \left(\frac{\delta\Delta X}{\Delta X}\right)_P \cong \pm\ 0.0 \text{ percent} \quad .$$

5. FLOWRATE UNCERTAINTY

The turbine meter outputs a squarewave frequency that is proportional to the flowrate as

Q = k · frequency.

And so the uncertainty in the flowrate is composed of transducer error and ADACS error;

$$\left(\frac{\delta Q}{Q}\right)^2 = \left(\frac{\delta Q}{Q}\right)^2_{transducer} + \left(\frac{\delta Q}{Q}\right)^2_{ADACS} \quad . \tag{B-15}$$

73

The manufacturer of the turbine meter gives the errors as

±0.75 percent of reading - linearity, and

±0.10 percent of reading - repeatability.

The former is predominately bias error while the latter is precision error. The manufacturer also gives an uncertainty in the proportionality constant, k, as ±5 percent, but for research applications the value of k for an individual meter is determined before the meter is shipped. This more exact k value was estimated to have an uncertainty of ±1.0 percent. It was assumed that this uncertainty is a bias error.

The uncertainty in the ADACS's reading of the frequency is ±0.02 percent. This error was assumed to be bias as it could be calibrated out; however, this is unnecessary as this error is negligible.

Therefore

$$\left(\frac{\delta Q}{Q}\right)^2_B = (0.75\%)^2 + (1.0\%)^2 + (0.02\%)^2$$

$$\left(\frac{\delta Q}{Q}\right)_B = \pm 1.25 \text{ percent,}$$

and

$$\left(\frac{\delta Q}{Q}\right)_P = \pm 0.10 \text{ percent.}$$

6. PROPAGATION OF ERRORS

Finally the bias in the friction factor is

$$\left(\frac{\delta f}{f}\right)^2_B = \left(\frac{\delta \Delta P}{\Delta P}\right)^2 + \left(\frac{\delta \rho}{\rho}\right)^2 + 25\left(\frac{\delta D}{D}\right)^2 + 4\left(\frac{\delta Q}{Q}\right)^2 + \left(\frac{\delta \Delta X}{\Delta X}\right)^2$$

or

$$\left(\frac{\delta f}{f}\right)^2_B = (1.5\%)^2 + (0.054\%)^2 + 25(0.74\%)^2 + 4(1.25\%)^2 + (0.013\%)^2$$

$$\left(\frac{\delta f}{f}\right)^2_B = 2.25 + 0.0029 + 13.69 + 6.25 + 0.0002$$

74

which is

$$\left(\frac{\delta f}{f}\right)_B = \pm 4.71 \text{ percent.}$$

Likewise the precision error in the friction factor is

$$\left(\frac{\delta f}{f}\right)^2_P = \left(\frac{\delta \rho}{\rho}\right)^2 + 25 \left(\frac{\delta D}{D}\right)^2 + 4 \left(\frac{\delta Q}{Q}\right)^2 ,$$

or

$$\left(\frac{\delta f}{f}\right)^2_P = (0.017\%)^2 + 25(0.01\%)^2 + 4(0.10\%)^2$$

$$\left(\frac{\delta f}{f}\right)^2_P = 0.0003 + 0.0025 + 0.04$$

which is

$$\left(\frac{\delta f}{f}\right)_P = \pm 0.21 \text{ percent.}$$

Combining the final bias and precision errors in the friction factor by the root sum square yields

$$\left(\frac{\delta f}{f}\right) = \pm 4.72 \text{ percent.}$$

It is worth noting that the largest contributor to the uncertainty in the friction factor is the error in the measurement of the diameter. However the error in the diameter cannot be greatly reduced because of the nature of the silicone sheets.

7. REYNOLDS NUMBER UNCERTAINTY

The friction factor is normally plotted as a function of the Reynolds number; and since the Reynolds number is calculated from the measured parameters in the experiment, it is important to examine the uncertainty associated with it. The Reynolds number written as a function of volumetric flowrate is

$$Re = \frac{4 \rho Q}{\pi \mu D} . \tag{B-16}$$

75

The uncertainty in the Reynolds number is then

$$\left(\frac{\delta Re}{Re}\right)^2 = \left(\frac{\delta\rho}{\rho}\right)^2 + \left(\frac{\delta D}{D}\right)^2 + \left(\frac{\delta Q}{Q}\right)^2 + \left(\frac{\delta\mu}{\mu}\right)^2 \quad . \tag{B-17}$$

The uncertainties in the density, diameter, and flowrate were previously calculated. The viscosity, like the density, is a function of the water temperature. A standard curvefit expression from the National Bureau of Standards, as given in the 1979 CRC Handbook of Chemistry and Physics, for the viscosity is as follows

$$\mu(N\text{-}s/m^2) = 1.002 \times 10^{-3}(10^a) \tag{B-18}$$

where

$$a = \frac{-0.001053T^2 - 1.2851T + 26.1228}{T + 105}$$

and T is in °C.

And so the uncertainty in the viscosity is

$$(\delta\mu)^2 = \left(\frac{\partial\mu}{\partial T}\,\delta T\right)^2$$

where

$$\frac{\partial\mu}{\partial T} = -0.00472 \; N\text{-}s/(m^2\text{-}°C) \quad .$$

Recalling that

$$(\delta T)_B = \pm\,0.20°C \quad (\pm\,0.36°F) \text{ and}$$

$$(\delta T)_P = \pm\,0.06°C \quad (\pm\,0.10°F)$$

then

$$(\delta\mu)_B = 3.82 \times 10^{-6} \; N\text{-}s/m^2 \quad \text{and}$$

$$(\delta\mu)_P = 1.14 \times 10^{-6} \; N\text{-}s/m^2.$$

The viscosity at a nominal water temperature of 27°C (80°F) is 851 x 10^{-6} N-s/m^2. So the uncertainties in percentage form are

$$\left(\frac{\delta\mu}{\mu}\right)_B = \pm\ 0.45 \text{ percent} \quad \text{and} \quad \left(\frac{\delta\mu}{\mu}\right)_P = \pm\ 0.13 \text{ percent.}$$

The uncertainties in the Reynolds number are

$$\left(\frac{\delta Re}{Re}\right)_B = \pm\ 1.52 \text{ percent} \quad \text{and} \quad \left(\frac{\delta Re}{Re}\right)_P = \pm\ 0.17 \text{ percent,}$$

and combining these bias and precision errors by the root sum square yields

$$\left(\frac{\delta Re}{Re}\right) = \pm\ 1.53 \text{ percent.}$$

APPENDIX C
TABULATION OF EXPERIMENTAL DATA

This appendix presents the data for the 13 surfaces tested in this experimental program. The data, given in Tables C-1 through C-13, include the Reynolds numbers and the corresponding friction factors. The standard deviation of the mean value of the friction factor is also presented. This value was determined by

$$s_m = \frac{s}{\sqrt{N}} \qquad (C-1)$$

where

$$s = [\frac{1}{N-1} \sum (f_i - \bar{f})^2]^{1/2} \quad ,$$

and N = 8 for every data point. The value of s_m presented in the following tables has been rounded up to 1 for all cases where $s_m \leq 1$. In addition, the water temperature and flow rate are given. The diameters of each of the test sections are given in Table C-14.

The following is a summary of the nomenclature used in the data listings.

Re   Reynolds number

f   Friction factor

s_m Standard deviation of the mean friction factor, percent of f

T   Temperature, °C

Q   Flow rate, m^3/hr.

Table C-1

Bare Wall Test Section Data

North Orientation

Re	f	s_m	T	Q
11600	0.00664	4	25.1	1.5
13400	0.00587	3	25.5	1.8
15700	0.00650	3	25.1	2.1
17900	0.00605	3	25.6	2.3
21300	0.00656	3	25.2	2.8
23900	0.00571	2	25.6	3.1
28700	0.00598	2	25.2	3.8
31900	0.00557	2	25.7	4.2
38800	0.00586	2	25.3	5.1
42600	0.00534	2	25.7	5.6
55800	0.00503	2	25.7	7.3
71100	0.00485	2	25.7	9.2
75100	0.00481	2	25.8	9.7
95000	0.00456	2	25.5	12.4
100600	0.00449	2	25.1	13.3
128000	0.00427	2	25.3	16.8
134900	0.00423	2	25.0	17.8
174500	0.00417	3	25.4	22.8
180400	0.00395	3	25.0	23.8
234600	0.00391	3	25.7	30.5
246000	0.00369	3	25.1	32.4
317600	0.00358	4	26.0	41.0
331500	0.00357	4	25.4	43.3
432500	0.00333	5	26.5	55.2

Unknown Orientation

Re	f	s_m	T	Q
11900	0.00791	4	25.2	1.6
15000	0.00711	3	25.4	2.0
21900	0.00642	1	25.4	2.9
28900	0.00602	1	25.4	3.8
37800	0.00570	2	25.5	4.9
50000	0.00538	2	25.4	6.5
60200	0.00512	2	25.7	7.8
72400	0.00488	2	26.1	9.3
80000	0.00505	3	24.9	10.6
94500	0.00459	2	25.0	12.5
109600	0.00449	2	25.1	14.4
129800	0.00433	2	25.2	17.1
150200	0.00426	3	25.2	19.7
175400	0.00405	3	25.3	23.0
226400	0.00377	3	25.5	29.6
295900	0.00353	4	25.7	38.5
375800	0.00341	4	26.2	48.5
427700	0.00331	4	26.9	54.3
505200	0.00325	5	27.6	62.9

South Orientation

Re	f	s_m	T	Q
14500	0.00652	10	25.2	1.9
19400	0.00670	2	25.3	2.6
21900	0.00643	3	25.3	2.9
34900	0.00576	2	25.4	4.6
39900	0.00588	1	25.4	5.2
45000	0.00564	2	25.5	5.9
48000	0.00570	2	25.6	6.3
81500	0.00490	2	25.4	10.7
112600	0.00454	3	25.3	14.8
153500	0.00426	3	25.5	20.1
208000	0.00409	4	25.8	27.0
280500	0.00371	5	26.0	36.2

Table C-2

Molded Smooth Silicone Skin Data

North Orientation

Re	f	s_m	T	Q
13500	0.00733	8	25.1	1.8
18000	0.00722	9	25.1	2.3
23900	0.00667	3	25.1	3.1
30100	0.00570	1	25.2	3.9
31900	0.00617	3	25.1	4.1
39900	0.00581	2	25.2	5.2
42800	0.00595	2	25.2	5.5
49600	0.00570	1	25.3	6.4
56100	0.00552	2	25.4	7.2
60000	0.00555	1	25.5	7.7
71200	0.00527	2	25.8	9.1
74900	0.00514	2	25.8	9.6
75500	0.00529	1	24.5	9.9
79500	0.00520	2	26.0	10.1
99600	0.00500	1	24.8	13.0
99800	0.00489	2	25.0	13.0
134400	0.00464	2	25.1	17.4
179800	0.00465	2	25.2	23.3
246100	0.00416	3	25.3	31.8
331400	0.00401	4	25.6	42.5
447500	0.00408	7	26.6	56.2
603600	0.00388	7	28.0	73.5

Table C-3

Large Hemispherical Roughness Data
Surface A-1 ($L/d_o = 2$)

North Orientation						South Orientation				
Re	f	s_m	T	Q		Re	f	s_m	T	Q
11800	0.02029	1	25.1	1.5		13500	0.02054	1	26.3	1.7
13500	0.02051	1	25.3	1.7		18000	0.02038	1	26.2	2.3
15300	0.02063	1	25.0	2.0		23900	0.01956	1	26.3	3.0
17800	0.02017	1	25.3	2.3		32000	0.01904	1	26.3	4.1
20500	0.02031	1	25.0	2.7		42700	0.01858	1	26.4	5.4
23600	0.01969	1	25.3	3.1		56000	0.01808	1	26.5	7.1
27500	0.01956	1	25.0	3.6		74500	0.01893	2	26.4	9.4
32000	0.01890	1	25.4	4.1		76100	0.01776	1	26.8	9.5
37200	0.01882	1	25.0	4.9		99500	0.01828	2	26.3	12.6
43000	0.01829	1	25.4	5.5		120100	0.01715	1	26.3	15.2
49400	0.01834	1	25.1	6.4		135100	0.01716	2	26.3	17.1
56400	0.01782	1	25.6	7.3		144800	0.01713	2	26.4	19.3
64800	0.01785	1	25.2	8.4		153400	0.01702	2	26.4	19.4
75600	0.01757	1	25.9	9.6		174800	0.01711	2	26.4	22.1
86500	0.01871	2	24.7	11.3		209500	0.01723	2	26.5	26.4
98800	0.01812	2	25.7	12.7		234700	0.01725	2	26.6	29.5
108000	0.01789	1	24.3	14.3		274800	0.01792	2	26.7	34.4
119200	0.01742	2	25.5	15.4		279100	0.01732	2	26.8	35.0
126400	0.01731	2	24.2	16.8		374700	0.01805	2	27.3	46.4
133800	0.01740	2	25.4	17.3						
139100	0.01728	2	24.2	18.4						
144200	0.01710	2	25.4	18.6						
147500	0.01725	2	24.2	19.6						
152300	0.01704	2	25.4	19.7						
162600	0.01713	2	24.3	21.5						
175100	0.01710	2	25.5	22.6						
191700	0.01716	2	24.3	25.4						
209900	0.01687	2	25.6	27.0						
222300	0.01699	2	24.4	29.3						
233700	0.01703	2	25.6	30.0						
254400	0.01714	2	24.5	33.5						
279700	0.01715	2	25.8	35.8						
300200	0.01715	2	24.8	39.3						
320700	0.01683	2	26.2	40.7						
320800	0.01690	2	25.1	41.7						
321200	0.01678	2	26.2	40.8						
322400	0.01697	2	25.0	42.0						
353600	0.01676	2	25.5	45.6						
381500	0.01674	2	26.6	47.9						
416700	0.01670	2	26.3	52.7						
440500	0.01649	2.	27.2	54.6						
480900	0.01647	2	27.2	59.6						

81

Table C-4

Large Hemispherical Roughness Data
Surface A-2 (L/d_o = 4)

North Orientation					South Orientation				
Re	f	s_m	T	Q	Re	f	s_m	T	Q
13500	0.01258	2	27.8	1.7	11700	0.01245	3	25.4	1.5
17900	0.01190	1	28.2	2.2	15500	0.01180	3	25.4	2.0
24000	0.01125	1	28.3	2.9	20400	0.01150	3	25.4	2.6
31900	0.01117	2	28.4	3.9	27600	0.01121	4	25.4	3.6
42700	0.01063	2	28.6	5.1	37000	0.01069	4	25.5	4.8
56300	0.01013	2	28.7	6.8	49500	0.01039	5	25.6	6.4
74600	0.01005	3	28.9	8.9	65200	0.01014	5	25.8	8.3
91100	0.01003	2	28.5	11.0	85000	0.01005	5	25.6	10.9
93100	0.00993	2	26.0	12.5	108900	0.00951	5	25.4	14.1
99900	0.00993	2	28.5	12.0	127500	0.00933	6	25.4	16.5
118400	0.00958	3	27.5	14.6	138800	0.00905	5	25.4	17.9
119600	0.00958	3	25.8	15.3	147300	0.00891	5	25.4	19.0
135000	0.00941	3	25.7	17.3	164400	0.00978	6	25.5	21.2
145100	0.00905	2	25.6	18.5	191300	0.00863	6	25.5	24.6
153300	0.00889	2	25.5	19.7	220300	0.00858	6	25.5	28.3
174500	0.00884	3	25.6	22.4	255100	0.00858	6	25.7	32.7
205600	0.00869	3	25.6	26.9	299700	0.00864	7	25.9	38.3
233400	0.00873	3	25.6	30.0	322400	0.00849	7	26.0	41.0
280300	0.00869	4	25.8	35.9	352500	0.00887	7	26.3	44.5
319200	0.00860	4	26.0	40.7	353100	0.00861	7	26.2	44.8
319200	0.00861	4	26.0	40.7	411000	0.00873	7	26.3	51.9
375900	0.00867	4	26.5	47.3	413400	0.00894	7	26.6	51.9
379700	0.00859	4	26.3	48.1	472900	0.00975	7	27.2	58.7
432700	0.00856	4	26.8	54.2	531400	0.00870	7	27.9	65.0
435000	0.00864	4	25.5	54.7					
507700	0.00952	4	27.4	62.6					

Table C-5

Large Hemispherical Roughness Data
Surface A-3 ($L/d_o = 8$)

North Orientation						South Orientation				
Re	f	s_m	T	Q		Re	f	s_m	T	Q
11500	0.01038	5	25.7	1.5		11800	0.00956	2	26.5	1.5
13200	0.00958	3	24.0	1.8		13300	0.01032	2	25.9	1.7
15700	0.00973	7	25.7	2.0		13400	0.01145	3	25.7	1.7
18200	0.00887	2	24.6	2.4		15900	0.00875	1	26.5	2.0
20800	0.00890	2	25.5	2.7		18000	0.00888	2	25.8	2.3
23900	0.00832	2	25.0	3.1		20800	0.00832	2	26.5	2.6
27900	0.00806	2	25.7	3.6		24000	0.00808	2	25.8	3.1
32000	0.00794	1	25.3	4.1		27800	0.00781	3	25.5	3.5
37000	0.00777	2	25.7	4.8		32100	0.00777	3	25.7	4.1
43200	0.00746	1	25.4	5.6		37000	0.00745	3	26.5	4.7
48900	0.00725	2	25.8	6.3		43000	0.00726	4	25.7	5.5
56000	0.00713	2	25.4	7.2		49100	0.00707	4	26.5	6.2
65100	0.00692	2	26.0	8.3		58400	0.00655	5	25.8	7.2
75900	0.00676	2	25.6	9.8		64700	0.00668	5	26.8	8.1
89500	0.00672	2	26.4	10.8		75400	0.00665	6	26.1	9.6
98900	0.00657	3	25.3	12.3		88400	0.00644	5	26.7	10.8
115400	0.00650	3	25.7	14.8		99100	0.00613	7	25.9	12.7
115700	0.00633	3	25.3	14.8		117000	0.00595	8	26.5	14.7
134500	0.00620	3	25.2	17.4		134200	0.00579	8	25.7	17.2
134700	0.00634	3	24.9	17.6		134800	0.00599	8	25.7	17.3
155200	0.00623	3	25.7	20.0		155900	0.00575	9	26.5	19.5
175800	0.00595	4	25.1	23.4		180000	0.00553	9	25.7	23.1
210400	0.00575	4	25.7	27.0		210300	0.00533	10	25.7	26.4
245700	0.00563	5	25.2	31.9		249500	0.00514	11	25.3	31.8
294200	0.00572	5	25.9	36.3		285400	0.00503	12	26.3	35.7
334800	0.00590	5	25.4	43.2		333900	0.00497	12	26.1	42.5
385100	0.00560	5	26.3	48.9		399300	0.00497	13	27.3	48.2
454500	0.00553	6	26.0	57.9		451800	0.00494	14	25.7	56.7
						518300	0.00492	15	23.2	63.9

Table C-8

Conical Roughness Data
Surface A-6 ($L/d_o = 8$)

North Orientation						South Orientation				
Re	f	s_m	T	Q		Re	f	s_m	T	Q
13400	0.00859	2	27.6	1.7		11700	0.01030	2	26.1	1.5
18000	0.00839	2	27.5	2.2		15600	0.00854	2	26.2	2.0
23800	0.00797	2	27.4	2.9		20800	0.00810	2	26.2	2.6
31800	0.00760	2	27.5	3.9		27500	0.00772	2	26.2	3.5
42600	0.00703	2	27.5	5.2		37200	0.00731	3	26.3	4.7
55900	0.00677	3	27.6	6.9		48900	0.00691	2	26.5	6.2
74800	0.00645	4	27.9	9.1		65300	0.00648	2	26.6	8.2
99400	0.00594	3	27.6	12.2		85600	0.00651	2	27.4	10.6
133900	0.00569	3	27.4	16.5		116100	0.00593	3	26.4	14.7
134900	0.00559	3	27.5	16.6		116700	0.00601	3	26.2	14.8
180400	0.00540	3	27.5	22.2		155800	0.00573	3	26.5	19.6
198700	0.00521	3	26.7	24.9		210600	0.00531	3	26.7	26.4
201500	0.00515	3	27.5	24.8		283000	0.00516	4	26.9	35.3
245700	0.00493	4	27.5	30.3		386200	0.00509	4	27.3	47.8
330200	0.00488	5	27.8	40.4		521800	0.00506	4	28.0	63.6
402300	0.00483	5	26.7	50.4						

Table C-9

Small Hemispherical Roughness Data
Surface B-1 ($L/d_o = 2$)

North Orientation						South Orientation				
Re	f	s_m	T	Q		Re	f	s_m	T	Q
13400	0.01603	1	25.5	1.7		11600	0.01427	1	26.4	1.5
18000	0.01549	1	25.5	2.3		15700	0.01513	1	26.5	2.0
23800	0.01577	1	25.5	3.1		20900	0.01537	1	26.5	2.7
31600	0.01572	1	25.5	4.1		28100	0.01563	1	26.5	3.6
42900	0.01565	1	25.6	5.5		37200	0.01569	1	26.6	4.7
56100	0.01545	1	25.7	7.2		49100	0.01549	1	26.9	6.2
74600	0.01514	1	26.0	9.6		65000	0.01518	1	27.1	8.2
99600	0.01529	1	25.7	12.9		85700	0.01575	1	28.0	10.5
135000	0.01420	2	25.6	17.5		115700	0.01489	1	26.9	14.6
179800	0.01406	2	25.7	23.3		157500	0.01400	1	26.9	19.8
245000	0.01401	2	25.8	31.6		209400	0.01409	1	26.9	26.3
329700	0.01418	2	26.3	42.0		288700	0.01411	1	27.1	36.2
331700	0.01413	2	26.1	42.5		385300	0.01423	1	27.6	47.7
451400	0.01426	2	26.9	56.8		387900	0.01421	1	27.7	47.9
						523200	0.01432	1	28.9	63.2

Table C-10

Small Hemispherical Roughness Data
Surface B-2 ($L/d_o = 4$)

North Orientation						South Orientation				
Re	f	s_m	T	Q		Re	f	s_m	T	Q
13400	0.00989	3	25.5	1.7		11700	0.01113	5	26.2	1.5
17900	0.00931	4	25.5	2.3		15600	0.00947	4	26.4	2.0
23700	0.00924	2	25.5	3.1		20900	0.00911	3	26.4	2.6
31900	0.00929	2	25.6	4.1		27700	0.00922	3	26.5	3.5
42600	0.00912	2	25.6	5.5		37100	0.00910	3	26.5	4.7
55400	0.00865	2	25.7	7.1		49500	0.00889	4	26.6	6.2
75300	0.00875	2	25.9	9.6		64900	0.00876	4	26.8	8.1
100300	0.00861	2	25.6	12.9		85800	0.00848	4	27.2	10.7
100700	0.00838	2	25.8	12.9		115100	0.00823	4	26.7	14.4
134200	0.00822	3	25.6	17.3		155600	0.00786	4	26.7	19.6
179600	0.00759	3	25.7	23.1		208700	0.00737	5	26.7	26.2
245900	0.00742	3	25.7	31.5		284600	0.00731	5	26.9	35.6
331300	0.00739	3	26.0	42.2		369000	0.00712	6	27.3	48.2
452100	0.00732	3	26.6	56.8		389400	0.00715	6	27.3	48.2
455000	0.00722	3	26.8	57.0		518600	0.00714	6	28.1	63.1
613000	0.00723	3	28.0	74.7						

Table C-11

Small Hemispherical Roughness Data
Surface B-3 ($L/d_o = 8$)

North Orientation						South Orientation				
Re	f	s_m	T	Q		Re	f	s_m	T	Q
13400	0.00901	5	26.7	1.7		11300	0.00935	5	25.9	1.5
18000	0.00772	3	26.5	2.3		15400	0.00818	3	25.8	2.0
23900	0.00735	4	26.7	3.0		20700	0.00709	5	25.9	2.7
31700	0.00726	4	26.7	4.0		27700	0.00684	3	25.9	3.5
42600	0.00686	3	26.8	5.4		37100	0.00662	3	26.0	4.7
55700	0.00651	4	27.0	7.0		48900	0.00643	3	26.2	6.2
75100	0.00619	6	27.2	9.3		65000	0.00616	3	26.4	8.2
99000	0.00616	4	27.0	12.4		84600	0.00594	4	27.8	10.4
135200	0.00573	5	26.9	16.9		117000	0.00559	4	26.3	14.8
136800	0.00565	5	26.5	17.3		156300	0.00527	4	26.3	19.8
180100	0.00553	5	26.8	22.6		157100	0.00538	4	26.4	19.9
249700	0.00511	6	27.1	31.2		209400	0.00497	4	26.5	25.4
333200	0.00502	6	27.3	41.4		287600	0.00463	5	25.8	36.1
447600	0.00491	7	27.9	54.9		387000	0.00460	6	27.2	48.2
						526400	0.00446	6	28.0	64.4
						610800	0.00437	6	29.8	73.4

Table C-12

Roughness Mixture 1 Data
Surface A-7

North Orientation					South Orientation				
Re	f	s_m	T	Q	Re	f	s_m	T	Q
13500	0.01236	1	25.6	1.7	11700	0.01233	2	26.1	1.5
17900	0.01170	1	25.6	2.3	15600	0.01215	2	26.2	2.0
23900	0.01154	1	25.5	3.1	20800	0.01133	2	26.2	2.6
31700	0.01101	1	25.6	4.1	27900	0.01108	2	26.3	3.5
42600	0.01056	2	25.7	5.5	37100	0.01050	2	26.3	4.7
55700	0.01022	2	25.8	7.1	49400	0.01009	2	26.4	6.2
75300	0.00993	2	26.1	9.6	65100	0.00979	2	26.6	8.2
99600	0.00968	2	25.7	12.8	85300	0.00962	3	26.4	10.8
100000	0.00948	2	25.9	12.8	115100	0.00919	2	26.1	14.6
135200	0.00929	2	25.7	17.3	116200	0.00906	2	26.2	14.7
180600	0.00860	2	25.7	23.2	156000	0.00845	2	25.8	20.0
245100	0.00852	2	25.8	31.4	211300	0.00832	2	25.7	27.1
331600	0.00851	2	26.1	42.2	286200	0.00826	2	25.9	36.5
449200	0.00842	3	27.0	56.0	385000	0.00825	2	26.5	48.5
455600	0.00842	3	25.8	57.1	385400	0.00818	2	26.4	48.7
612000	0.00833	3	28.4	73.9	525000	0.00816	2	27.4	64.8

Table C-13

Roughness Mixture 2 Data
Surface B-4

North Orientation					South Orientation				
Re	f	s_m	T	Q	Re	f	s_m	T	Q
13600	0.01064	1	25.9	1.7	11600	0.00998	3	26.9	1.5
19100	0.01009	1	26.0	2.3	15500	0.01013	1	26.9	2.0
24100	0.00965	1	26.0	3.1	20600	0.00979	1	26.9	2.6
31600	0.00928	1	26.1	4.1	27800	0.00919	2	26.9	3.5
42600	0.00890	1	26.2	5.5	36900	0.00889	1	26.9	4.6
56200	0.00856	1	26.3	7.1	49100	0.00855	1	27.0	6.1
75100	0.00819	1	26.7	9.5	64800	0.00822	2	27.2	9.1
100200	0.00796	1	26.5	12.7	85900	0.00806	2	27.6	10.6
136200	0.00741	2	26.4	17.2	114600	0.00750	1	27.0	14.3
136300	0.00753	2	26.5	17.2	115300	0.00777	1	27.0	14.4
182000	0.00703	2	26.5	23.0	156600	0.00729	1	27.0	19.6
244900	0.00683	2	26.7	30.8	205600	0.00576	2	27.1	26.1
332900	0.00675	3	27.0	41.6	285400	0.00561	2	27.2	35.5
450400	0.00663	3	27.7	55.4	386800	0.00553	2	27.5	47.8
451000	0.00667	3	27.6	55.6	526000	0.00549	2	28.3	54.0
616400	0.00643	4	28.9	74.0					

Table C-14

Test Section Diameters

Surface	Diameter (mm)
Bare Wall	52.17
Smooth Silicone Skin	51.38
A-1	51.46
A-2	51.46
A-3	51.51
A-4	51.31
A-5	51.41
A-6	51.46
B-1	51.89
B-2	51.51
B-3	51.64
Mixture 1	51.46
Mixture 2	51.61